Response to reviewers

August 28, 2019

Summary:

We thank both reviewers for their comments. As detailed in the point-by-point response below, we have done two major modifications to the manuscript:

1. Now we explicitly take into account rain evaporation and horizontal advection in our model. These effects are described as simply as possible in the main text, and technical details are given in appendix. This allows us to rigorously quantify these effects on δD_0 variations and to address all the related comments. This also simplifies the interpretation of r_{orig} variations. We also address explicitly the effect of rain evaporation and horizontal advection on z_{orig} estimates, and have modified our abstract and conclusion accordingly.
2. Now we better document and discuss the spatio-temporal variability of free tropospheric profiles. However, since this is not the core of the paper, and consistent with reviewer 1's suggestion, we have moved this discussion to the appendix.

1 Reviewer 1

We thank reviewer 1 for his/her comments.

This paper presents an analytical steady state vertical mixing model to investigate the controls on the water vapor isotopic composition in the subcloud layer over the tropical oceans. It is a nicely simple model that considers the most important processes, which are surface evaporation and vertical mixing and predicts the subcloud layer water vapour isotope composition from a combination of mass balance equations for all isotope species. I enjoyed reading this paper very much, I particularly like the approach chosen for testing this analytical model, which combines model simulation data and ship-based observations. The ideas presented in this paper are exciting and very valuable for upcoming large field campaigns in which isotope observations are planned in different parts of the lower troposphere.

I thus recommend minor revisions with the following minor points:

1) In the abstract it should be clearly stated that the proposed analytical model is a steady state formulation, which neglects horizontal gradients and thus the impact of horizontal advection.

- Regarding the steady state formulation. Now we write in the abstract: "The model relies on the assumption that δD profiles are steeper than mixing lines, and that the SCL is at steady state, restricting its applications to time scales longer than daily."
- Regarding horizontal advection. Now we account for it explicitly. We write in the abstract: "We extend previous simple box models of the SCL by prescribing the shape of δD vertical profiles as a function of humidity profiles and by accounting for rain evaporation and horizontal advection effects."

2) P. 1, L. 10: "When the air mixing into the SCL is lower in altitude it is moister": I think this is true most of the time and certainly in a climatological sense, but of course when including differential advection elevated moist layers can occur. I guess adding "it is generally moister" would make me very happy.

We modify as suggested.

3) P. 3, L. 4: Shouldn't cloud top cooling be mentioned here as well?

We modify as: "driven by cloud-top radiative cooling, mixing and evaporative cooling of droplets"

4) P. 5, L. 4: Neglecting the large-scale horizontal gradients in air properties, particularly in the trade wind regions seems to me like a strong assumption. Given the sensitivity of dD to SST and the considerable SST gradient across the North Atlantic, I find that this caveat could be discussed a bit more explicitly here.

We agree that the neglect of horizontal advection was an important caveat. Therefore, now we rigorously estimate the effect of horizontal advection of isotopic gradients on our results. This is detailed in section 2 in the main text. Eq. (8) provides the new equation for R_0 as a function of , the ratio of water vapor coming from horizontal advection to that coming from surface evaporation, and β, the ratio of isotopic ratios of horizontal advection to that of the SCL.

Coming back to the effect of horizontal gradients in the North Atlantic: our figure 7h shows that the effect of horizontal advection is not stronger in the North Atlantic than elsewhere. But it is larger near the Saharan coast. A later comment from you can be used to explain this feature: section 4.1: "Horizontal advection is slightly enriching in deep convective regions and depleting in coastal regions (e.g. off the coasts of California, Peru, Mauritania, Namibia, India and Australia). For example, the Saharan layer in front of the North-Western African Coast leads to a strong effect of horizontal advection there ([Lacour et al., 2017]). "

5) P. 5, L. 20: "qs is the saturation specific humidity at SST"
corrected

6) P. 6, L26: In the closure section and the discussion of the free tropospheric profile the role of horizontal advection is again neglected. This is maybe a good assumption in the tropic but it should still be mentioned explicitly.
Now we account for the effect of horizontal advection on δD_0 in our box model. However, our closure assumption does not need to neglect horizontal advection. Horizontal advection effects are implicitely taken into account through the α_{eff}: we now clarify this: section 2.2: "Effects of horizontal advection and rain evaporation are encapsulated into α_{eff}. "

7) P. 8, L26: "Depending on microphysical details that are too complex to be addressed here", Graf et al. 2019 could be referenced here
We add this reference.

8) P. 9. Fig. 3: Which value was chosen for the SST? This could be mentioned in the caption as well as a reference to which equilibrium fractionation factor was used

We add this information in the caption: "For this illustrative purpose, we assume SST=30°C, $h_0 = 0.8$ $\delta D_{oce} = 0$‰ and $\phi = \eta = 0$. ". We also add it to Fig. 4.

9) P. 12, L. 2: "However, if the end member is defined below 500 hPa (e.g. 600 hPa), results are not always reasonable", why is this so?

Now we explain this in the text: section 3.3: "However, the end member should be defined above 500 hPa to ensure that it is well above boundary layer processes. If the end member is defined below 500 hPa (e.g. 600 hPa), there are a few cases where q increases with altitude ($q_f > q_0$) due to horizontal advection or convective detrainment from nearby moister regions. Meanwhile, δD decreases monotonically, leading to unrealistic values for α_{eff}.".

10) P. 12, L. 7: In my opinion, this makes it difficult to interpret rorig. But probably there are conditions when rorig and thus zorig are more physically meaningful than others. Could the authors maybe add a list with explicit and quantitatively expressed conditions in which they would argue that the assumptions involved in Eq. 9 are satisfied?

Now we explicitly account for rain evaporation and horizontal advection. Equations are given in the main text, so anyone can calculate these effects in their own cases. The contributions of these effects are plotted as maps in Fig. 7 g and h, and as composites as a function of ω_{500} and EIS in Fig. 8. Table 2 compares the effect of r_{orig} if these effects are neglected or not. The effect of rain evaporation and horizontal advection on z_{orig} estimates are plotted in Fig. 14b.

Note that a list of conditions would not be easy, since the effect of rain evaporation depends on parameters η and α_{evap} which are very difficult to estimate in nature, and horizontal advection depends on parameters ϕ and β which are resolution-dependent and depend on several variables (wind, humidity and δD profiles in the SCL).

11) P. 13, L. 4-5: Is there a literature reference that the authors could indicated for this calculation of zi from observations?

We now give several literature references and more explanation on this calculation method: section 3.4: "The temperature inversion is an abrupt increase in temperature that caps the boundary layer. Therefore, a method to automatically estimate its altitude is to detect a maximum in the vertical gradient of potential temperature ([Stull, 1988, Oke, 1988, Sorbjan, 1989, Garratt, 1994, Siebert et al., 2000]). This method is sensitive to the resolution of vertical profiles ([Siebert et al., 2000, Seidel et al., 2010]). Therefore, we adapted this method in order to yield z_i values that best agree with what we would estimate from visual inspection of individual temperature profiles. In LMDZ, we calculate z_i as the first level at which the vertical potential temperature gradient exceeds 3 times the moist-adiabatic lapse rate. In observations, we calculate z_i as the first level at which the vertical potential temperature gradient exceeds 5 times the moist-adiabatic lapse rate, because radio-soundings are noisier than simulated profiles. "

12) P. 13, L. 15: I did not immediately understand what was meant by composites belonging to a given interval of omega500, I was expecting a map. A reference to the results figure referred to here would have helped me.

We now explain better how the composites are calculated, and we add a reference to Fig. 10 as an example. Section 3.5: "The type of clouds and mixing processes depends strongly on the large-scale velocity at 500 hPa (ω_{500}, map shown in Fig. 6a), with shallow clouds in subsiding regions and deeper clouds in ascending regions (Fig. 1). Therefore, it is convenient to plot variables as composites as a function of ω_{500} ([Bony et al., 2004]). To make such plots, we divide the ω_{500} range from -30 to 50 hPa/d into intervals of 5 hPa/d. In each given interval, we average all seasonal-mean values at all locations over tropical oceans for which seasonal-mean ω_{500} belongs to this interval (e.g. Fig. 10a will be an example). .

The cloud cover strongly correlates with the inversion strength, which can be quantified by the Estimated Inversion Strength (EIS, [Wood and Bretherton, 2006], map shown in Fig. 6b) as a measure of inversion strength. We thus also plot variables as composites as a function of EIS. To make such plots, we divide the EIS range from -1 K to 9 K into intervals of 0.5K. In each given interval, we average all seasonal-mean values at all locations over tropical oceans for which seasonal-mean EIS belongs to this interval (e.g. Fig. 10b will be an example). "

13) P. 13, L. 22: By how much (range of variability) were the four factors varied?

The four factors were varied from a control value to their simulated value.

Now we explain better the calculation with the contribution of r_{orig} as an example, and we give all equations for other contributions in Table 1. Section 3.6: "To understand what controls the δD_0 spatio-temporal variations, δD_0 is decomposed into 4 contributions based on Eq. (8). First, we define $r_{orig,bas} = 0.3$, $\alpha_{eff,bas} = 1.09$, SST_{bas}=25°C, $h_{0,bas} = 0.7$, $\phi_{bas} = 0$, $\eta_{bas} = 0$, $\beta_{bas} = 1$ and $\alpha_{evap,bas} = 1$ as a basic state. We call $\delta D_{0,func}(r_{orig}, \alpha_{eff}, SST, h_0, \phi, \beta, \eta, \alpha_{evap})$ the function giving δD_0 as a function of r_{orig}, α_{eff}, SST, h_0, ϕ, β, η and α_{evap} following Eq. (8), and $\delta D_{0,bas} = \delta D_{0,func}(r_{orig,bas}, \alpha_{eff,bas}, SST_{bas}, h_{0,bas}, \phi_{bas}, \beta_{bas}, \eta_{bas}, \alpha_{evap,bas})$. The relative contribution of r_{orig} to δD_0 is estimated as $\delta D_{0,func}(r_{orig}, \alpha_{eff,bas}, SST_{bas}, h_{0,bas}, \phi_{bas}, \beta_{bas}, \eta_{bas}, \alpha_{evap,bas}) - \delta D_{0,bas}$. Similarly, the contributions of α_{eff}, SST, h_0, ϕ and η are to δD_0 are estimated as detailed in Table 1. All the contributions have the same units as δD_0 (‰).".

14) P. 14, Section 4.1: This section seemed very technical for me. I also see it more as a methodological aspect than a result. I would recommend to either shift it to a technical appendix (since the paper is quite long) or to the methods section.

We have now shifted this section to the appendix D.2. We have deeply modified this section to address comments from you and the other reviewer.

15) P. 15, Fig. 7: Mention that these are different random (?) grid points in the caption. I would have liked a more general evaluation also describing the temporal and spatial variability in the vertical profiles simulation by LMDZ.

We have removed this figure, which was misleading, and replaced it by a more general documentation of the temporal and spatial variability in vertical profiles simulated by LMDZ, to address this comment and those from the other reviewer. This discussion is in appendix D: "LMDZ free tropospheric profiles". We add a figure showing maps of a parameter $f = \frac{\delta D_{LMDZ} - \delta D_{Rayleigh}}{\delta D_{mix} - \delta D_{Rayleigh}}$ at 1000 m and 4000 m, representing how close is the simulated δD compared to the Rayleigh and mixing lines (Fig. 16b,d). This documents the spatial variability in the shape of δD profiles. To document the temporal variability, we add maps of the standard deviation of f (Fig. 16c,e).

16) P. 15, L. 3: could the authors mention the region where they think that alphaeff may also reflect horizontal advection effects?

We now quantify the effect of horizontal advection on δD_0, i.e. in the SCL. However, the effect of horizontal advection on α_{eff} is a completely different subject that is beyond the scope of this paper. Therefore, we only reply based on the litterature: in appendix D: "The pattern of α_{eff} may also reflect horizontal advection effects, where strong isotopic gradients align with winds (e.g. from the Eastern to the Western Pacific, [Dee et al., 2018]). "

To clarify the scope of this paper, we start appendix D by stating: "The goal of this appendix is to document the spatio-temporal variability in the shape and steepness of simulated free tropospheric δD profiles. Note that a detailed interpretation of these profiles is beyond the scope of this paper. This paper aims at understanding δD_0, which is the first step towards understanding full tropospheric profiles. In turn, understanding full tropospheric profiles in future studies will help refine our model for δD_0."

17) P.16: I find it interesting that the mixing and Rayleigh lines have large biases in front of the eastern continental boundaries where the inversion is strongest and, where there is a strong decoupling between the FT and BL. In particular in these regions, I would expect horizontal advection to play a key role, (e.g. the SAL layer in front of the eastern North African Coast, see Lacour et al. 2017, ACP). Maybe the authors find a good way to shortly note this in the text.

The map showing RMS errors was misleading. For example, if the simulated δD behaves smoothly and is half-way between Rayleigh lines and mixing lines, it will result in local maxima in RMS values, but when we plot the new parameter $f = \frac{\delta D_{LMDZ} - \delta D_{Rayleigh}}{\delta D_{mix} - \delta D_{Rayleigh}}$, representing how close is the simulated δD compared to the Rayleigh and mixing lines, nothing special emerges. This is the case in front of the Saharan coast. Therefore, we have not added this discussion here.

However, this comment is relevant for interpreting horizontal advection effects on δD_0: "Horizontal advection is slightly enriching in deep convective regions and depleting in coastal regions (e.g. off the coasts of California, Peru, Mauritania, Namibia, India and Australia). For example, the Saharan layer in front of the North-Western African Coast lead to a strong effect of horizontal advection ([Lacour et al., 2017])."

18)P. 17, L. 2: Maybe one could add oceanic upwelling and atmospheric deep convection. Jumping from upwelling to deep convection in the same sentence, I was not sure whether deep convection in the ocean or the atmosphere was meant here.

We modify as suggested.

19) P. 17, L. 4: "Decreases as omega500 is more strongly ascending or descending" -> "with increasing vertical winds (omega500) of both signs"

We modify as suggested.

20) P. 17, L. 11: "in more ascending regions" -> a reference to Fig. 8d would have helped me here.

We add this reference

21) P. 17, L. 25: "The fact that the effect..." I had difficulties to understand this sentence.

We remove this sentence that was not so useful.

22) P. 17, L. 33: h_0 (62%) is the largest explained fraction of all the variables considered and should thus be put first. This could be a hint that large-scale horizontal advection plays an important role at the synoptic timescale in these regions.

The numbers have changed because (1) we now account for rain evaporation and horizontal advection, and (2) we now add an additional condition to make our calculation: section 3.1: "to avoid numerical problems when estimating effect of horizontal advection and rain evaporation, only grid boxes and days where $E > 0.5$ mm/d are considered. This represents 99.7% of all tropical oceanic grid boxes."

With the new values, the effect of h_0 is reduced and the effect of r_{orig} is enhanced (table 3). Section 4.1: "In subsiding regions, the effect of SST is muted due to its slow variability, and r_{orig} (82 %) becomes the main factor. "

23) P. 19, Fig. 10: The bin sizes (number of data points per bin should be added).

We now add this information in Fig 8, and we write in the caption: "The number of samples in each bin is indicated on a logarithmic scale on the right-hand-side (dotted black line)."

If I understood correctly from the caption, the authors used the seasonal averaged fields from LMDZ. Why not making these composites using the 6-hourly outputs? For me there is a timescale discrepancy between the processes (mixing, evaporation) that the authors look at and the averaging timescale of the used fields.

The composites are based on seasonal-mean EIS or ω_{500} because this allows a better link with the large-scale dynamical regime. Mixing and evaporation are processes that act at short time scales, but their relationship to the large-scale circulation is best constrained by energetics at time scales longer than synoptic. Let's consider $\omega_{500,}$ for example. It relates to convective activity and other diabatic processes through the conservation equation of moist static energy. Adiabatic cooling by large-scale ascent balances latent heating by convection ([Yanai et al., 1973]), or adiabatic heating by large-scale subsidence balances radiative cooling ([Emanuel et al., 1994]). The stationarity in the conservation of moist static equation is most valid at time scales longer than synoptic, otherwise, the storage term becomes important ([Masunaga and Sumi, 2017]). This is why in [Bony et al., 2004] and subsequent papers (e.g. [Bony et al., 2013]) based on ω_{500}, monthly-mean ω_{500} is used, which yields similar results to seasonal-mean.

A similar rationale applies to EIS. This is why many papers on EIS use seasonal-mean values, notably the paper defining this quantity ([Wood and Bretherton, 2006]).

We now explain this in section 3.5: "Note that such composites are done on seasonal-mean ω_{500} because cloud processes and their associated diabatic heating are tied to the large-scale circulation through energetic constrains ([Yanai et al., 1973, Emanuel et al., 1994]) that are best valid at longer time scales (otherwise, the energy storage term may become significant, e.g. [Masunaga and Sumi, 2017]). This is why ω_{500} is generally averaged over a month or longer (e.g. [Bony et al., 1997, Williams et al., 2003, Bony et al., 2004, Wyant et al., 2006, Bony et al., 2013]). In addition, we primarily focus on understanding the seasonal and spatial distribution of δD_0."

and for EIS: "Using seasonal-mean values is consistent with [Wood and Bretherton, 2006] and with the better link at longer time scales between cloud processes and the large-scale dynamical regime.".

In addition, we do not look at the diurnal variations: the stationarity assumption in our simple model would be violated. We now explain this in the abstract: "the steady-state assumption restricts the application of this model to time scales longer than daily." and in section 2.1: "We assume that the SCL is at steady state. For example, its depth is constant. Since the SCL properties may exhibit a diurnal cycle ([Duynkerke et al., 2004]), this hypothesis restricts the application of this model to time scales longer than daily. "

24) P. 27, L. 28: a reference to a more technical paper such as Aemisegger et al. 2012 AMT, would be nice here.

We add this reference

Small technical comments:

1) P. 2, L. 22 : "suffers **from** a low bias"

2) P. 3, L. 28: “capturing **the** second-order...”
3) P. 8, L. 26: no parenthesis after B)
4) P. 12, L.7: “based” -> “biased”
5) P. 15, L . 1: Figure 8d
6) P. 15, L. 4: “Values **of** alphaeff...”
7) P. 15, L. 5: using a fractionation coefficient alpha eq **as** a function of temperature”
8) P. 17, L. 14: space missing between rorig and (
9) P. 18, L. 1: “Overall, **the** results...”
We correct all these mistakes.
10) In general, the authors do not consistently use B15 for Benetti et al. (2015)
We now use B15 consistently.

11) P. 21, L. 2: “with **the** strongest inversion”
12) P. 27, L. 27: measurement errors
13) P. 28, L. 2: “if **we** measure...”
14) P. 29, L. 14: very precise
15) P. 30, L. 11: **from** which altitude the air comes
We correct all these mistakes.

2 Reviewer 2

We thank reviewer 2 for his/her comments.

This paper presents a simple box model solving the water isotope budget in the sub-cloud layer to quantify the relative contributions of sea surface temperature, relative humidity, mid-tropospheric depletion, and the fraction of moisture from the free troposphere (rorig) on the variability of δD in near-surface water vapor (δD_0). The contribution of r_{orig} is further separated into contributions of specific humidity at the surface, and the height (z_{orig}), relative humidity and temperature from which the free tropospheric air originates. Zorigis found to be an important factor explaining the seasonal-spatial and daily variations of δD_0. This means that measurements of Dδ0, if precise enough, can potentially be used to estimate z_{orig} and distinguish between different mixing processes in the atmosphere.

The paper is interesting and well written, and it nicely demonstrates the use of measuring water vapor isotopes on short time scales. The box model's theoretical framework is describedin detail and its drawbacks are clearly identified by the authors. I only have a few comments about the methods, the rest are mainly ideas for clarifying the paper. I recommend that the paper be published after minor revisions.

General comments

1) I like the method for quantifying the contributions of different factors by linear regression. I see how this works when the contributing factors have the same units as the variable of interest, which was the case in the previous studies that used this method and are cited in this paper (Risi et al. 2010, Oueslati et al., 2016). Here the different factors all have different units, and the slope therefore depends on the units, or how much the components vary. I assume this was accounted for somehow, as the slopes in the tables are all unitless, but it is not clear from the text, and makes me a bit skeptical about the results. More explanation on that would be useful.

The contributing factors have the same units as the variable of interest, i.e. permil. We now clarify this in the text. We also explain better the calculation with the contribution of r_{orig} as an example, and we give all equations for other contributions in Table 1. Section 3.6: “To understand what controls the δD_0 spatio-temporal variations, δD_0 is decomposed into 4 contributions based on Eq. (8). First, we define $r_{orig,bas} = 0.3$, $\alpha_{eff,bas} = 1.09$, SST_{bas}=25°C, $h_{0,bas} = 0.7$, $\phi_{bas} = 0$, $\eta_{bas} = 0$, $\beta_{bas} = 1$ and $\alpha_{evap,bas} = 1$ as a basic state. We call $\delta D_{0,func}(r_{orig}, \alpha_{eff}, SST, h_0, \phi, \beta, \eta, \alpha_{evap})$ the function giving δD_0 as a function of r_{orig}, α_{eff}, SST, h_0, ϕ, β, η and α_{evap} following Eq. (8), and $\delta D_{0,bas} = \delta D_{0,func}(r_{orig,bas}, \alpha_{eff,bas}, SST_{bas}, h_{0,bas}, \phi_{bas}, \beta_{bas}, \eta_{bas}, \alpha_{evap,bas})$. The relative contribution of r_{orig} to δD_0 is estimated as $\delta D_{0,func}(r_{orig}, \alpha_{eff,bas}, SST_{bas}, h_{0,bas}, \phi_{bas}, \beta_{bas}, \eta_{bas}, \alpha_{evap,bas}) - \delta D_{0,bas}$. Similarly, the contributions of α_{eff}, SST, h_0, ϕ and η are to δD_0 are estimated as detailed in Table 1. All the contributions have the same units as δD_0 (‰).”.

2) As stated in the paper, the methods rely on the assumption that the δD profile follows a Rayleigh-like line, and that there is no effect of rain evaporation. Figures 7 and 8 show that the δD profile is often closer to a mixing line than a Rayleigh line, and the large contribution of r_{orig} mainly comes from ascending regions, where clouds are most likely precipitating. It would be nice to see some quantification of how this impacts the results. A possible way to do this is to remove days/locations where the RMSE of the mixing line is smaller than the RMSE of the Rayleigh line and where there is precipitation, then repeat the analysis for these new fields and add the results in brackets in Tables 1, 2 and as dotted lines in Figures 10, 12.

- Effect of rain evaporation. Now we explicitly account for the effect of rain evaporation. Equations are given in the main text. The contributions of this effect are plotted as maps in Fig. 7g, and as composites as a function of ω_{500} and EIS in Fig. 8. Table 2 compares the effect of r_{orig} if rain evaporation and horizontal advection are neglected or not. The effect of rain evaporation on z_{orig} estimates are plotted in Fig. 14b.
- Effect of the deviation of the δD profile from a Rayleigh distillation line. This is more difficult to quantify. Now we discuss this in detail in the discussion section: subsection 6.5 untitled "Rayleigh assumption for the shape of δD profiles": "Finally, a fifth source of uncertainty comes the assumption that the δD profile follows a Rayleigh distillation line (section 2.2). However, both in LMDZ (appendix D) and nature ([Sodemann et al., 2017]), δD profiles are usually intermediate between Rayleigh and mixing lines. The precision of our z_{orig} estimate is maximum in the Rayleigh distillation case. When trying to directly find a numerical solution for z_{orig} from Eq. (6), a solution can be found only in 0.1 % of cases. This is because... However, it is possible that δD profiles simulated by LMDZ are closer to mixing lines than real profiles, since GCMs are known to overestimate vertical mixing through the troposphere ([Risi et al., 2012]) and to mix the lower free troposphere too frequently by deep convection in trade-wind regions ([Nuijens et al., 2015b, Nuijens et al., 2015a]). Therefore, the shape of δD profiles simulated by LMDZ is not a sufficient reason to reject the Rayleigh assumption. The uncertainty associated with this assumption is very difficult to quantify in LMDZ. More measurements of full δD profiles are very welcome to help quantify it."

3) The paper presents the new box model as an extension of the model by Benetti et al. (2015), which is technically true, but can be a bit misleading because its application is different. Rather than predicting δD_0 from zorig, it predicts z_{orig} from δD_0 and therefore requires δD_0 to be known. This means it cannot be applied to initialize Rayleigh models like the model by Benetti et al. (2015), which assumes constant zorig. This could be written more clearly (e.g., from the abstract it seems like the model can be used to predict δD_0, which is only possible if z_{orig} is known).

The model can be used both ways, either to predict δD_0 as a function of z_{orig}, or to estimate z_{orig} from δD_0. We now clarify this:

- in the abstract: "The model express δD_0 as a function of z_{orig}, humidity and temperature profiles, surface conditions a parameter describing the steepness of the δD vertical gradient and a few parameters describing rain evaporation and horizontal advection effects. ".
- in section 2.2: "If the goal is to predict R_0 from z_{orig} , we can apply Eq. (6) if we know the q and δD vertical profiles. Conversely, if the goal is to predict z_{orig} from R_0, we can numerically solve Eq. (6) if we know the q and δD vertical profiles.".

4) Changing some of the colors and colormaps could make the figures easier to understand. For example, I think the contributions of different factors and how they add up in Figures 9 and 11 would be more intuitive with a perceptually uniform colormap going from light to dark colors. Also, the red and pink lines in Figures 3, 4, 7, 10, 12, 15 look very similar to each other. It would be good to use a different color for one of them.

- Now all maps are colored in shaded of blue for negative values and shaded of red for positive values.
- We now change the line color from pink to purple to distinguish it from red (Figures 3, 4, 5), or from red to dark red to distinguish it from pink (Figures 8, 10, 13).

Specific comments

P1 L13: [D]/[H] instead of [HDO]/[H2O]

We modify.

P2 L22: high bias instead of low bias?

Corrected.

P2 L30: Please introduce the abbreviation for LCL

Done.

P3 L4: pointed **out** the important role

Corrected.

P3 L15: "We do not call it entrained": The word entrained/entrainment still appears a few times in the text (e.g. in Fig. 2, the title of section 4.4)

We modify all the occurences of "entrainment", except when it really refers to entrainment.

P3 L23: during **a** field campaign, global outputs **of** an isotope-enabled GCM.

Corrected.

P3 L24: "at the global scale": Really? There are no global maps. Are the numbers in Tables 1, 2 and the lines in Figures 10, 12 from global output, or from the region shown on the maps?

We now modify by "in the Tropics". We precise in the captions for these Tables and Figures: "All seasons and locations over tropical oceans ($30°N - 30°S$, ocean fraction>80%) are considered."

P3 L28: capturing **the** second-order parameter d-excess

Corrected.

P3 L32: "MJ79 already performs quite well for d-excess": Pfahl and Wernli (2009) would probably disagree.

Now we modify as (section 1.3): "In addition, the need for an extension of MJ79 is more needed for δD than for d-excess, since the effect of convective mixing is larger on δD than on d-excess ([Risi et al., 2010, Benetti et al., 2014])."This does not contradict Pfahl and Wernli (2009).

P5 L23: r $\rightarrow r_{orig}$

Corrected.

P6 L20: measurement**s**

Corrected.

P6 L20: "Therefore, variations of δD_0 that are mediated by q_0 or h_0 do not interest us": But δD in the FT is prescribed as a function of q (confusing).

We remove this confusing sentence and we write (section 2.1): "We attempt to express neither h_0 as a function of q_0 as in B15, and nor the q profile as a function of q_0".

P8 L11: Refer to l'Hopital's rule?

Now we add: "(L'Hopital's rule was used to calculate this limit)." (section 2.2°

P8 L21: follows a**s** mixing line

Corrected.

P9: Fig.3: $\alpha_{eff} = \alpha_{eq}$ instead of $\alpha_{eff} = 1/\alpha_{eq}$

Corrected.

P11 L25: "Only profiles during the ascending phase of the balloons are considered": (Why?)

We now justify this choice: “Only profiles during the ascending phase of the balloon are considered, because the descent phase is often located far away from the initial launch point ([McGrath et al., 2006, Seidel et al., 2011]). “ (section 3.2)

P11 L27 (title): write somewhere that these results are based on LMDZ output (not observations)

Now we write (section 3.3): “Here we explain how z_{orig} is estimated based on LMDZ outputs.”. Later in the section, we write: “When estimating z_{orig} from observations, we follow the same methodology except that...”.

P12 Fig. 5: Describe abbreviations (LCL, EIS, SCL) in caption.

Done

P12 L2: “if the end member is defined below 500hPa (e.g. 600hPa) results are not always reasonable”: In what sense? Why?

Now we write: “However, the end member should be defined above 500 hPa to ensure that it is well above boundary layer processes. If the end member is defined below 500 hPa (e.g. 600 hPa), there are cases where q increases with altitude ($q_f > q_0$) due to horizontal advection or convective detrainment from nearby moister regions; meanwhile, δD decreases monotically, leading to unrealistic values for α_{eff}.”

P15 Fig. 7: What meteorological conditions do these examples represent? Would it be possible to show all (/more) simulated profiles in the background, e.g. in some transparent color, to get a better feeling for the variability? Also, I suggest adding markers to highlight where the levels are.

We have removed this figure, because it was misleading. We replace it by Fig. 16 in appendix D to better document the temporal and spatial variability in free tropospheric profiles. Maps show parameter $f = \frac{\delta D_{LMDZ} - \delta D_{Rayleigh}}{\delta D_{mix} - \delta D_{Rayleigh}}$ describing whether simulated δD is closer to Rayleigh line or a mixing line (Fig 16b,d). We also show maps for the standard deviation of f to illustrate the temporal variability (Fig 16 c,e).

In addition, markers are added in Fig 16a to highlight the model levels.

P15 L1: Figure 8d instead of 8c.

Corrected

P15 L5: α_{eq} **as** a function of temperature

Corrected

P16 Fig. 8: in **boreal** winters of all years

Corrected

P17 L22: “in the cold upwelling regions”: for example where?

Now we add: “cold upwelling regions, for example off Peru or Namibia” (section 4.1)

P17 L23: probably reflect**s**

This sentence was removed because r_{orig} cannot reflect rain evaporation any more.

P17 L24: “the effect of r_{orig} can be seen on the composites as a function of EIS and not as a function of ω_{500} ”: I don’t see this, please elaborate.

This sentence was removed.

P17 L30: followed by h_0 **(23%)**, r_{orig} (16%), ...

Corrected

P18 Fig. 9: Are the correlations significant everywhere? Otherwise, add hatching where not significant?

In this figure (now Fig. 7), we do not show the correlations, but rather the contributions to δD_0 on a ‰ scale. We now explain better in the text how these contributions are calculated (section 3.6), and we add table 1 to give the exact equations used to calculate each contribution.

The spatial-seasonal correlations are shown in Table 2. We now write between brackets when correlations are not statistically significant at 99%. We write in the caption: "The threshold for the correlation coefficient to be statistically significant at 99 % is 0.15 or lower in all cases. We write correlation coefficient and slope values between brackets when they are not significant at 99%."

P19 Fig.10: ω_{500} (hPa/**d**)
Corrected

P20 Tab. 2: q_0 seems to be important in Fig. 12, but the slope is 0.0 here, h_0 seems to be unimportant in Fig. 12 but slope is 0.91 here. Why is that?
We now explain this: section 4.2: "Note that this effect can be seen only in most stable regions, but when considering all subsiding regions, the contribution is small (Table 2). "

P20 L1: "it would translate into a lower zorig.": Why?

For example, in case of deep convection with depleting rain evaporation, a larger r_{orig} is necessary to match the depleted δD_0, and a lower z_{orig} is necessary to match this large r_{orig}.
Now this sentence is removed, since we explicitely account for rain evaporation and horizontal advection. We do not need this kind of rationale any more.

P22 Fig.12: ω_{500}(hPa/d)
Corrected

P25 L6: the cruises goes
Corrected

P25 L8: "when considering only the 6 data points when $z_{orig} < 2000$m": Rationale behind this?

We now clarify what we mean: section 5: "Remarkably, there are 6 days when z_{orig} coincides with z_i with a root means square error of 31‰ and correlation coefficient of 0.996 (Fig. 15c). This indicates that the air exactly comes from the inversion layer. When recalling that z_{orig} and z_i are estimated from completely independent observations, the coincidence is remarkable and lends support to the fact that on these days, our z_{orig} estimate is physical. However, there remains 9 days when z_{orig} is much higher than z_i. This may reflect more penetrative downdrafts as we approach deeper convective regimes. But it may also be an artifact of our neglect of horizontal advection. For example, on these days which are characterized by lower h_0, neglecting the advection of enriched water vapor from nearby regions with higher h_0 could be mis-interpreted as lower r_{orig} and thus higher z_{orig}. ".

P25 L14: ... at the seasonal-spatial and daily scale is the proportion of the water vapor in the SCL that is originates from above
Corrected

P26 Fig. 15: r $\rightarrow$ r_{orig}
Corrected

P27 L1: there $\rightarrow$ they
Corrected

P27 L13: the **temporal** variability of α_{eff}. Is it possible to estimate the uncertainty from the spatial variability of α_{eff} as well (in the vertical, i.e. how much the δ profile differs from a Rayleigh line with constant α_{eff})?

We now better document the spatio-temporal variability in the shape of free tropospheric δD profiles in the appendix D.1. To address this specific comment, we now plot parameter $f = \frac{\delta D_{LMDZ} - \delta D_{Rayleigh}}{\delta D_{mix} - \delta D_{Rayleigh}}$ describing whether simulated δD is closer to Rayleigh line or a mixing line. We show vertical profiles and maps of f at both 1000 m and 4000 m (Fig 16 b,d).
We tried to compare the z_{orig} estimate with and without the assumption that the δD profile follows a Rayleigh line. However, it didn't work as well as expected. We now explain this when examining all errors on z_{orig} (section

6.5): "When trying to find a numerical solution for z_{orig} directly from Eq. (6), a solution can be found only in 0.1 % of cases.". We explain why, and we also explain why it may work better in nature.

P27 L21: estimating z_{orig} from δD_0measurements **on a daily basis** (?)

Now we write: "estimating z_{orig} from daily δD_0 measurements cannot be useful unless we measure δD profiles on a daily basis as well."

P28 L2: and if **we** measure
Corrected

P28 L3: swap trade-wind cumulus and strato-cumulus clouds
Corrected

P29 L14: very precise**d** estimates
Corrected

P29 L18: the altitude from which the air **is** originates, and is not **to** biase**d** by
Corrected

References

[Benetti et al., 2014] Benetti, M., Reverdin, G., Pierre, C., Merlivat, L., Risi, C., and Vimeux., F. (2014). Deuterium excess in marine water vapor: Dependency on relative humidity and surface wind speed during evaporation. *J. Geophys. Res*, 119:584–593, DOI: 10.1002/2013JD020535.

[Bony et al., 2013] Bony, S., Bellon, G., Klocke, D., Sherwood, S., Fermepin, S., and Denvil, S. (2013). Robust direct effect of carbon dioxide on tropical circulation and regional precipitation. *Nature Geoscience*, 6(6):447–451.

[Bony et al., 2004] Bony, S., Dufresne, J.-L., Le Treut, H., Morcrette, J.-J., and Senior, C. (2004). On dynamic and thermodynamic components of cloud changes. *Climate Dynamics*, 22:71–86.

[Bony et al., 1997] Bony, S., Lau, K., and Sud, Y. (1997). Sea surface temperature and large-scale circulation influences on tropical greenhouse effect and cloud radiative forcing. *Journal of Climate*, 10(8):2055–2077.

[Dee et al., 2018] Dee, S. G., Nusbaumer, J., Bailey, A., Russell, J. M., Lee, J.-E., Konecky, B., Buenning, N. H., and Noone, D. C. (2018). Tracking the strength of the walker circulation with stable isotopes in water vapor. *Journal of Geophysical Research: Atmospheres*, 123(14):7254–7270.

[Duynkerke et al., 2004] Duynkerke, P. G., de Roode, S. R., van Zanten, M. C., Calvo, J., Cuxart, J., Cheinet, S., Chlond, A., Grenier, H., Jonker, P. J., Köhler, M., et al. (2004). Observations and numerical simulations of the diurnal cycle of the eurocs stratocumulus case. *Quarterly Journal of the Royal Meteorological Society: A journal of the atmospheric sciences, applied meteorology and physical oceanography*, 130(604):3269–3296.

[Emanuel et al., 1994] Emanuel, K., Neelin, D., and Bretherton, C. (1994). On large-scale circulations in convecting atmospheres. *Quaterly Journal of the Royal Meteorological Society*, 120:1111–1143.

[Garratt, 1994] Garratt, J. R. (1994). The atmospheric boundary layer. *Earth-Science Reviews*, 37(1-2):89–134.

[Lacour et al., 2017] Lacour, J.-L., Flamant, C., Risi, C., Clerbaux, C., and Coheur, P.-F. (2017). Importance of the saharan heat low in controlling the north atlantic free tropospheric humidity budget deduced from iasi δd observations. *Atmospheric Chemistry and Physics*, 17:9645–9663.

[Masunaga and Sumi, 2017] Masunaga, H. and Sumi, Y. (2017). A toy model of tropical convection with a moisture storage closure. *Journal of Advances in Modeling Earth Systems*, 9(1):647–667.

[McGrath et al., 2006] McGrath, R., Semmler, T., Sweeney, C., and Wang, S. (2006). Impact of balloon drift errors in radiosonde data on climate statistics. *Journal of climate*, 19(14):3430–3442.

[Nuijens et al., 2015a] Nuijens, L., Medeiros, B., Sandu, I., and Ahlgrimm, M. (2015a). The behavior of trade-wind cloudiness in observations and models: The major cloud components and their variability. *Journal of Advances in Modeling Earth Systems*, 7(2):600–616.

[Nuijens et al., 2015b] Nuijens, L., Medeiros, B., Sandu, I., and Ahlgrimm, M. (2015b). Observed and modeled patterns of covariability between low-level cloudiness and the structure of the trade-wind layer. *Journal of Advances in Modeling Earth Systems*, 7(4):1741–1764.

[Oke, 1988] Oke, T. R. (1988). *Boundary layer climates.* Halsted press, New York.

[Risi et al., 2010] Risi, C., Landais, A., Bony, S., Masson-Delmotte, V., Jouzel, J., and Vimeux, F. (2010). Understanding the 17O-excess glacial-interglacial variations in Vostok precipitation. *J. Geophys. Res*, 115, D10112:doi:10.1029/2008JD011535.

[Risi et al., 2012] Risi, C., Noone, D., Worden, J., Frankenberg, C., Stiller, G., Kiefer, M., Funke, B., Walker, K., Bernath, P., Schneider, M., Wunch, D., Sherlock, V., Deutscher, N., Griffith, D., Wernberg, P., Bony, S., Lee, J., Brown, D., Uemura, R., and Sturm, C. (2012). Process-evaluation of tropical and subtropical tropospheric humidity simulated by general circulation models using water vapor isotopic observations. Part 2: an isotopic diagnostic of the mid and upper tropospheric moist bias. *J. Geophy. Res.*, 117:D05304.

[Seidel et al., 2010] Seidel, D. J., Ao, C. O., and Li, K. (2010). Estimating climatological planetary boundary layer hheight from radiosonde observations: comparison of methods and uncertainty analysis. *J. Geophy. Res.*, 115, D16113.

[Seidel et al., 2011] Seidel, D. J., Sun, B., Pettey, M., and Reale, A. (2011). Global radiosonde balloon drift statistics. *Journal of Geophysical Research: Atmospheres*, 116(D7).

[Siebert et al., 2000] Siebert, P., Beyrich, F., Gryning, S. E., Joffre, S., and Rasmussen, A. (2000). Review and intercomparison of operational methods for the determination of the mixing height. *Atmos. Environ.*, 34:1001–1027.

[Sodemann et al., 2017] Sodemann, H., Aemisegger, F., Pfahl, S., Bitter, M., Corsmeier, U., Feuerle, T., Graf, P., Hankers, R., Hsiao, G., Schulz, H., et al. (2017). The stable isotopic composition of water vapour above corsica during the hymex sop1 campaign: insight into vertical mixing processes from lower-tropospheric survey flights. *Atmospheric Chemistry and Physics*, 17(9):6125–6151.

[Sorbjan, 1989] Sorbjan, Z. (1989). *Structure of the atmospheric boundary layer.* Prentice Hall, Englewood Cliffs, N. J.

[Stull, 1988] Stull, R. B. (1988). *An intruduction to boundary layer meteorology.* Dordrect Kluwer.

[Williams et al., 2003] Williams, K., Ringer, M., and Senior, C. (2003). Evaluating the cloud response to climate change and current climate variability. *Climate Dynamics*, 20(7-8):705–721.

[Wood and Bretherton, 2006] Wood, R. and Bretherton, C. S. (2006). On the relationship between stratiform low cloud cover and lower-tropospheric stability. *Journal of climate*, 19(24):6425–6432.

[Wyant et al., 2006] Wyant, M. C., Bretherton, C. S., Bacmeister, J. T., Kiehl, J. T., Held, I. M., Zhao, M., Klein, S. A., and Soden, B. J. (2006). A comparison of low-latitude cloud properties and their response to climate change in three agcms sorted into regimes using mid-tropospheric vertical velocity. *Climate Dynamics*, 27:261–279.

[Yanai et al., 1973] Yanai, M., Esbensen, S., and Chu, J.-H. (1973). Determination of bulk properties of tropical cloud clusters from large-scale heat and moisture budgets. *Journal of the Atmospheric Sciences*, 30(4):611–627.

Controls on the water vapor isotopic composition near the surface of tropical oceans and role of boundary layer mixing processes

Camille Risi[1], Joseph Galewsky[2], Gilles Reverdin[3], and Florent Brient[4]

[1]Laboratoire de Météorologie Dynamique, IPSL, CNRS, Sorbonne Université, Paris, France
[2]Department of Earth and Planetary Sciences, University of New Mexico, Albuquerque, USA
[3]Sorbonne Université, CNRD/IRD/MNHN, LOCEAN, IPSL, Paris, France
[4]CNRM, Université de Toulouse, Météo-France, CNRS, Toulouse, France

Correspondence: Camille Risi (Camille.Risi@lmd.jussieu.fr)

Abstract. Understanding what controls the water vapor isotopic composition of the sub-cloud layer (SCL) over tropical oceans (δD_0) is a first step towards understanding the water vapor isotopic composition everywhere in the troposphere. We propose an analytical model to predict δD_0 ~~as a function of sea surface conditions, humidity and temperature profiles, and the~~ motivated by the hypothesis that the altitude from which the free tropospheric air originates (z_{orig}) ~~. To do so, we extend previous studies by (1)~~ is an important factor: when the air mixing into the SCL is lower in altitude, it is generally moister, and thus it depletes more efficiently the SCL. We extend previous simple box models of the SCL by prescribing the shape of δD vertical profiles ~~, and (2) linking δD_0 to z_{orig}~~ as a function of humidity profiles and by accounting for rain evaporation and horizontal advection effects. The model relies on the ~~hypotheses~~ assumption that δD profiles are steeper than mixing lines~~and no clouds are precipitating.~~ , and that the SCL is at steady state, restricting its applications to time scales longer than daily. The model express δD_0 as a function of z_{orig}, humidity and temperature profiles, surface conditions, a parameter describing the steepness of the δD vertical gradient and a few parameters describing rain evaporation and horizontal advection effects. We show that δD_0 does not depend on the intensity of entrainment, dampening hope that δD_0 measurements could help constrain this long-searched quantity.

Based on an isotope-enabled general circulation model simulation, we show that δD_0 variations are mainly controlled by mid-tropospheric depletion and rain evaporation in ascending regions, and by sea surface temperature and z_{orig} in subsiding regions. ~~When the air mixing into the SCL is lower in altitude, it is moister, and thus it depletes more efficiently the SCL.~~

In turn, could δD_0 measurements help estimate z_{orig} and thus discriminate between different mixing processes? ~~Estimates that are accurate enough~~ For such isotope-based estimates of z_{orig} to be useful~~would be difficult to achieve in practice, requiring measuring daily~~ , we would need a precision of a few hundreds meters in deep convective regions and smaller than 20 m in strato-cumulus regions. To reach this target, we would need daily measurements of δD ~~profiles, and measuring~~ in the mid-troposphere and accurate measurements of δD_0 ~~with an accuracy of~~ (accuracy down to 0.1 ‰ ~~and 0.4 ‰ in trade-wind cumulus and~~ in the case of strato-cumulus clouds, which is currently difficult to obtain). We would also need information on the horizontal distribution of δD to account for horizontal advection effects, and full δD profiles to quantify the uncertainty associated with the assumed shape for δD profiles. Finally, rain evaporation is an issue in all regimes, even in strato-cumulus clouds~~respectively.~~ . Innovative techniques would need to be developed to quantify this effect from observations.

Copyright statement.

1 Introduction

1.1 What controls the water vapor isotopic composition?

The water vapor isotopic composition (e.g. $\delta D = (R/R_{SMOW} - 1) \times 1000$ expressed in ‰, where ~~$R = HDO/H_2O$~~ R is the D/H ratio and SMOW is the Standard Mean Ocean Water reference) has been shown to be sensitive to a wide range of atmospheric processes (Galewsky et al., 2016), such as continental recycling (Salati et al., 1979; Risi et al., 2013), unsaturated downdrafts (Risi et al., 2008, 2010a), rain evaporation (Worden et al., 2007; Field et al., 2010), the degree of organization of convection (Lawrence et al., 2004; Tremoy et al., 2014), the convective depth (Lacour et al., 2017b), the proportion of precipitation that occurs as convective or large-scale precipitation (Lee et al., 2009; Kurita, 2013; Aggarwal et al., 2016), vertical mixing in the lower troposphere (Benetti et al., 2015; Galewsky, 2018a, b), mid-troposphere (Risi et al., 2012b) or upper-troposphere (Galewsky and Samuels-Crow, 2014), convective detrainment (Moyer et al., 1996; Webster and Heymsfield, 2003), ice microphysics (Bolot et al., 2013). It is therefore very challenging to quantitatively understand what controls the isotopic composition of water vapor.

A first step towards this goal is to understand what controls the water vapor isotopic composition in the sub-cloud layer (SCL) of tropical (30°S-30°N) oceans. Indeed, this water vapor is ~~a~~ an important source moistening air masses traveling to land regions (Gimeno et al., 2010; Ent and Savenije, 2013) and towards higher latitudes (Ciais et al., 1995; Delaygue et al., 2000). It is also ultimately the only source of water vapor in the tropical free troposphere, since water vapor in the free troposphere ultimately originates from convective detrainment (Sherwood, 1996), and convection ultimately feeds from the SCL air (Bony et al., 2008). Therefore, the water vapor isotopic composition in the SCL of tropical oceans serves as initial conditions to understand the isotopic composition in land waters and in the tropospheric water vapor everywhere on Earth. We focus here on the SCL because, by definition, there is no complication by cloud condensation processes.

The goal of this paper is thus to propose a simple analytical equation that allows us to understand and quantify the factors controlling the δD in the water vapor in the SCL of tropical oceans. So far, the most famous analytical equation for this purpose has been the closure equation developed by ~~Merlivat and Jouzel (1979)~~ Merlivat and Jouzel (1979) (MJ79). This closure equation can be derived by assuming that all the water vapor in the SCL air originates from surface evaporation. The water balance of the SCL can be closed by assuming a mass export at the SCL top (e.g. by convective mass fluxes) and a totally dry entrainment into the SCL to compensate this mass export. The MJ79 equation has proved very useful to capture the sensitivity of δD and second-order parameter d-excess to sea-surface conditions ~~(Merlivat and Jouzel, 1979; Ciais et al., 1995; Risi et al., 2010d)~~ Merlivat and Jouzel (1979); Ciais et al. (1995); Risi et al. (2010d). However, the δD calculated from this equation suffers ~~a low~~ from a high bias in tropical regions ~~(Jouzel and Koster, 1996)~~Jouzel and Koster (1996). This bias can be explained by the neglect of vertical mixing between the SCL and air entrained from the free troposphere (FT). The MJ79 equation can better reproduce surface water vapor observation when extended to take into account this mixing ~~(Benetti et al., 2015)~~(Benetti et al. (2015), hereafter B15). ~~However, this~~ This extension requires to know the specific humidity (q) and water vapor δD of the entrained air~~, which are often unknown. In addition, they assumed~~ . To get these values, they assume that the air entrained into the boundary layer comes from a constant altitude~~, which does not reflects~~ . However, this does not reflect the complexity of entrainment and mixing processes in marine boundary layers.

1.2 Entrainment and mixing mechanisms

Figure 1 summarizes our knowledge about these entrainment and mixing processes. In strato-cumulus regions, clouds are thin and the inversion is just above the ~~LCL~~lifting condensation level (LCL). Air is entrained from the FT by cloud-top entrainment driven by radiative cooling or wind shear instabilities (Mellado, 2017), possibly amplified by evaporative cooling of droplets (Lozar and Mellado, 2015). Both Direct Numerical Simulations (Mellado, 2017) and observations of tracers (Faloona et al., 2005) and cloud holes (Gerber et al., 2005) show that air is entrained from a thin layer above the inversion, thinner than 80m and as small as 5m. The boundary layer itself is animated by updrafts, downdrafts and associated turbulent shells that bring air from the cloud layer downward (Brient et al., 2019; Davini et al., 2017).

In trade-wind cumulus regions, the cloudy layer is a bit deeper. Observational studies and large-eddy simulations have pointed out the important role of thin subsiding shells around cumulus clouds, driven by cloud-top radiative cooling, mixing and evaporative cooling of droplets (Jonas, 1990; Rodts et al., 2003; Heus and Jonker, 2008; Heus et al., 2009; Park et al., 2016). This brings air from the cloudy layer to the SCL. Subsiding shells may also cover overshooting plumes of the cumulus clouds, entraining FT air into the cloud layer (Heus and Jonker, 2008).

In deep convective regions, unsaturated downdrafts driven by rain evaporation (Zipser, 1977) are known to contribute significantly to the energy budget of the SCL (Emanuel et al., 1994). Large-eddy simulations show that subsiding shells, similar to those documented in shallow convection, also exist around deep convective clouds (Glenn and Krueger, 2014). In the clear-sky environment between clouds, turbulent entrainment into the SCL may also play a significant role (Thayer-Calder and Randall, 2015).

Therefore, whatever the cloud regime, air entering the SCL from above may originate either from the cloud layer or from the free troposphere, depending on the mixing mechanism. Therefore, in this paper in contrast with ~~Benetti et al. (2015)~~ Benetti et al. (2015), we let the altitude from which the air originates, z_{orig}, be variable. We do not call it “entrained” air because entrainment sometimes refer to mixing processes through an interface (e.g. ~~De Rooy et al. (2013); Davini et al. (2017)~~ De Rooy et al. (2013); Davini et al. (2017)), whereas air in the SCL may also enter through deep, coherent and penetrative structures such as unsaturated downdrafts. We do not call it FT air either, since it may originate from the cloudy layer.

1.3 Goal of the article

To acknowledge the diversity and complexity of mixing mechanisms, we extend the B15 framework in ~~two~~ several ways. First, we assume that we know the ~~relationship between~~ shape of δD ~~and~~ profiles as a function of q~~in the FT, which allows us to get rid of one unknown~~. Second, we write the specific humidity of the air originating from above the SCL as a function of z_{orig}. Third, we account for rain evaporation and horizontal effects.

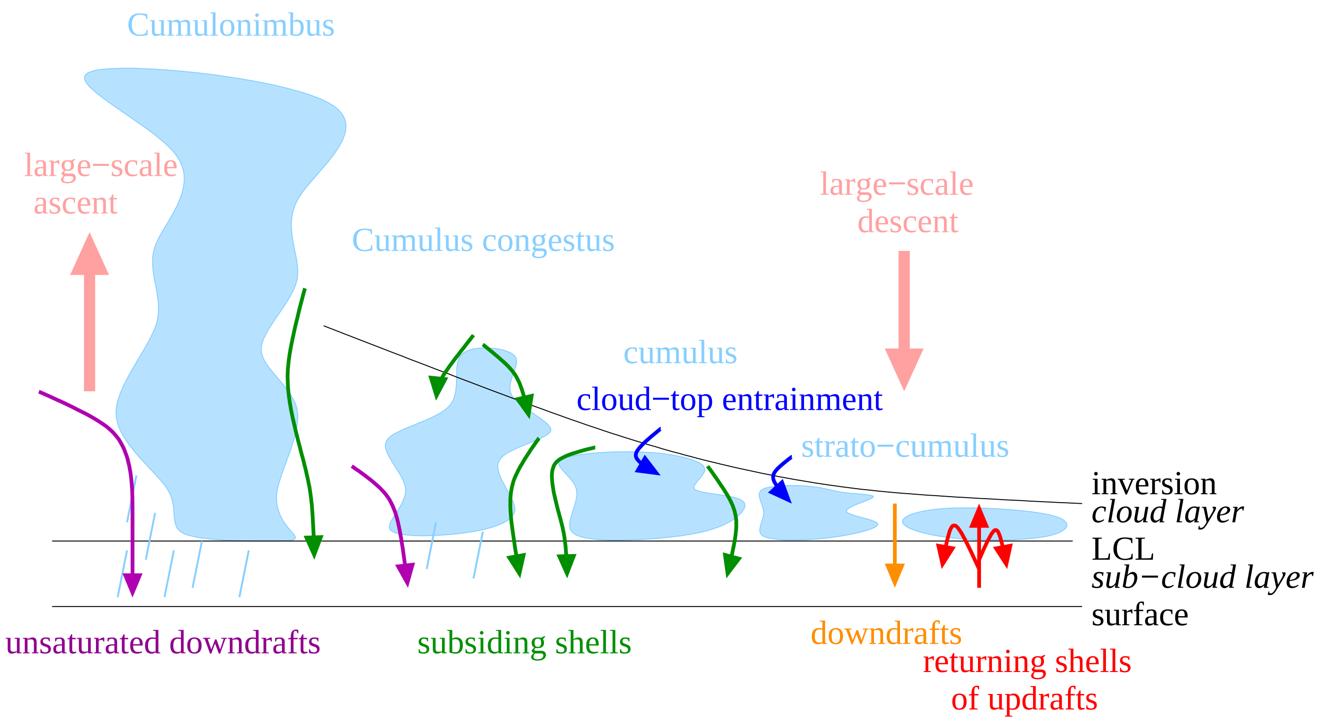

Figure 1. Schematics showing the different types of clouds and mixing processes as a function of the large-scale circulation.

While B15 focused on observations during a field campaign, we also apply the extended equation to global outputs of an isotope-enabled general circulation model, with the aim to quantify the different factors controlling the δD variability ~~at the global scale~~in the Tropics. The variable z_{orig} will emerge as an important factor. Therefore, we discuss the possibility that δD measurements at the near surface and through the lower FT could help estimate z_{orig}, and thus the mixing processes between the SCL and the air above.

Note that we focus on δD only. Results for $\delta^{18}O$ are similar. We do not aim at capturing the second-order parameter d-excess, because our model requires some knowledge about free tropospheric vertical profiles of isotopic composition. While δD is known to decrease with altitude (Ehhalt, 1974; Ehhalt et al., 2005; Sodemann et al., 2017), vertical profiles of d-excess are more diverse and less well understood (Sodemann et al., 2017)). In addition, the need for an extension of MJ79 is more needed for δD than for d-excess~~anyway, since MJ79 already performs quite well for~~ , since the effect of convective mixing is larger on δD than on d-excess (Risi et al., 2010d; Benetti et al., 2014).

2 Theoretical framework

2.1 ~~Assumptions leading to the Benetti et al 2015 equation~~Box model and budget equations

~~In this section, we recall how the equation in Benetti et al. (2014)~~ Building on Benetti et al. (2014) and B15~~was derived and explicit all underlying assumptions.~~

~~We~~, we consider a simple box representing the SCL (Fig. 2). We assume that the air ~~may come~~ comes from above (M) ~~or from the~~ and from the incoming large-scale horizontal ~~convergence ($D<0$~~advection (F_{adv}), and is exported through the SCL top (N, e.g. turbulent mixing or convective mass flux) ~~or~~ and by outgoing large-scale horizontal ~~divergence ($D>0$~~advection ($F_{adv,out}$). We assume that the SCL is at steady state. ~~In particular~~For example, its depth is constant. Since the SCL properties may exhibit a diurnal cycle (Duynkerke et al., 2004), this hypothesis restricts the application of this model to time scales longer than daily. The air mass budget of the SCL thus writes:

$$M + F_{adv} = N + \cancel{D}F_{adv,out} \tag{1}$$

These fluxes also transport water vapor and isotopes. In addition, surface evaporation E ~~imports~~ and rain evaporation F_{evap} import water vapor and isotopes (Fig. 2). ~~We neglect import of water vapor and isotopes by rain evaporation (Albrecht, 1993) and will test the sensitivity to this effect in appendix B.~~

Hereafter, to simplify equations, we use the isotopic ratio R instead of δD.

The SCL is usually well-mixed (Betts and Ridgway, 1989; Stevens, 2006; De Roode et al., 2016)~~, so that we can~~. We thus assume that the humidity and isotopic properties are constant vertically and horizontally in the SCL. They are noted (q_0, R_0). The humidity and isotopic properties of the mass flux export N are thus also (q_0, R_0). ~~In case of net horizontal divergence ($D>0$), the~~ The properties of the ~~divergence flux are also (q_0, R_0). In case of net convergence ($D<0$), we neglect large-scale~~ flux M are noted (q_{orig}, R_{orig}). The properties of the incoming air by horizontal advection are noted (q_{adv}, R_{adv}). For simplicity we neglect here the effect of horizontal gradients in ~~air properties, so that the properties of the convergence flux are also (q_0, R_0). The properties of the flux M are noted (q_{orig}, R_{orig})~~ humidity (i.e. $q_{adv} = q_0$), assuming that the main effect of horizontal advection on δD_0 arises from horizontal gradients in δD. Appendix C explains how R_{adv} can be calculated. At steady state, the water budget of the SCL writes:

$$M \cdot q_{orig} + E + F_{evap} + F_{adv} \cdot q_0 = (N + \cancel{D}F_{adv,out}) \cdot q_0 \tag{2}$$

This model is consistent with SCL water budgets that have already been derived in previous studies (Bretherton et al., 1995), except that we consider steady state. This equation can be solved for q_0:

$$q_0 = q_{orig} + \cancel{E/M}\frac{E + F_{evap}}{M} \tag{3}$$

The SCL humidity q_0 is thus sensitive to M, justifying that it can be used to estimate the mixing intensity or the ~~entrainment velocity~~ “entrainment velocity” $w_e = M/\rho_0$ (ρ being the air volumic mass) (Bretherton et al., 1995).

At steady state, the water isotope budget of the SCL writes:

$$M \cdot q_{orig} \cdot R_{orig} + E \cdot R_E + F_{evap} \cdot R_{evap} + F_{adv} \cdot q_0 \cdot R_{adv} = (N + D F_{adv,out}) \cdot q_0 \cdot R_0 \tag{4}$$

where R_E is the isotopic composition of the surface evaporation. It is assumed to follow the ~~Craig and Gordon (1965)~~ Craig and Gordon (1965) equation:

$$R_E = \frac{R_{oce}/\alpha_{eq} - h_0 \cdot R_0}{\alpha_K \cdot (1 - h_0)} \tag{5}$$

where R_{oce} is the isotopic ratio in the surface ocean water, α_{eq} is the equilibrium fractionation calculated at the ocean surface temperature (SST) (Majoube, 1971), α_K is the kinetic fractionation coefficient (MJ79) and h_0 is the relative humidity normalized at the SST ($h_0 = q_0/q_s(SST, P_0)$ where q_s is the saturation specific humidity at ~~saturation function~~ SST and P_0 is the surface pressure).

We write the isotopic composition of the rain evaporation, R_{evap}, as:

$$R_{evap} = \alpha_{evap} \cdot R_0$$

where α_{evap} is an effective fractionation coefficient. For example, if droplets are formed near the cloud base, some of them precipitate and evaporate totally into the SCL (e.g. in non-precipitating shallow cumulus clouds), then $\alpha_{evap} = \alpha(T_{cloudbase})$. In contrast, if droplets are formed in deep convective updrafts after total condensation of the SCL vapor, and then a very small fraction of the rain is evaporated into a very dry SCL, then $\alpha_{evap} = 1/\alpha(T_{SCL})/\alpha_K$ (Stewart, 1975).

We note $\eta = F_{evap}/E$ the ratio of water vapor coming from rain evaporation to that of surface evaporation, and $\phi = F_{adv} \cdot q_{adv}/E$ the ratio of water vapor coming from horizontal advection to that coming from surface evaporation. We note $\beta = R_{adv}/R_0$ the ratio of isotopic ratios of horizontal advection to that of the SCL.

Note that in all our equations, we assume that temperature and humidity profiles and all basic surface meteorological variables are known. We attempt to express neither h_0 as a function of q_0 as in B15, nor the q profile as a function of q_0. Our ultimate goal is to assess the added value of δD assuming that meteorological measurements are already routinely done.

By combining all these equations, we get:

$$R_0 = \frac{(1 - r_{orig}) \cdot R_{oce}/\alpha_{eq} + \alpha_K \cdot (1 - h_0) \cdot r \cdot R_{orig}}{(1 - r_{orig}) \cdot h_0 + \alpha_K \cdot (1 - h_0)} \frac{(1 - r_{orig}) \cdot R_{oce}/\alpha_{eq} + \alpha_K \cdot (1 - h_0) \cdot r_{orig} \cdot (1 + \eta) \cdot R_{orig}}{(1 - r_{orig}) \cdot h_0 + \alpha_K \cdot (1 - h_0) \cdot (1 + \eta + (1 - r_{orig}) \cdot (\phi \cdot (1 - \beta) - \eta \cdot \alpha_{evap})} \tag{6}$$

where $r_{orig} = q_{orig}/q_0$ is the proportion of the water vapor in the SCL that originates from above.

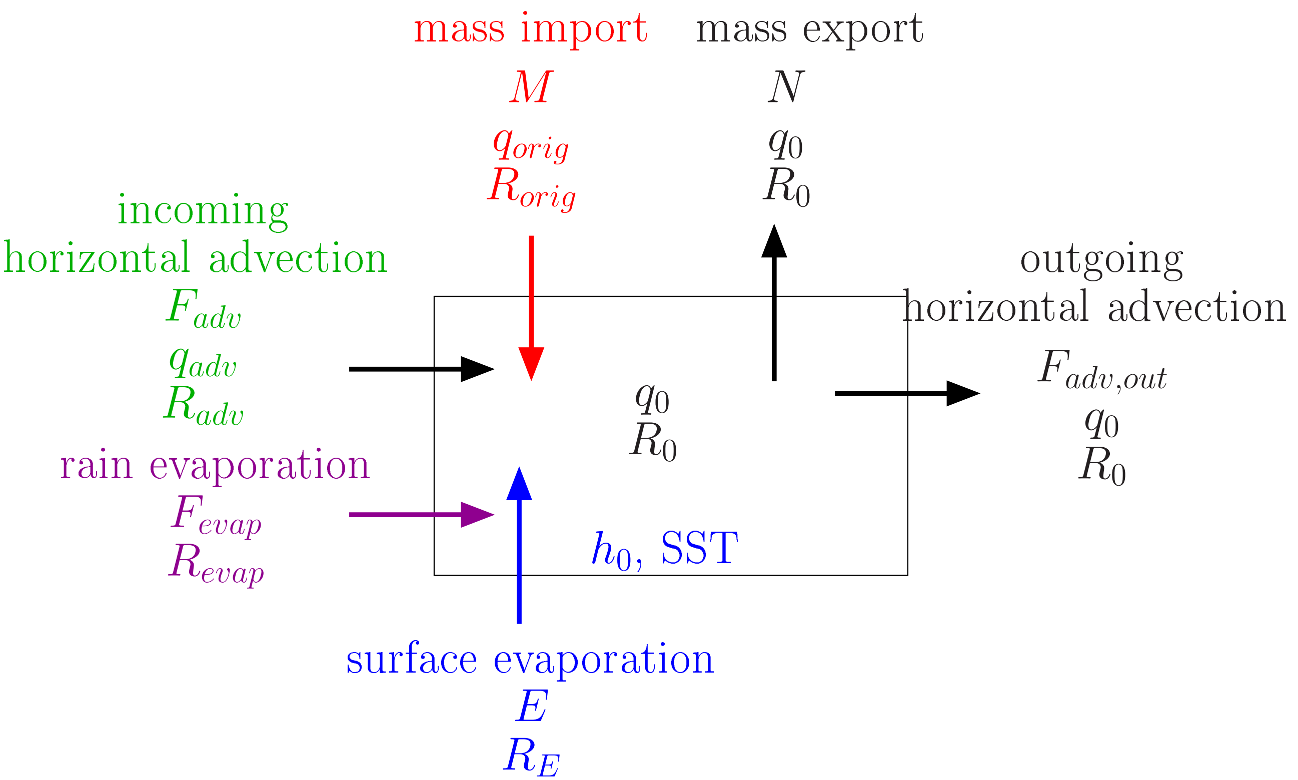

~~Equation~~

Figure 2. Schematics showing the simple box model on which the theoretical framework is based, and illustrating the main notations.

An intriguing aspect of this equation is that the sensitivity to M disappears. In contrast to q_0, R_0 is not sensitive to M. Therefore, it appears illusory to promise that water vapor isotopic measurements could help constrain the entrainment velocity that many studies have ~~strived~~ striven to estimate (Nicholls and Turton, 1986; Khalsa, 1993; Wang and Albrecht, 1994; Bretherton et al., 1995; Faloona et al., 2005; Gerber et al., 2005, 2013). The lack of sensitivity of R_0 to M is explained physically by the fact that for a given q_0 and q_{orig}, if M increases, then ~~E~~ $E + F_{evap}$ increases in the same proportion to maintain the water balance. Therefore, the relative proportion of the water vapor originating from surface ~~evaporation and~~ and rain evaporation to that coming from above, to which R_0 is sensitive, remains constant. Rather, since q and R vary with altitude, R_0 is sensitive to the altitude from which the air originates~~, as argued in the next paragraph~~.

2.2 ~~Two additional assumptions to close the equation~~

2.2 Closure if δD profile follows a Rayleigh distillation line

Eq. (6) requires to know q_{orig} and R_{orig}. B15 ~~closed it by taking the values of q_{orig} and R_{orig}~~ take these values from GCM outputs at 700 hPa~~from GCM outputs. We modify this in two ways.~~

~~First, we want to~~ . In contrast, here we acknowledge the diversity and complexity of mixing mechanisms by ~~taking~~ keeping the possibility to take q_{orig} and R_{orig} at a variable altitude z_{orig}~~:~~ .

~~$q_{orig} = h(z_{orig}) \cdot q_s(\bar{T}(z_{orig}) + \delta T(z_{orig}), P(z_{orig}))$~~

~~where $\bar{T}(z_{orig}) + \delta T(z_{orig}) = T(z_{orig})$ is the temperature at altitude~~ If the goal is to predict R_0 from z_{orig} , ~~$\bar{T}$ is the tropical-ocean-mean temperature profiles, $h(z_{orig})$~~ we can apply Eq. (6) if we know the q and ~~$P(z_{orig})$ are the relative humidity and pressure at~~ δD vertical profiles. Conversely, if the goal is to predict z_{orig} ~~, and $\delta T(z_{orig})$ is the temperature perturbation compared to $\bar{T}$. Therefore,~~ from R_0, we can numerically solve Eq. (6) if we know the q and δD vertical profiles. No analytical solution exists in the ~~unknown q_{orig} is replaced by the unknown~~ general case, but a numerical solution can be searched for z_{orig} ~~.~~ based on Eq. (6). However, the existence and unicity of the solution is not warranted for all kinds of profiles (e.g. appendix A).

~~Note that in all our equations, we assume that temperature and humidity profilesand all basic surface meteorological variables are known. We make no attempt to express h_0 as a function of q_0 as in B15. Our ultimate goal is to assess the added value of δD assuming that meteorological measurement are already routinely done. Therefore, variations of δD_0 that are mediated by q_0 or h_0 do not interest us.~~

~~Second, to deal with R_{orig} in Eq. (6) and get an analytical solution, we assume~~ In practice, full isotopic profiles are costly to measure. In addition, our goal is to develop an analytical model. Therefore, in the following we simplify the problem by assuming that the vertical profile of R follows a known relationship as a function of q. Measured vertical profiles of δD are usually bounded by two curves when plotted in a (q, δD) diagram (Sodemann et al., 2017): Rayleigh distillation curve and mixing line. ~~We explore these two extreme cases in the next section and in appendix A respectively.~~

~~Schematics showing the simple box model on which the theoretical framework is based, and illustrating the main notations.~~

2.3 ~~Closure if the tropospheric profile follows a Rayleigh line~~

~~Here we assume that R_{orig} is uniquely related to q_{orig} by Rayleigh distillation~~ First, we explore the case of a Rayleigh distillation curve (Dansgaard, 1964), as in ~~Galewsky and Rabanus (2016)~~Galewsky and Rabanus (2016):

$$R_{orig} = R_0 \cdot r_{orig}^{\alpha_{eff}-1} \quad (7)$$

where α_{eff} is an effective fractionation coefficient. Typically, q decreases with altitude, so R also decreases with altitude. However, in observations and models, vertical profiles of R can be very diverse (Bony et al., 2008; Sodemann et al., 2017). The water vapor may be more (Worden et al., 2007) or less (Sodemann et al., 2017) depleted than predicted by Rayleigh curve using a realistic fractionation factor that depends on local temperature. Therefore, here we let α_{eff} be a free parameter larger than 1. Rather than assuming a true Rayleigh curve, we simply assume that R and q are logarithmically related. Effects of horizontal advection and rain evaporation on tropospheric profiles are encapsulated into α_{eff}.

Injecting Eq. (7) into Eq. (6), we get:

$$R_0 = \frac{R_{oce}}{\alpha_{eq}} \cdot \frac{1}{h_0 + \alpha_K \cdot (1-h_0) \cdot \left((1+\eta) \cdot \frac{1-r_{orig}^{\alpha_{eff}}}{1-r_{orig}} - \eta \cdot \alpha_{evap} + \phi \cdot (1-\beta) \right)} \tag{8}$$

A simpler form can be found if neglecting horizontal advection and rain evaporation effects ($\phi = \eta = 0$):

$$R_0 = \frac{R_{oce}}{\alpha_{eq}} \cdot \frac{1}{h_0 + \alpha_K \cdot (1-h_0) \cdot \frac{1-r_{orig}^{\alpha_{eff}}}{1-r_{orig}}} \tag{9}$$

As a consistency check, in the limit case where the air coming from above is totally dry ($r_{orig} = 0$), ~~we find~~ Eq. (9) becomes the MJ79 equation:

$$R_0 = \frac{R_{oce}}{\alpha_{eq}} \cdot \frac{1}{h_0 + \alpha_K \cdot (1-h_0)} \tag{10}$$

Equation (~~9~~8) tells us that whenever $\alpha_{eff} > 1$, R_0 decreases as r_{orig} increases (Fig. 3 red), i.e. as q_{orig} is moister. Therefore, R_0 decreases as z_{orig} is lower in altitude. This result may be counter-intuitive, but can be physically interpreted as follows. If z_{orig} is high, mixing brings air with very depleted water vapor, but since the air is dry, the depleting effect is small. In contrast, if z_{orig} is low, mixing brings air with water vapor that is not very depleted, but since the air is moist, the depleting effect is large (Fig. 4a).

Figure 3 (red) shows that the range of possible δD values is restricted to -70 ‰ to -85 ‰. This explains why in quiescent conditions near the sea level in tropical ocean locations, the water vapor δD varies little ~~Benetti et al. (2014) (~~(Benetti et al. (2014), F. Vimeux pers. comm.). In the limit case where $r_{orig} \rightarrow 1$ (i.e. the air comes from the SCL top), $R_0 \rightarrow \frac{R_{oce}}{\alpha_{eq}} \cdot \frac{1}{h_0 + \alpha_K \cdot (1-h_0) \cdot \alpha_{eff}}$ (L'Hopital's rule was used to calculate this limit). This lower bound is not so depleted compared to the more depleted water vapor observed in regions of deep convection (e.g. ~~Lawrence et al. (2002); Lawrence et al. (2004); Kurita (2013)~~Lawrence et al. (2002); Lawr). This is because when $r_{orig} \rightarrow 1$, the water vapor coming from above has a composition very close to that of the SCL, so the depleting effect is limited. In addition, surface evaporation strongly damps the depleting effect of mixing. Only rain evaporation or liquid-vapor exchanges (Lawrence et al., 2004; Worden et al., 2007) can further decrease R_0 (appendix B).

Figure 3 (green) shows that the sensitivity to α_{eff} is relatively small but cannot be neglected. Therefore, predicting ~~water vapor δD~~ δD_0 requires to have some knowledge about the steepness of the isotopic profiles in the FT. Rain evaporation and horizontal advection can have either an enriching or depleting effect, but do not qualitatively change the results (Fig. 3 purple and blue).

~~Assuming a Rayleigh shape for the δD profile allows us to find a good-looking analytical solution, but our~~ Now we consider the case of a mixing line. Detailed calculation in appendix A show that the sensitivity to r_{orig} is lost. An infinity of FT end members can lead to the same δD_0 when mixed with the surface evaporation, as illustrated in Fig. 4b and analytically demonstrated in appendix A. Our main results (more depleted δD_0 as r_{orig} increases, restricted range of δD_0 variations, relationship with z_{orig}) ~~would hold for any~~ hold only for δD ~~profile that is steeper than the~~ profiles that are steeper than a mixing line. ~~If the profile follows as~~ This is the case for profiles that are intermediate between a Rayleigh and a mixing line, ~~however, our results would not hold any more, because no single end member can be identified, as illustrated in Fig. 4b and analytically demonstrated in appendix A. Therefore, in the remaining of the paper, we will assume that R follows a logarithmic line. We will assess the validity of this assumption in section D1.~~ as is usually the case in nature (Sodemann et al., 2017) or in a general circulation model (appendix D1).

~~An important assumption that led to Eq. (9) is the neglect of SCL moistening by rain evaporation. We propose an extended equation including rain evaporation in appendix B). Rain evaporation can have a depleting or enriching effect (e.g. pink and blue curves in Fig. 3), depending on microphysical details that are too complex to be addressed here. Therefore, we neglect rain evaporation effects and our results will be valid only in regions covered by non-precipitating clouds, e.g. subsiding regions covered by non-precipitating trade-wind cumulus, strato-cumulus or stratus clouds.~~

3 Model simulations, observations and methods

3.1 LMDZ simulations

We use an isotope-enabled general circulation model (GCM) as a laboratory to test our hypotheses and investigate ~~isotopic controls~~ what controls the isotopic composition. We use the LMDZ5A version of LMDZ (Laboratoire de Météorologie Dynamique Zoom), which is the atmospheric component of the IPSL-CM5A coupled model (Dufresne et al., 2012) that took part in CMIP5 (Coupled Model Intercomparison Project, ~~Taylor et al. (2012)~~Taylor et al. (2012)). This version is very close to LMDZ4 (Hourdin et al., 2006). Water isotopes are implemented the same way as in its predecessor LMDZ4 (Risi et al., 2010c). We use 4 years (2009-2012) of an AMIP (Atmospheric Model Intercomparison Project)-type simulation (Gates, 1992) that was initialized in 1977. The winds are nudged towards ERA-40 reanalyses (Uppala et al., 2005) to ensure a more realistic simulation. Such a simulation has already been described and extensively validated for isotopic variables in both precipitation and water vapor (Risi et al., 2010c, 2012a). The ocean surface water δD_{oce} is assumed constant and set to 4 ‰. The resolution is 2.5° in latitude $\times$ 3.75° in longitude, with 39 vertical levels. Over the ocean, the first layer extends up to 64 m, and a typical SCL extending up to 600 m is resolved by 6 layers. Around 2500 m, a typical altitude for the inversion for trade-wind cumulus clouds, the resolution is about 500 m.

For our calculations, we only use tropical grid boxes (30°S-30°N) over tropical oceans (>80% ocean fraction in the grid box). In addition, to avoid numerical problems when estimating effect of horizontal advection and rain evaporation, only grid boxes and days where $E > 0.5$ mm/d are considered. This represents 99.7% of all tropical oceanic grid boxes.

Specific diagnostics for horizontal advection and rain evaporation are detailed in appendix B and C.

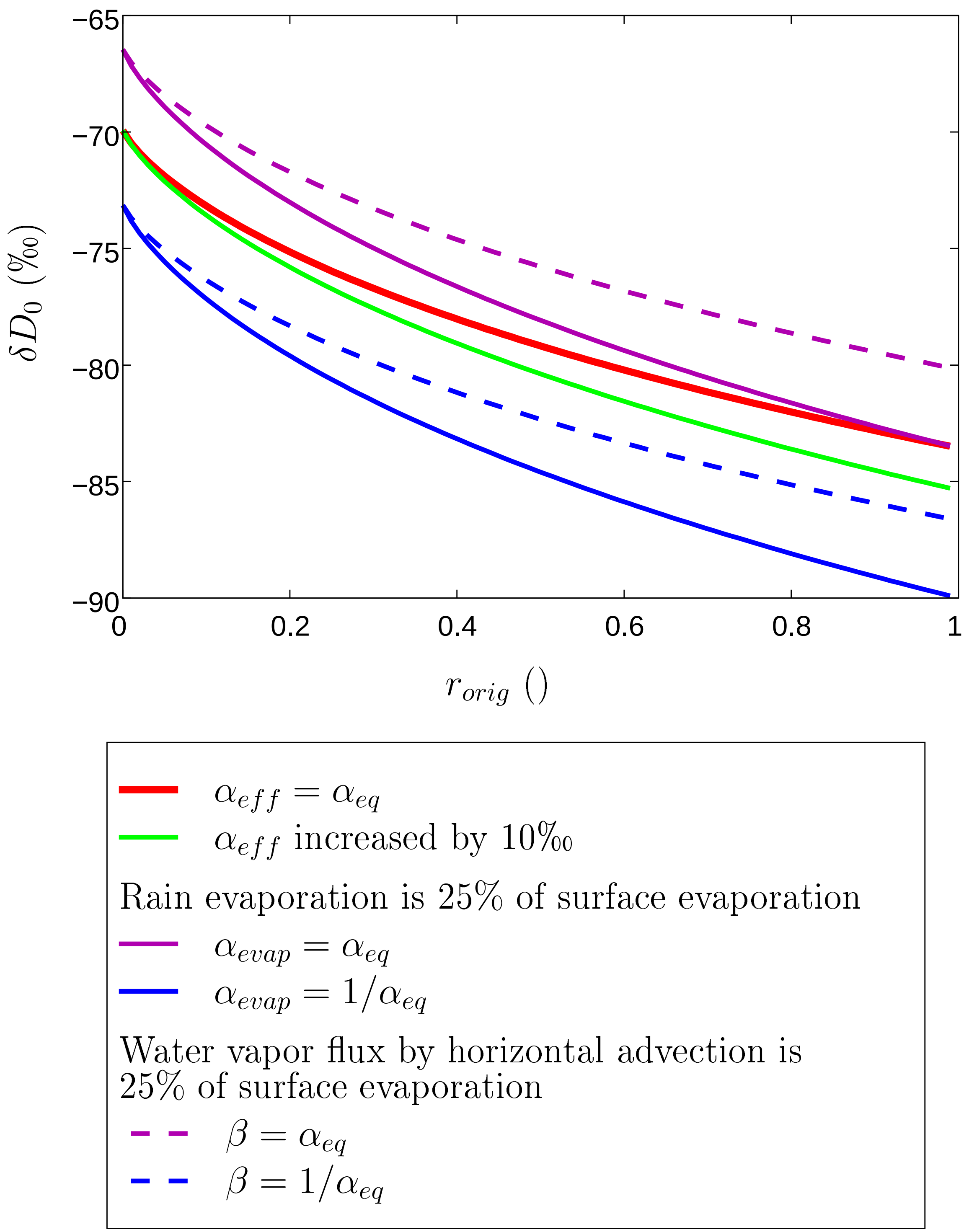

Figure 3. δD_0 as a function of r_{orig} according to Eq. (9), with $\alpha_{eff} = \alpha_{eq}$ as an example (red). For this illustrative purpose, we assume SST=30°C, $h_0 = 0.8$, $\delta D_{oce} = 0$‰ and $\phi = \eta = 0$. The sensitivity to the effective fractionation factor α_{eff} (green) is shown. ~~In case of~~ If rain evaporation ~~fractionation~~is 25% of surface evaporation ($\eta = 0.25$), the solid pink and blue curves show the sensitivity to the effective fractionation factor ~~α_{re} (see appendix B)~~ α_{evap}. If the incoming water vapor by horizontal advection is ~~shown~~ 25% of surface evaporation (~~pink~~$\phi = 0.25$), the dashed pink and blue ~~)~~curves show the sensitivity to the isotopic gradient quantified by β.

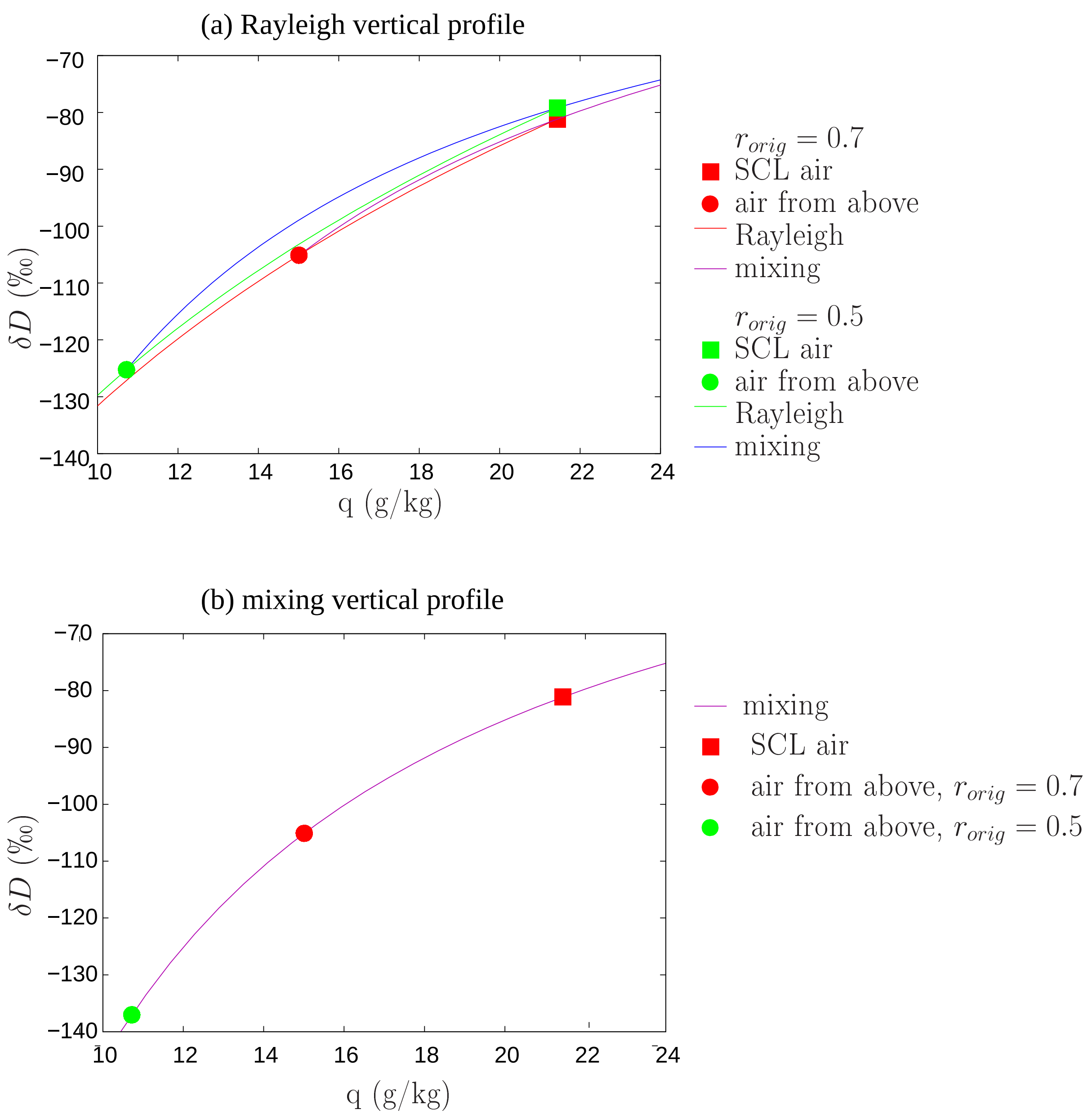

Figure 4. Idealized $q - \delta D$ diagrams showing how the SCL water vapor δD is set. For this illustrative purpose, we assume SST=30°C, $h_0 = 0.8$, $\delta D_{oce} = 0$‰ and and $\phi = \eta = 0$. (a) If δD profiles follow Rayleigh distillation. The red curve shows the Rayleigh profile starting from the SCL and the pink curve shows the mixing line connecting the air coming from above to the surface evaporation, in the case $r_{orig} = q_{orig}/q_0 = 0.7$. The green curve shows the the Rayleigh profile starting from the SCL and the blue curve shows the mixing line connecting the air coming from above to the surface evaporation, in the case $r_{orig} = q_{orig}/q_0 = 0.5$. One can visually see that when r_{orig} is lower, the mixing line is more curved, leading to more enriched values. (b) If δD profiles follow a mixing line. The ~~pink~~ purple curve joins the SCL air and the air at all altitudes above the SCL. One can see that different values for r_{orig} can lead to the same value of δD in the SCL.

3.2 STRASSE observations

We also apply our theoretical framework to observations during the STRASSE (subtropical Atlantic surface salinity experiment) cruise that took place in the Northern subtropical ocean in August and September 2012 (Benetti et al., 2014). This campaign accumulates several advantages that are important for our analysis: (1) continuous δD_0 measurements in the surface water vapor (17m) at a high temporal frequency during one month (Benetti et al., 2014, 2015, 2017b), (2) associated surface meteorological measurements, including SST and h_0, (3) 22 radio-soundings relatively well distributed over the campaign period and providing vertical profiles of altitude, temperature, relative humidity and pressure, (4) ocean surface water δD_{oce} measurements (Benetti et al., 2017a), (5) a variety of conditions ranging from quiescent weather to convective conditions, (6) on many vertical profiles, a well defined temperature inversion allows to calculate the inversion altitude.

We use δD_0 measurements on a 15-minute time step. The measurements in ocean water were interpolated on the same time steps using a Gaussian filter with a width of 3 days. The radio-soundings are used together with all water vapor isotopic measurements that are within 30 minutes of the radio-sounding launch. Only profiles during the ascending phase of the balloon are considered, because the descent phase is often located far away from the initial launch point (McGrath et al., 2006; Seidel et al., 2011)
.

3.3 Estimating the altitude from which the air originates

~~First, α_{eff} is estimated assuming that~~ Here we explain how z_{orig} is estimated based on LMDZ outputs. First, we assume that the q and δD at 500 hPa (q_f, δD_f) ~~at 500hPa follows~~ belong to a Rayleigh distillation line starting from the surface with effective fractionation α_{eff}:

$$\alpha_{eff} = 1 + \frac{ln(R_f/R_0)}{ln(q_f/q_0)}$$

In a real field campaign, this assumption means that we do not need to measure the full vertical profile of δD, but only δD_f at a given free tropospheric altitude (e.g. 500 hPa).

We checked that results are similar when defining the end member at 400 hPa rather than 500 hPa. However, ~~if~~ the end member ~~is~~ should be defined above 500 hPa to ensure that it is well above boundary layer processes. If the end member is defined below 500 hPa (e.g. 600 hPa), ~~results are not always reasonable~~there are a few cases where q increases with altitude ($q_f > q_0$) due to horizontal advection or convective detrainment from nearby moister regions; meanwhile, δD decreases monotonically, leading to unrealistic values for α_{eff}.

Second, r_{orig} is estimated based on Eq. (9), using α_{eff}, α_{eq}, α_K , δD_{oce}, h_0 and δD_0 simulated by LMDZ.

Third, the altitude z_{orig} is estimated from r_{orig}. Using the q vertical profile, we find z_{orig} so that $q(z_{orig}) = r_{orig} \cdot q_0$ (Fig. 5, red).

~~Note that~~ When estimating z_{orig} from observations, we follow the same methodology except that in absence of measurements for q_f and δD_f we assume a constant $\alpha_{eff} = 1.07$ based on LMDZ simulation, and that α_{eq}, α_K , δD_{oce}, h_0 and δD_0 come from surface observations.

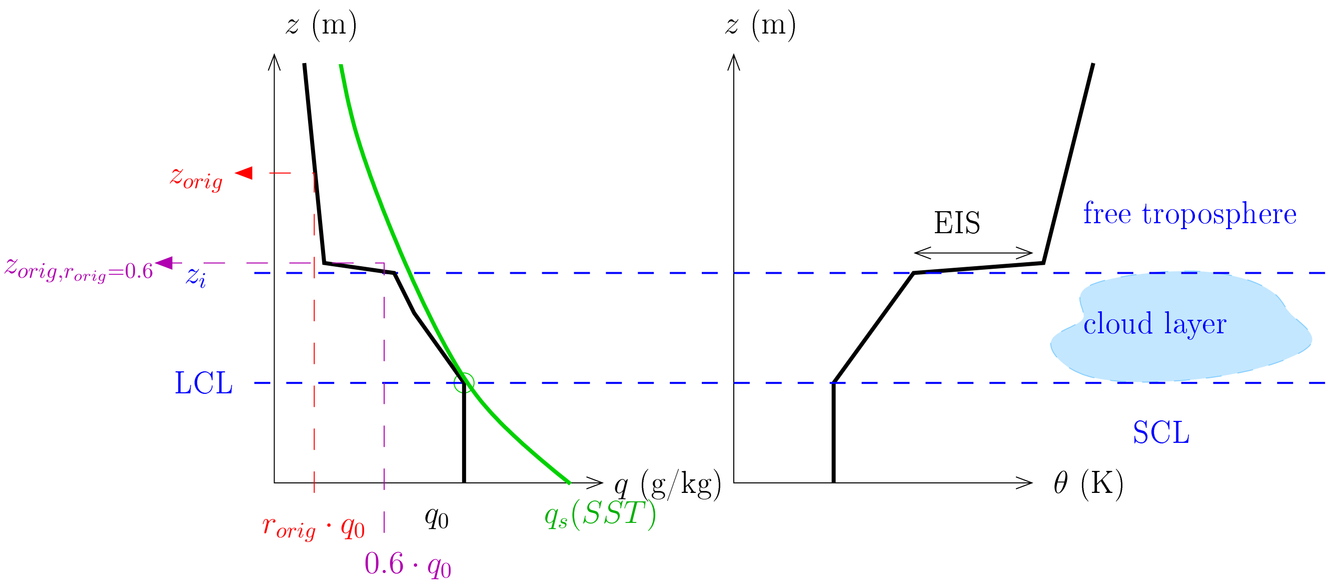

Figure 5. Schematics illustrating the typical structure of tropical marine boundary layers. The sub-cloud layer (SCL) extends from the surface to the lifting condensation level (LCL) and the cloud layer extends from the LCL to the inversion (z_i). EIS stands for the estimated inversion strength. Left: shape of the vertical profile in q (black) and q_s (green). Right: shape of the vertical profile in potential temperature θ, inspired by ~~Wood and Bretherton (2006)~~(Wood and Bretherton, 2006). The LCL, z_{orig} , $z_{orig,r_{orig}=0.6}$ and z_i altitudes defined in section 3.4 are indicated.

Note that r_{orig} and z_{orig} are not direct diagnostics from the simulation, but rather a-posteriori estimates to match the simulated δD_0. Therefore, if assumptions underlying Eq. (9) are violated, then the estimate of r_{orig}, and subsequently z_{orig}, will be ~~based~~biased. The estimate of r_{orig} encapsulates the effect of mixing processes, but also all other processes that have been neglected in our theoretical framework, such as temporal variations in SCL depth, q_0 or δD_0 ~~, horizontal gradients in~~ or vertical variations of q_0 or δD_0 ~~, or rain evaporation. For example, in case of deep convection, depleting rain evaporation will reflect into an artificially larger r_{orig} and lower z_{orig}. We have to keep this in mind when interpreting the results~~within the SCL.

3.4 Boundary layer structure diagnostics

Figure 5 illustrates the structure of a typical tropical marine boundary layer covered by strato-cumulus or cumulus clouds (Betts and Ridgway, 1989; Wood, 2012; Wood and Bretherton, 2004; Neggers et al., 2006; Stevens, 2006). The cloud base corresponds to the lifting condensation level (LCL). Below is the well-mixed SCL. Above is the cloud layer, topped by a temperature inversion. Above the inversion is the FT.

The LCL is calculated as the altitude at which the specific humidity near the surface equals the specific humidity at saturation of a parcel that is lifted following a dry adiabat (Fig. 5). ~~In LMDZ, the inversion~~

The temperature inversion is an abrupt increase in temperature that caps the boundary layer. Therefore, a method to automatically estimate its altitude z_i is ~~calculated~~ to detect a maximum in the vertical gradient of potential temperature (Stull, 1988; Oke, 1988; Sorbjan, 1 . This method is sensitive to the resolution of vertical profiles (Siebert et al., 2000; Seidel et al., 2010). Therefore, we adapted this method in order to yield z_i values that best agree with what we would estimate from visual inspection of individual temperature profiles. In LMDZ, we calculate z_i as the first level at which the vertical potential temperature ~~gradients~~ gradient exceeds 3 times the moist-adiabatic lapse rate. In observations, we calculate z_i ~~is calculated~~ as the first level at which the vertical potential temperature ~~gradients~~ gradient exceeds 5 times the moist-adiabatic lapse rate, because radio-soundings are noisier than simulated profiles. ~~These estimates are consistent with what we would estimate from visual inspection of vertical profiles.~~

Finally, we calculate $z_{orig,r_{orig}=0.6}$, which is the z_{orig} altitude if r_{orig} is set to 0.6. This usually coincides with the altitude of strong humidity decrease near the inversion (Fig. 5).

3.5 Averages and composites

All calculations are done on daily values for LMDZ, and on 15-minute values for observations.

For LMDZ, when analyzing spatial and seasonal variability, seasonal averages are calculated at each grid box over tropical oceans by averaging all days of all years that belong to each season. Seasons are defined as boreal winter (December-January-February), spring (March-April-May), summer (June-July-August) and fall (September-October-November). For illustration purpose, all maps are plotted for boreal winter. Standard deviations are also calculated among all days of all years for each season.

The type of clouds and mixing processes depends strongly on the large-scale velocity at 500 hPa (ω_{500}, map shown in Fig. 6a), with shallow clouds in subsiding regions and deeper clouds in ascending regions (~~(Bony et al., 2004),~~ Fig. 1). Therefore, ~~composites are calculated by averaging~~ it is convenient to plot variables as composites as a function of ω_{500} (Bony et al., 2004). To make such plots, we divide the ω_{500} range from -30 to 50 hPa/d into intervals of 5 hPa/d. In each given interval, we average all seasonal-mean values at all locations ~~that belong to a given interval of~~ over tropical oceans for which seasonal-mean ω_{500} belongs to this interval (e.g. Fig. 8a will be an example). Note that such composites are done on seasonal-mean ω_{500} because cloud processes and their associated diabatic heating are tied to the large-scale circulation through energetic constrains (Yanai et al., 1973; Emanuel et al., 1994) that are best valid at longer time scales (otherwise, the energy storage term may become significant, e.g. Masunaga and Sumi (2017)). This is why ω_{500} is generally averaged over a month or longer (e.g. Bony et al. (1997); Williams et al. (2003); Bony et al. (2004); Wyant et al. (2006); Bony et al. (2013)). In addition, we primarily focus on understanding the seasonal and spatial distribution of δD_0.

The cloud cover strongly ~~depends on~~ correlates with the inversion strength, ~~with increasing cloud fraction as inversion strength increases. We use~~ which can be quantified by the Estimated Inversion Strength (EIS~~) (Wood and Bretherton, 2006) (~~, Wood and Bretherton (2006), map shown in Fig. 6b) as a measure of inversion strength. ~~Composites as~~ We thus also plot variables as composites as a function of EIS~~are calculated by averaging~~ . To make such plots, we divide the EIS range from -1 K to 9 K into intervals of 0.5K. In each given interval, we average all seasonal-mean values at all locations ~~that belong~~

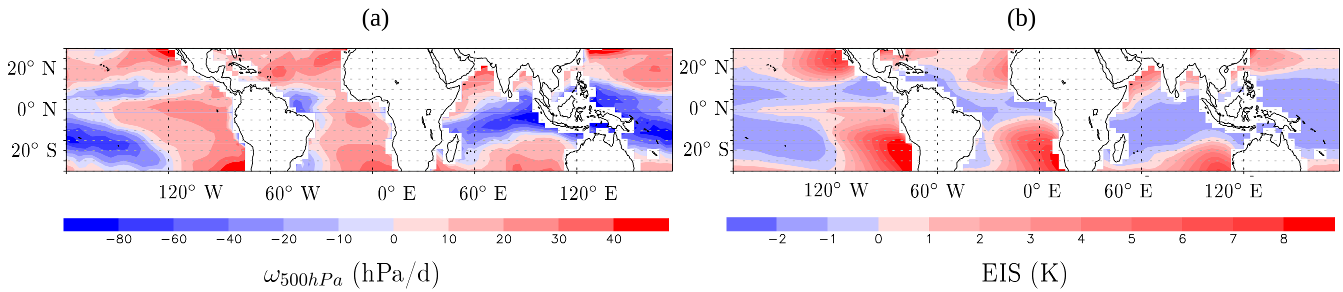

Figure 6. Maps of winter-mean ω_{500} (a) and EIS (b) simulated by LMDZ.

~~to a given interval of EIS.~~over tropical oceans for which seasonal-mean EIS belongs to this interval (e.g. Fig. 8b will be an example). Using seasonal-mean values is consistent with Wood and Bretherton (2006) and with the better link at longer time scales between cloud processes and the large-scale dynamical regime.

3.6 Decomposition method for δD_0

To understand what controls the δD_0 spatio-temporal variations, δD_0 is decomposed into 4 contributions based on Eq. (~~9). The 4 factors, r_{orig}~~8). First, we define $r_{orig,bas}=0.3$, ~~α_{eff}~~$\alpha_{eff,bas}=1.09$, ~~SST and h_0, are alternatively varied each one at a time, assuming that all other factors are constant ($r_{orig}=0.6$, $\alpha_{eff}=1.09$, SST~~SST_{bas}=25°C, ~~$h_0=0.8$). This yields 4 components~~ $h_{0,bas}=0.7$, ~~representing the effects of the variability of~~ $\phi_{bas}=0$, $\eta_{bas}=0$, $\beta_{bas}=1$ and $\alpha_{evap,bas}=1$ as a basic state. We call $\delta D_{0,func}(r_{orig},\alpha_{eff},SST,h_0,\phi,\beta,\eta,\alpha_{evap})$ the function giving δD_0 as a function of r_{orig}, α_{eff}~~, SST and~~ , SST, h_0~~on δD_0.~~ , ϕ, β, η and α_{evap} following Eq. (8), and $\delta D_{0,bas}=\delta D_{0,func}(r_{orig,bas},\alpha_{eff,bas},SST_{bas},h_{0,bas},\phi_{bas},\beta_{bas},\eta_{bas},\alpha_{evap,bas})$. The relative contribution of r_{orig} to δD_0 is estimated as $\delta D_{0,func}(r_{orig},\alpha_{eff,bas},SST_{bas},h_{0,bas},\phi_{bas},\beta_{bas},\eta_{bas},\alpha_{evap,bas})-\delta D_{0,bas}$. Similarly, the contributions of α_{eff}, SST, h_0, ϕ and η are to δD_0 are estimated as detailed in table 1. All the contributions have the same units as δD_0 (‰). The sum of these components yields a quantity that is very close to the simulated δD_0, which confirms the validity of this linear decomposition. These components and their sum can be plotted as maps: Fig. 7 provides an example.

The relative ~~contribution~~ contributions of each of these ~~effects~~ components to the δD variability ~~is~~ are quantified by performing a linear regression of each of the components as a function of δD_0. If the correlation coefficient is significant for a given factor, then the slope quantifies the contribution of this factor to the variability of δD_0. The sum of all contributions may not always be 1 due to non-linearity. Such a method has already been applied in previous studies (e.g.~~Risi et al. (2010b); Oueslati et al. (2016)~~ Risi et al. (2010b); Oueslati et al. (2016)). The contributions to the seasonal-spatial variability of δD_0 can be quantified by performing the regression among all locations and seasons. The contributions to the daily variability of δD_0 can be quantified by performing the regression among all days of a given season at a given location.

Contribution	Calculation	Physical meaning
r_{orig}	$\delta D_{0,func}(r_{orig},\alpha_{eff,bas},SST_{bas},h_{0,bas},\phi_{bas},\beta_{bas},\eta_{bas},\alpha_{evap,bas})-\delta D_{0,bas}$	Altitude from which the air originates
α_{eff}	$\delta D_{0,func}(r_{orig,bas},\alpha_{eff},SST_{bas},h_{0,bas},\phi_{bas},\beta_{bas},\eta_{bas},\alpha_{evap,bas})-\delta D_{0,bas}$	Steepness of the δD vertical gradient in the FT
SST	$\delta D_{0,func}(r_{orig,bas},\alpha_{eff,bas},SST,h_{0,bas},\phi_{bas},\beta_{bas},\eta_{bas},\alpha_{evap,basic})-\delta D_{0,bas}$	SST
h_0	$\delta D_{0,func}(r_{orig,bas},\alpha_{eff,bas},SST_{bas},h_0,\phi_{bas},\beta_{bas},\eta_{bas},\alpha_{evap,bas})-\delta D_{0,bas}$	h_0
ϕ	$\delta D_{0,func}(r_{orig,bas},\alpha_{eff,bas},SST_{bas},h_{0,bas},\phi,\beta,\eta_{bas},\alpha_{evap,bas})-\delta D_{0,bas}$	Horizontal advection through horizontal δD gradients
η	$\delta D_{0,func}(r_{orig,bas},\alpha_{eff,bas},SST_{bas},h_{0,bas},\phi_{bas},\beta_{bas},\eta,\alpha_{evap})-\delta D_{0,bas}$	Rain evaporation in the SCL

Table 1. Equations to calculate the relative contributions of r_{orig}, α_{eff}, SST, h_0, ϕ and η to δD_0, and the physical meaning of these contributions.

3.7 Decomposition method for r_{orig}

To understand what controls r_{orig}, a similar method as for the decomposition of δD_0 can be applied~~, based on Eq. (??)~~. We can write r_{orig} as:

$$r_{orig} = \frac{h(z_{orig}) \cdot q_s(\bar{T}(z_{orig}) + \delta T(z_{orig}), P(z_{orig}))}{q_0} \tag{11}$$

where $\bar{T}(z_{orig}) + \delta T(z_{orig}) = T(z_{orig})$ is the temperature at altitude z_{orig}, $\bar{T}$ is the tropical-ocean-mean temperature profiles, $h(z_{orig})$ and $P(z_{orig})$ are the relative humidity and pressure at z_{orig}, and $\delta T(z_{orig})$ is the temperature perturbation compared to $\bar{T}$. Therefore, the variability of r_{orig} is decomposed into the effect of 4 factors: q_0, z_{orig}, $h(z_{orig})$ and $\delta T(z_{orig})$. In practice, r_{orig} and z_{orig} are calculated following section 3.3, then Eq. (11) is applied.

4 Results from LMDZ

4.1 ~~Does the tropospheric profile follow a mixing or Rayleigh line?~~

~~First, we test whether the δD vertical profiles simulated by LMDZ follow a Rayleigh or mixing curve as a function of q. For the Rayleigh curve, α_{eff} is estimated as explained in section 3.3. For the mixing line, the end member (q_f, R_f) is also taken at 500 hPa. Examples of vertical δD profiles simulated by LMDZ and predicted by the Rayleigh and mixing lines are plotted in Fig. **??**. We can see that simulated profiles are usually bounded by these two extreme lines, consistent with observations (Sodemann et al., 2017). Profiles are however much smoother than in observations, due to the coarse vertical resolution of the model. The coarse vertical resolution is a limitation to keep in mind when discussing the shape of vertical profiles.~~

~~When assuming a Rayleigh or mixing curve, the root mean square error (RMSE) on the δD profile from the surface to 500hPa ranges from 5 to 30 ‰ (Fig. D1a-b). In average, RMSE are slightly larger for Rayleigh, but this depends on the location and no generic curve fits perfectly well the vertical profiles. This is consistent with the diversity of observed profile shapes (Sodemann et al., 2017). In the following, we will assume that the Rayleigh curve is a good first order approximation. Our method of z_{orig} estimate remains valid even if δD vertical profiles do not follow Rayleigh, as long they follow a curve that is steeper than mixing. This is the case in LMDZ (Fig. **??**).~~

~~Figure D1c shows the estimated α_{eff} . It is maximum in regions of deep convection. This is consistent with the maximum depletion simulated in deep convective regions in the mid-troposphere simulated by models (Bony et al., 2008), leading to steeper δD profiles. The pattern of α_{eff} may also reflect horizontal advection effects (Dee et al., 2018).~~

~~Values α_{eff} are of the same order of magnitude as real fractionation factors, but the spatial variations do not reflect those predicted if using a fractionation coefficient α_{eq} a function of temperature T (Fig. D1f). Rayleigh curves using $\alpha_{eq}(T)$ poorly predict vertical profiles of δD (Fig. D1c), with RMSE values exceeding 20 ‰ at most locations.~~

~~Examples of vertical profiles simulated by LMDZ (red), predicted by a Rayleigh curve with α_{eff} estimated to fit the simulated δD at 500 hPa (section 3.3, green), and predicted by a mixing line with the dry end member at 500 hPa (pink). Three examples are given: (a) the simulated profile is closed to a mixing line, (b) the simulated profile is closed to a Rayleigh line, and (c) the simulated profile deviates both from a mixing and a Rayleigh line (c). The RMS values indicate the RMS difference between simulated profile and mixing line (pink) or Rayleigh curve (green).~~

~~a) Root mean square error (RMSE) between the simulated δD profile and a δD profile that would follow a mixing curve between the surface and 500 hPa. b) Same as a but for a profile that would follow a Rayleigh curve between the surface and 500 hPa, with α_{eff} determined based on simulated δD at 500 hPa. c) Same as b but for a profile that would follow a Rayleigh curve using equilibrium fractionation calculated as a function of temperature, $\alpha_{eq}(T)$. d) $\alpha_{eff} - 1$, where α_{eff} is the effective fractionation coefficient, expressed in ‰. e) Standard deviation of α_{eff} among all days in winter of all years, expressed in ‰. f) $\alpha_{eq}(T) - 1$ expressed in ‰. For a-d and f, all daily values are averaged over all days in winters of all years.~~

4.1 Decomposition of δD_0 variability

The spatial variations of δD_0 simulated by LMDZ (Fig. 7a) are characterized by depleted values near mid-latitudes and in dry subsiding regions (e.g. off the coast of Peru and over other ~~upwelling regions) and in deep convective regions~~ regions of oceanic upwelling) and regions of atmospheric deep convection (e.g. Maritime Continent). Consistently, δD_0 values exhibit a maximum for weakly ascending or subsiding regions: δD_0 decreases ~~as ω_{500} is more strongly ascending or descending~~ with increasing vertical velocity of both signs (Fig. 8a black); δD_0 decreases as EIS increases reflecting more stable, subsiding conditions (Fig. 8b black). This pattern is consistent with previous studies (e.g. ~~Good et al. (2015)~~Good et al. (2015)). For the first time, we propose a theoretical framework to interpret this pattern, decomposing it into ~~4~~ 6 contributions: r_{orig}, α_{eff}, SST~~and~~, h_0, rain evaporation and horizontal advection effects (section 3.6). We check that the reconstructed δD_0 from the sum of its 4 contributions is very similar to the simulated δD_0 (Fig. 7b, 8 dashed black).

In ascending regions, the main contribution explaining the more depleted δD_0 in deep convective regions is that of α_{eff} (Fig. 7d, 8a red). α_{eff} is higher in more ascending regions ~~.~~ (Fig. D1d). This means that the main factor depleting δD_0 in deep convective regions is the fact that the mid-troposphere is more depleted. This leads to a steeper gradient (higher α_{eff}), and thus a more efficient depletion by vertical mixing. This is consistent with deep convection depleting the water vapor most efficiently in the mid-troposphere ~~(Bony et al. (2008))~~(Bony et al., 2008). The second main contribution is that associated with r_{orig} (Fig. 7c, 8a green). r_{orig} is larger in deep convective regions ~~. However, we recall that Eq. (9) does not consider rain evaporation, which is a significant source of water vapor in deep convective regions (Worden et al. (2007)). Rain evaporation in deep convective regions is expected to deplete the water vapor (section B), so that neglecting rain evaporation leads to an over-estimate of r_{orig} in these regions. Therefore, the stronger r_{orig} in deep convective regions could be partially an artifact reflecting the effect of rain evaporation.~~ (as explained in section 4.2).

In subsidence regions, the main factor explaining the more depleted δD_0 as subsidence is stronger, or as EIS increases, is the cold SST (Fig. 7e, 8a pink), leading to larger α_{eq}, and to a lesser extent the dry h_0 (Fig. 7f, 8a purple). The contribution of r_{orig} is also a significant contribution to the depletion of δD_0 in the cold upwelling regions, for example off Peru or Namibia (Fig. 7c). ~~In subsidence regions, r_{orig}, is unlikely to be an artifact of rain evaporation there, and probably really reflect the importance of mixing processes.~~ The shallower boundary layer there are associated with higher r_{orig}. ~~The fact that the effect of r_{orig} can be seen on the composites as a function of EIS~~

The contribution of rain evaporation on δD_0 is minor compared to other contributions, except in the deepest convective regions (Fig. ~~8b, green)and not as a function of ω_{500} may reflect the fact that EIS reflects more faithfully the cloud and mixing processes in dry, stable regionsthan ω_{500} does (Wood and Bretherton, 2006)~~7g). Rain evaporation has a slightly depleting effect in regions of strong deep convection and a slightly enriching effect in regions of moderate deep convection. When the fraction of raindrops that evaporate is small, isotopic fractionation favors evaporation of the lighter isotopologues. Therefore in convective, moist regions, rain evaporation has a depleting effect on the SCL (Worden et al., 2007). In contrast, in drier regions, rain evaporates almost totally. The evaporation flux thus has almost the same composition as the initial rain, which is more enriched than the water vapor.

The contribution of horizontal advection to δD_0 is significant only where isotopic gradients are the largest (Fig. C1h). Horizontal advection has slightly enriching in deep convective regions and depleting in coastal regions (e.g. off the coasts of California, Peru, Mauritania, Namibia, India and Australia). For example, the Saharan layer in front of the North-Western African Coast leads to a strong effect of horizontal advection (Lacour et al., 2017a).

From a quantitative point of view, we can decompose the δD_0 seasonal-spatial variations into these different effects (section 3.6). In regions of large-scale ascent, α_{eff} is the main factor explaining the δD_0 seasonal-spatial variations (~~37~~ 33%), followed

Regime	ascending		Subsiding	
	correlation coefficient	slope	correlation coefficient	slope
r_{orig}	~~0.71~~ 0.59	~~0.17~~ 0.19	~~0.50~~ 0.52	~~0.16~~0.29
α_{eff}	~~0.75~~ 0.73	~~0.37~~ 0.33	~~0.36~~ 0.26	~~0.14~~0.10
SST	~~-0.20~~ -0.23	-0.06	0.89	0.54
h_0	~~0.09~~ (0.06)	~~0.03~~ (0.01)	~~0.35~~ 0.28	~~0.23~~0.13
rain evaporation	0.67	0.20	-0.36	-0.05
horizontal advection	-0.26	-0.12	(0.10)	(0.04)
r_{orig} if rain evaporation and horizontal advection are neglected	0.69	0.30	0.58	0.34

~~Decomposition of the spatial and seasonal variation in δD_0 into its 4 contributions: effect of~~

Table 2. Decomposition of the spatial and seasonal variation in δD_0 into its 6 contributions: effect of r_{orig}, α_{eff}, SST, h_0, rain evaporation and horizontal advection. For each contribution, we show the correlation coefficient of the linear regression of the contribution as a function of δD_0. The analysis is done separately for ascending and subsiding regimes. All seasons and locations over tropical oceans ($30°N-30°S$, ocean fraction>80%, surface evaporation>0.5 mm/d) are considered.The threshold for the correlation coefficient to be statistically significant at 99 % is 0.15 or lower in all cases. We write correlation coefficient and slope values between brackets when they are not significant at 99%.

~~by~~ rain evaporation (20%) and r_{orig} (~~17~~19 %) and (Table 2). In regions of large-scale descent, SST is the main factor explaining the seasonal-spatial variations (54 %), followed by r_{orig} (~~16~~29 %) h_0 (13%), and α_{eff} (~~14~~10 %) (~~table~~ Table 2). Note that the contribution of r_{orig} would be similar if we neglect rain evaporation and horizontal advection effects (Table 2).

The decomposition method can also be applied to decompose the δD_0 variability at the daily time scale at each location and for each season (Table 3). On average, in ascending regions, r_{orig} is the main factor (~~49~~52 %), followed by rain evaporation (48%) and α_{eff} (~~39~~35 %). In subsiding regions, the effect of SST is muted due to its slow variability, and r_{orig} (~~59~~82 %) ~~, α_{eff} (49 %) and h_0 (62 %) become the main factors~~becomes the main factor.

Overall, the results highlight the importance of r_{orig} as one of the main factors controlling the spatio-temporal variability of δD_0.

4.2 Decomposition of r_{orig} variability

Given the importance of r_{orig} in controlling the δD_0 variations, we now decompose r_{orig} into its 4 contributions: q_0, z_{orig}, h_{orig} and δT_{orig} (section 3.6). Spatially, r_{orig} is maximum in regions of strong large-scale ascent (Fig. 10a) such as the Maritime continent (Fig. 9a), and in very stable regions (Fig. 10b) such as upwelling regions (Fig. 10a). We check that the reconstructed r_{orig} from the sum of its 4 contributions is very similar to the simulated r_{orig} (Fig. 9b, 10 dashed black).

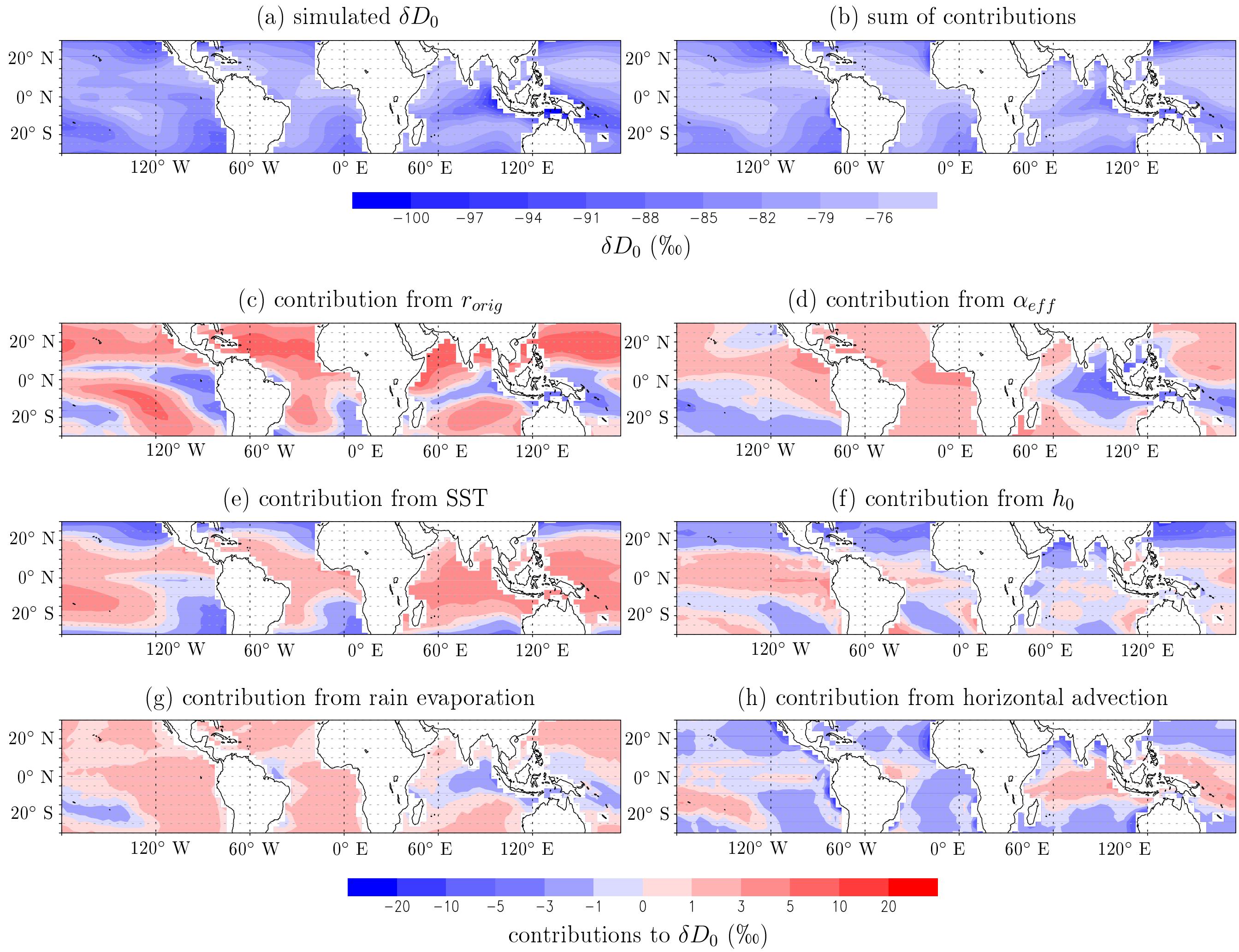

Figure 7. a) Map of winter-mean δD_0 simulated by LMDZ. b) Map of winter-mean δD_0 reconstructed as the sum of the 4 contributions. ~~Note that to focus on variations only and to get values of the same order of magnitude as the simulated~~ Tropical-mean δD_0 ~~field, we subtracted the mean of the 4 contributions and~~ was added ~~the mean of simulated δD_0~~ to compare with a on the ~~reconstructed δD_0 field~~same color scale. c) Map of the contribution of r_{orig} on winter-mean δD_0 calculated from Eq. (9) ~~if only r_{orig} varies~~ (see section 3.6). d) Same as b but ~~of only~~ for α_{eff} varies. e) Same as b but ~~if only~~ for SST~~varies~~. f) Same as b but ~~if only~~ for h_0~~varies~~.

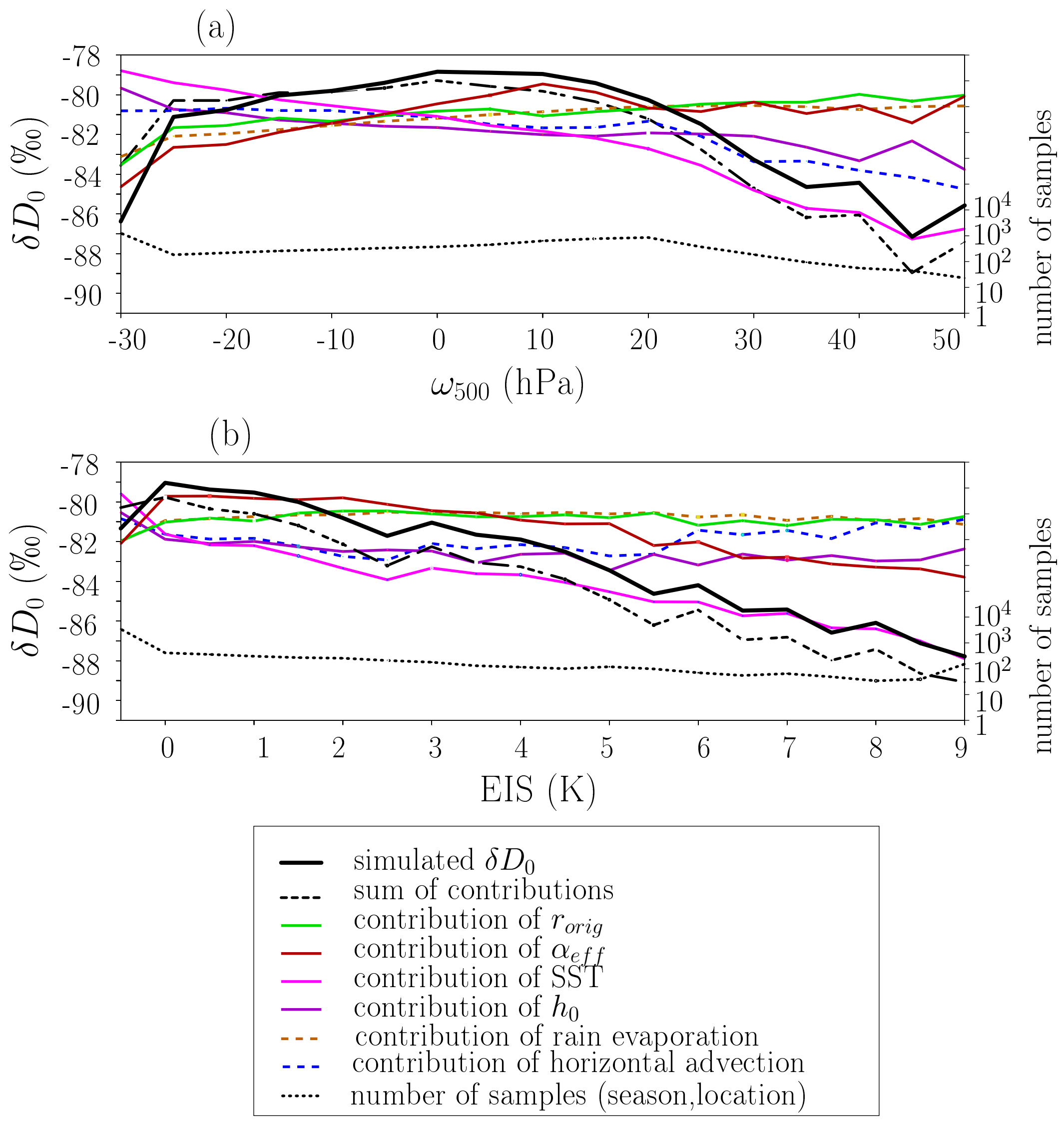

Figure 8. Composites as a function of ω_{500} (a) and of EIS (b) of the seasonal averages of δD_0 simulated by LMDZ over all tropical ocean locations (black). Same for the sum of the contributions (black dashed ~~)~~ and for each individual contribution to δD_0: r_{orig} varies (green), α_{eff} (dark red), SST (pink)~~and~~ , h_0 (purple), rain evaporation (dashed brown) and horizontal advection (dashed blue). the tropical mean δD_0 was added to each contribution to plot on the same scale as simulated δD_0. The number of samples in each bin is indicated on a logarithmic scale on the right-hand-side (dotted black line).

Regime	Ascending		Subsiding	
	correlation coefficient	slope	correlation coefficient	slope
r_{orig} ~~,~~	0.46	0.52	0.42	0.82
α_{eff} ~~,~~	0.34	0.35	0.14	0.40
SST ~~and~~	-0.12	-0.01	0.25	0.22
h_0 ~~variations. For each contribution, we show~~	0.06	0.26	0.15	0.39
rain evaporation	0.49	0.48	0.19	0.20
horizontal advection	-0.26	-0.24	-0.15	-0.31

Table 3. As in table 4 but at the ~~correlation coefficient of the linear regression of the contribution as a function of δD_0~~daily scale. The ~~threshold for the~~ correlation ~~coefficient to be statistically significant at 99 % is 0.15 or lower in~~ coefficients and slopes are averaged over all ~~cases. The analysis is done~~ seasons and locations over tropical oceans ($30°N-30°S$, ocean fraction>80%), separately for ascending and subsiding regimes. ~~All seasons and tropical oceans locations are considered.~~

In regions of strong large-scale ascent, r_{orig} is larger mainly because h_{orig} is larger (Fig. 9e, 10a pink). This ~~suggests that even though the effect of rain evaporation may artificially bias high the estimate of r_{orig} , a substantial part of the r_{orig} signal is actually physical. Indeed, if the large r_{orig} was purely an artifact of the neglect of rain evaporation, it would translate totally into a lower z_{orig}. Physically, the~~ is because the moister the FT, the higher the contribution of vapor coming from above to the vapor of the SCL, and thus the higher r_{orig} and the more depleted δD_0. This mechanism through which a moister FT leads to a more depleted δD_0 is consistent with that argued in B15. z_{orig} damps this effect: when convection is stronger and the FT moister, convection is also deeper, so the air originates from higher in altitude where the air is drier.

In very stable regions, r_{orig} is larger ~~mainly~~ because q_0 is ~~small~~ larger (Fig. 9c, 10b green), consistent with the drier conditions in these regions of large-scale descent~~, and~~. Note that this effect can be seen only in most stable regions, but when considering all subsiding regions, the contribution is small (Table 2). r_{orig} is larger also because z_{orig} is lower in altitude (Fig. 9d, 10b red)~~, consistent with the shallower boundary layers as EIS increases. Physically, the lower in altitude the~~. As EIS increases, the boundary layers are shallower, the air comes from ~~, the higher~~ lower in altitude, r_{orig} ~~and the more depleted~~is higher and thus δD_0 is more depleted. This mechanism was not considered in ~~Benetti et al. (2015)~~ B15 but our decomposition shows that it is a key mechanism driving r_{orig} and thus δD_0 variations in stable regions.

Quantitatively, in ascending regions, the main ~~factors~~ factor controlling the seasonal-spatial variations in r_{orig} ~~are~~ is h_{orig} (~~94~~182 %)~~and~~, dampened by z_{orig} (~~61~~-67 %) (Table 4). ~~Similarly, in~~ In descending regions, the main ~~factors are~~ factor is also h_{orig} (~~91~~96 %)~~and~~, followed by z_{orig} (~~72~~41 %) (Table 4). At the daily scale, the same two factors dominate the variability of r_{orig}: h_{orig} and z_{orig} contribute to ~~67~~78 % and ~~76~~39 % of r_{orig} variations in average over ascending regions, and to ~~104~~118 % and ~~73~~39 % in average over descending regions (Table 5).

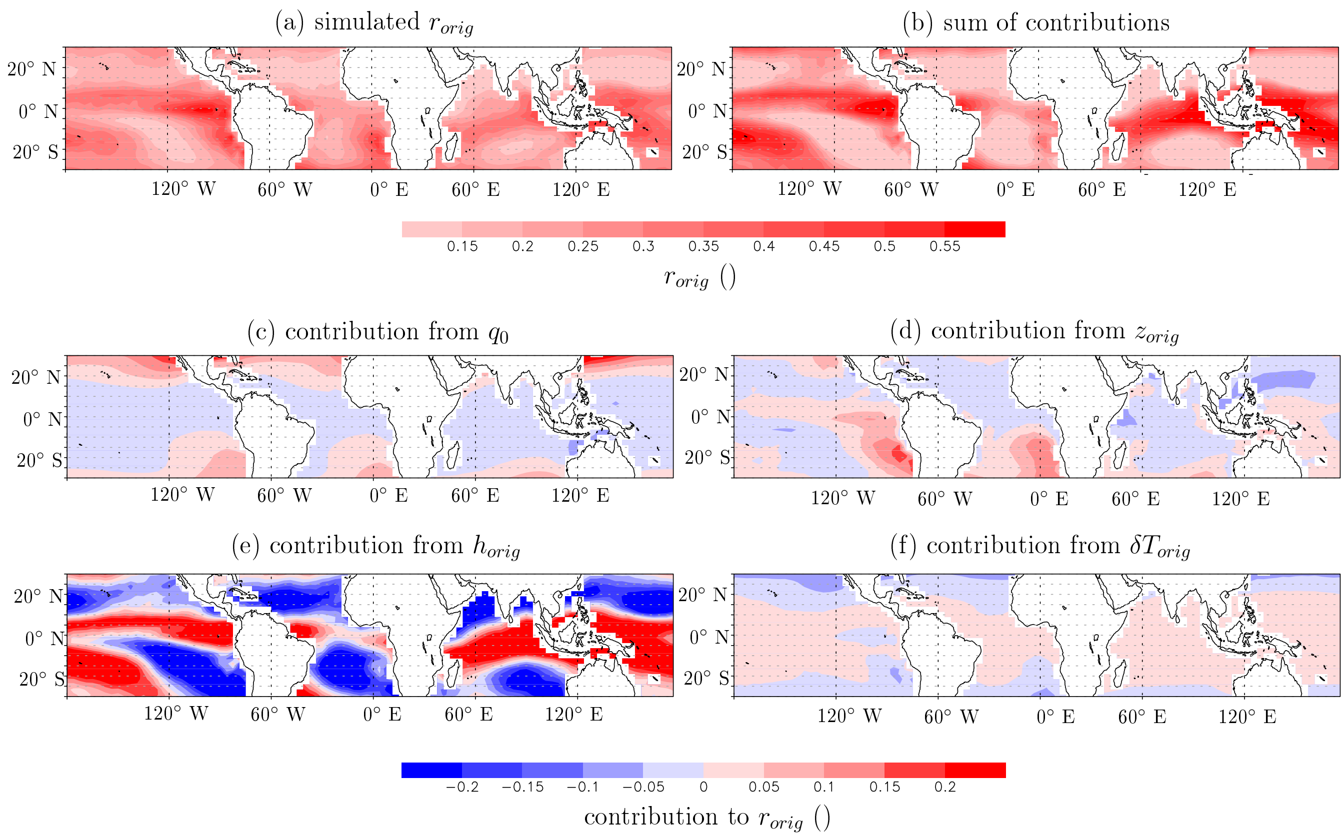

Figure 9. a) Map of winter-mean r_{orig} simulated by LMDZ. b) Map of winter-mean r_{orig} reconstructed as the sum of the 4 contributions. Tropical-mean r_{orig} was added to compare with a with the same color scale. c) Map of winter-mean r_{orig} calculated from Eq. (11) if only q_0 varies (see section 3.6). d) Same as b but of only z_{orig} varies. e) Same as b but if only $h(z_{orig})$ varies. f) Same as b but if only δT_{orig} varies.

4.3 ~~Entrainment~~ Estimating altitude ~~estimate~~ z_{orig}

Estimated altitude z_{orig} is minimum in dry subsiding regions, especially in upwelling regions (Fig. 11a, Fig. 12), corresponding to regions with the strongest inversion (Fig. 11). This contributes to the depleted δD_0 in these regions.

As explained in 3.3, our estimate of z_{orig} may be artificially biased due to the neglect of some processes in our theoretical framework. Ideally, to check whether z_{orig} really physically represents the altitude from which the air originates, additional model experiments where water vapor from different levels are tagged (Risi et al., 2010b) would be needed. While we leave this for future work, ~~in the meanwhile~~ we check whether z_{orig} estimates are consistent with what we expect based on what we know about mixing processes in the marine boundary layers. We expect that in strato-cumulus regions, air ~~is entrained~~ originates from a very shallow (a few tens of meters) layer above the inversion, whereas the mixing processes may be more diverse, and possibly deeper in the FT, as the boundary layer deepens (Fig. 1).

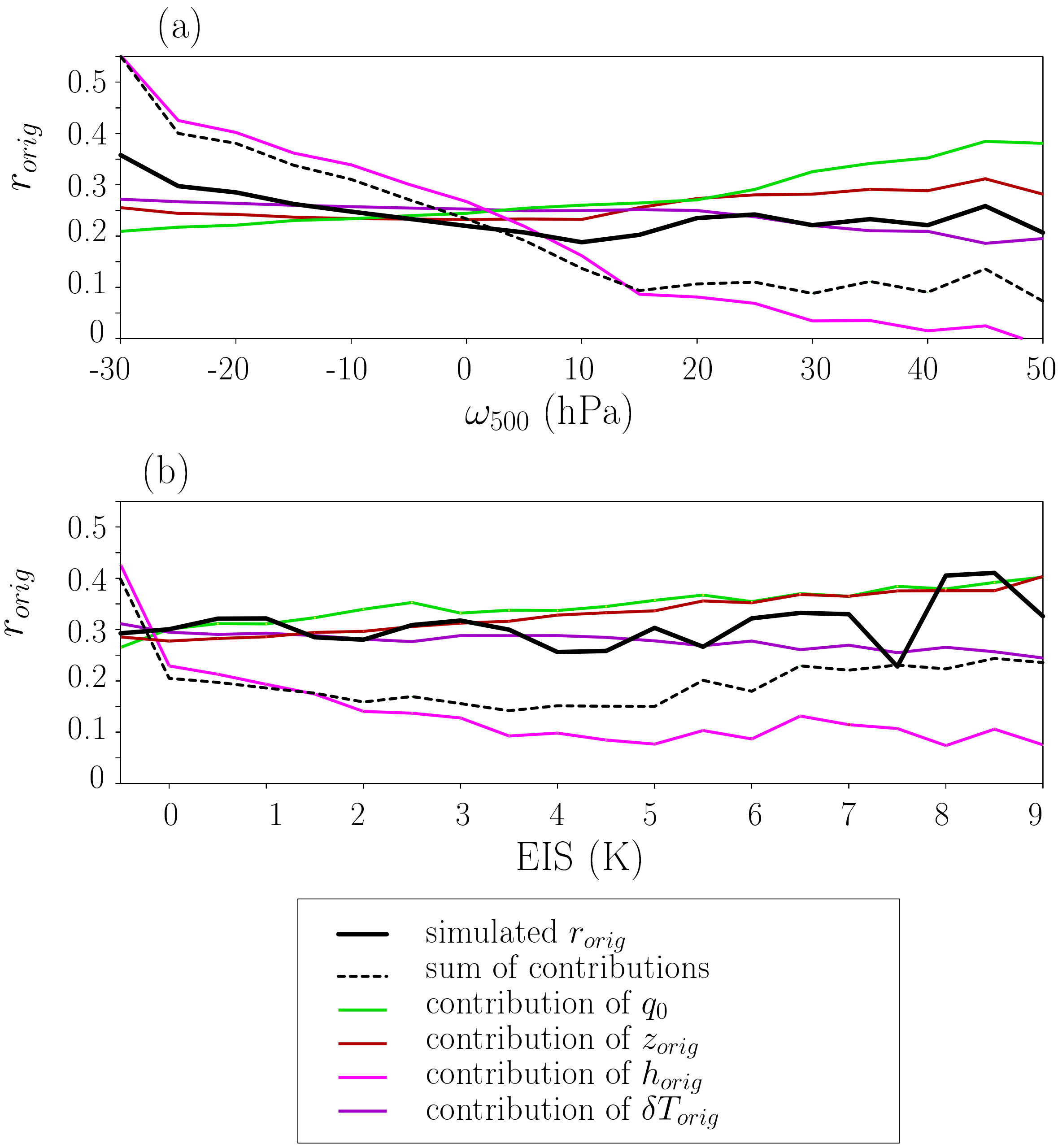

Figure 10. Composites as a function of ω_{500} (a) and of EIS (b) of the seasonal averages of r_{orig} simulated by LMDZ over all tropical ocean locations (black). Same for the sum of the contributions (black dashed) and for each individual contribution to r_{orig} : q_0 varies (green), z_{orig} (dark red), $h(z_{orig})$ (pink) and δT_{orig} (purple). The number of samples in each bin is indicated on a logarithmic scale on the right-hand-side as bars.

Regime	Ascending		Subsiding	
	correlation coefficient	slope	correlation coefficient	slope
q_0	~~-0.24~~ -0.82	~~0.0~~ -0.33	~~0.09~~ 0.21	~~0.0~~0.12
z_{orig}	~~0.88~~ -0.91	~~0.61~~ -0.67	~~0.65~~ 0.77	~~0.72~~0.41
h_{orig}	~~0.75~~ 0.98	~~0.94~~ 1.82	0.53	~~0.91~~0.96
δT_{orig}	~~0.33~~ 0.55	~~0.12~~ 0.06	~~-0.34~~ -0.37	~~-0.27~~ -0.12

~~Decomposition of the spatial-seasonal variation in r_{orig} into its 4 contributions: effect of~~

Table 4. Decomposition of the spatial-seasonal variation in r_{orig} into its 4 contributions: effect of q_0, z_{orig}, h_{orig} and δT_{orig} variations. For each contribution, we show the correlation coefficient of the linear regression of the contribution as a function of r_{orig}. The analysis is done separately for ascending and subsiding regimes. All seasons and locations over tropical oceans ($30°N - 30°S$, ocean fraction>80%) are considered. The threshold for the correlation coefficient to be statistically significant is 0.15 or lower in all cases. We write correlation coefficient and slope values between brackets when they are not significant at 99%.

Regime	Ascending		Subsiding	
	correlation coefficient	slope	correlation coefficient	slope
q_0 ~~,~~	-0.37	-0.04	-0.23	-0.07
z_{orig} ~~,~~	0.91	0.39	0.80	0.39
h_{orig} ~~and~~	0.58	0.78	0.58	1.18
δT_{orig} ~~variations. For each contribution, we show~~	-0.14	0.01	-0.23	-0.12

Table 5. As in table 4 but at the ~~correlation coefficient of the linear regression of the contribution as a function of r_{orig}~~daily scale. The ~~threshold for the~~ correlation ~~coefficient to be statistically significant is 0.15 or lower in~~ coefficients and slopes are averaged over all ~~cases. The analysis is done~~ seasons and locations over tropical oceans ($30°N - 30°S$, ocean fraction>80%), separately for ascending and subsiding regimes. ~~All seasons and tropical oceans locations are considered.~~

To check whether estimated z_{orig} is consistent with this picture, we compare z_{orig} to $z_{orig,r_{orig}=0.6}$ (z_{orig} that we would estimate is r_{orig} was set constant to 0.6) and z_i (section 3.4), which are measures of the altitude of the humidity drop and temperature inversion respectively. As expected from Fig. 1, they are minimum in dry upwelling regions, intermediate in trade-wind regions, and maximum values in convective regions (Fig. 11c-d, 12 green, blue). Therefore, the low z_{orig} in upwelling regions reflects the low z_i. Consistently, in subsiding regions, z_{orig} correlates well with $z_{orig,r_{orig}=0.6}$ (correlation coefficient of 0.52, statistically significant beyond 99 %). If we focus on very stable regions only (EIS>7 K), z_{orig} correlates well with both $z_{orig,r_{orig}=0.6}$ and z_i (correlation coefficient of 0.58 and 0.52 respectively, statistically significant beyond 99 %). The altitude z_{orig} is a few meters above the inversion in strato-cumulus regions, and up to 1km above the inversion in cumulus and deep convective regions (Fig. 12), consistent with our expectations from Fig. 1. This lends support to the fact that at least in subsiding regions, our isotope-based z_{orig} estimate effectively ~~reflect~~ reflects the origin of air coming from above.

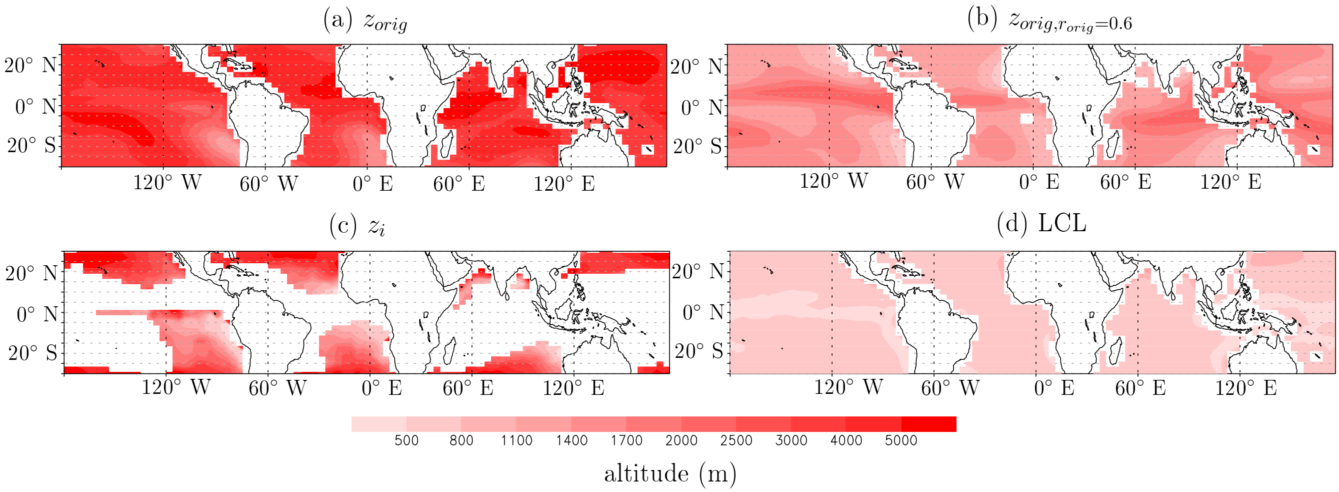

Figure 11. a) Map of winter-mean z_{orig} estimated from δD_0 simulated by LMDZ. b) Same as a but z_{orig} that we would estimate if r_{orig} was constant set to 0.6 ($z_{orig,r_{orig}=0.6}$). c). Same as a but for z_i simulated from LMDZ. Only days when EIS>2 K are considered, otherwise z_i is difficult to estimate. d) Same as a but for LCL simulated by LMDZ.

In ascending regions, in contrast, z_{orig} does not correlate significantly with $z_{orig,r_{orig}=0.6}$ or z_i. This may indicate either that our z_{orig} estimate is biased by neglected processes such as rain evaporation, or that in deep convective regions, the origin of FT air into the SCL is very diverse due to the variety of mixing processes (1).

5 Results from observations

To check whether our results obtained with LMDZ are realistic, we apply our methods to the measurements gathered during the STRASSE campaign. ~~In the absence of measured δD profiles, we assume that α_{eff} is 1.07 based on LMDZ simulation~~For simplicity and in absence of all necessary measurements, here we neglect the effects of rain evaporation and horizontal advection.

Throughout the cruise, δD_0 shows a large variability, ranging from around -75 ‰ in quiescent conditions to -120 ‰ during the two convective conditions (Benetti et al., 2014) (Fig. 13a red). Variability in r_{orig} is the major factor contributing to this variability (58 %) (Fig. 13a green, Table 6). This crucial importance of mixing processes is consistent with B15.

During the two convective events, the estimated r_{orig} saturates at 1 (Fig. 13b). This proves that r_{orig} estimated in these conditions is biased high because it encapsulates the effect of neglected processes, i.e. depletion by rain evaporation. Equation (9) is not valid in this case. In addition, at the scale of a few hours, the steady-state assumptions may be violated. Rain evaporation may strongly deplete the SCL before surface evaporation has the time to play its dampening role, hence the possibility to reach very low δD_0 that cannot be predicted even when considering rain evaporation (appendix B).

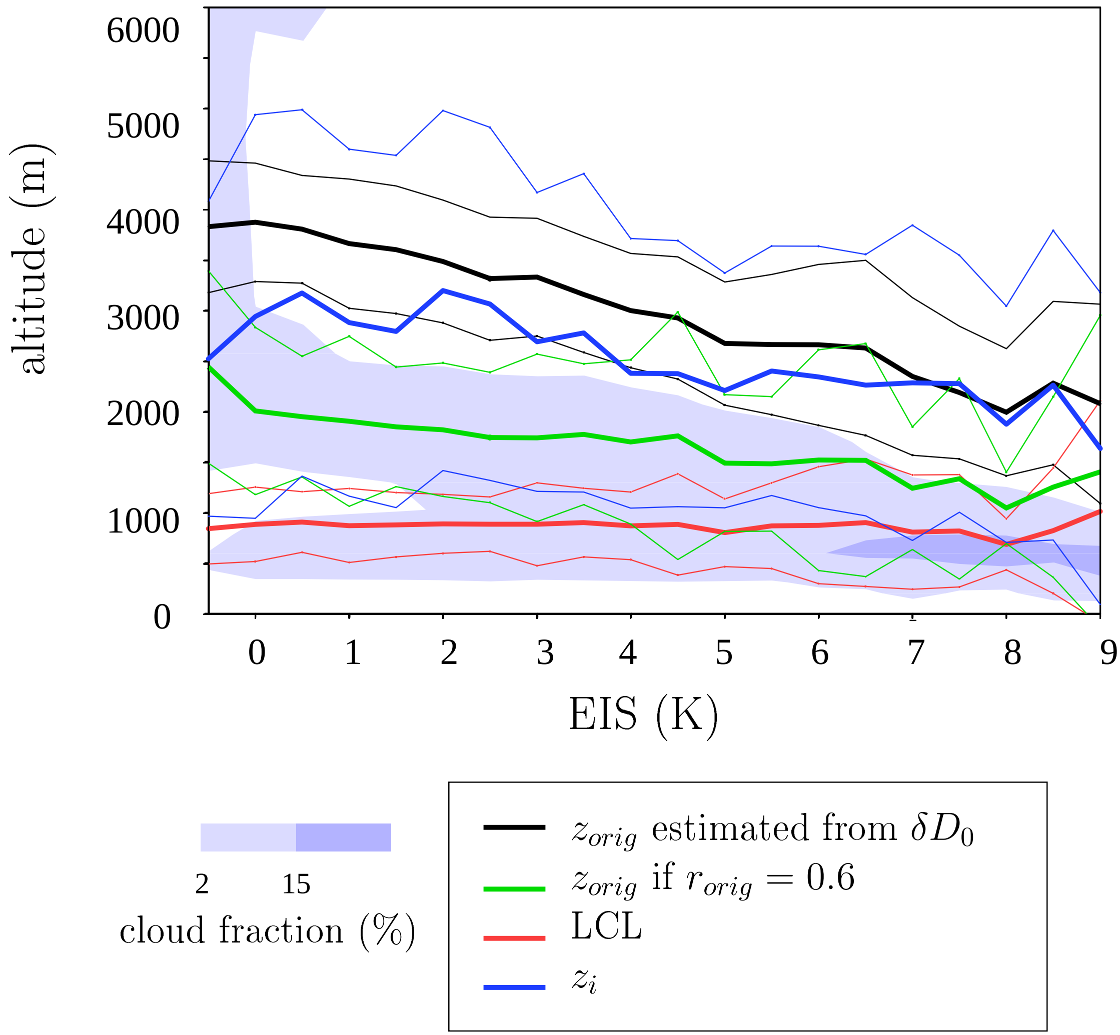

Figure 12. Composites as a function of EIS of seasonal-mean of z_{orig} (black), $z_{orig,r_{orig}=0.6}$ (green), z_i (blue) and LCL (red). The composite profiles of cloud cover are also shown, showing deep clouds when EIS is close to 0 and shallowest clouds when EIS is largest.

contributions to δD_0	correlation coefficient	slope
r_{orig}	0.77	0.58
SST	0.57	0.16
h_0	0.40	0.48

Table 6. Same as Table 2 but for the STRASSE observations. Linear regressions are calculated among 1977 data points.

contributions to r_{orig}	correlation coefficient	slope
q_0	-0.46	-1.49
z_{orig}	0.66	0.90
h_{orig}	0.81	0.70
δT_{orig}	-0.36	-0.91

Table 7. Same as Table 4 but for the STRASSE observations. Linear regressions are calculated among 55 data points, so that correlation coefficients above 0.35 are statistically significant at 99 %.

During the rest of the cruise, the main factors controlling the r_{orig} variability are z_{orig} (90 %) and h_{orig} (70 %). The importance of FT humidity in controlling r_{orig} was already highlighted in B15. However, in their paper, the variability in z_{orig} was neglected, whereas it appears here as the main factor.

Through September, the ~~cruises~~ cruise goes from a shallow boundary layer in early September to deeper boundary layers with higher inversions, before reaching the convective conditions (Fig. 13c). Consistently with this deepening boundary layer, the air ~~is entrained~~ originates from increasingly higher in altitude. ~~When considering only the~~ Remarkably, there are 6 ~~data points when z_{orig} <2000 m,~~ days when z_{orig} coincides ~~almost exactly~~ with z_i with a root means square error of 31‰ and correlation coefficient of 0.996 (Fig. 13c~~; the correlation coefficient between z_{orig} and z_i is 0.996~~). This indicates that the air ~~is entrained into the SCL exactly~~ exactly comes from the inversion layer. ~~Even if the number of sample is small, the coincidence is remarkable, especially when~~ When recalling that z_{orig} and z_i are estimated from completely independent observations~~. This~~ , the coincidence is remarkable and lends support to the fact that on these days, our z_{orig} estimate is physical. However, there remains 9 days when z_{orig} is much higher than z_i. This may reflect more penetrative downdrafts as we approach deeper convective regimes. But it may also be an artifact of our neglect of horizontal advection. For example, on these days which are characterized by lower h_0, neglecting the advection of enriched water vapor from nearby regions with higher h_0 could be mis-interpreted as lower r_{orig} and thus higher z_{orig}.

6 Discussion: what can we learn from water isotopes on mixing processes?

We have shown in the previous section that one of the main factors controlling δD_0 at the seasonal-spatial and daily scale are the proportion of the water vapor in the SCL that ~~is~~ originates from above (r_{orig}), and that one of the main factor controlling r_{orig} is the altitude from which the air originates (z_{orig}). In turn, could we use water vapor isotopic measurements to constrain

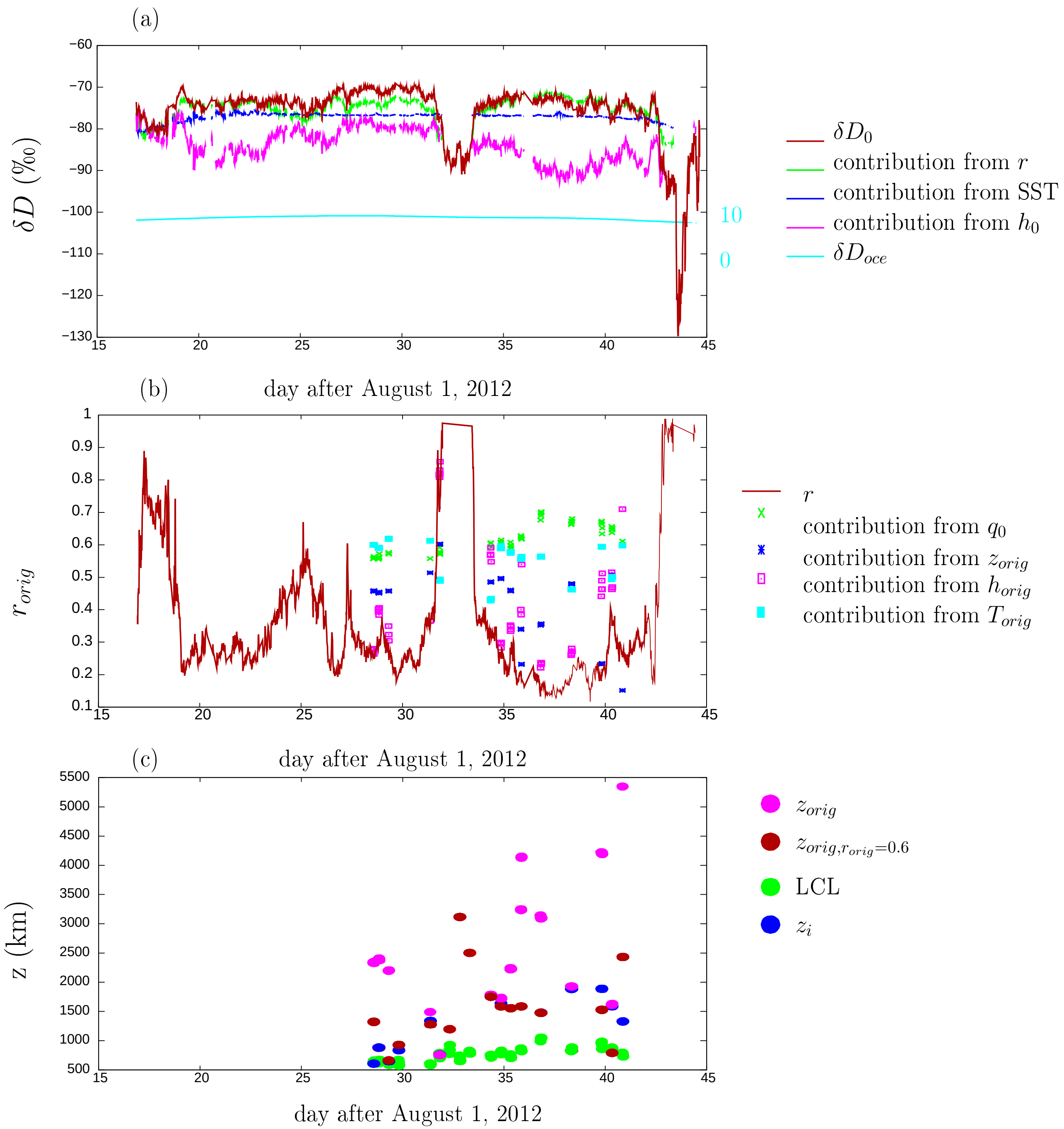

Figure 13. a) Time series of δD_0 observed during the STRASSE cruise, together with its 4 contributions. The δD of the surface ocean water is also plotted with the scale on the right. b) Time series of r_{orig} estimated from observations during the STRASSE campaign, together with its 4 contributions. c) Times series of z_{orig}, $z_{orig,r_{orig}=0.6}$, LCL and z_i estimated from the STRASSE observations.

z_{orig}? This would open the door to discriminating between different mixing processes at play (Fig. 1). Since mixing processes are crucial to determine the sensitivity of cloud fraction to SST (Sherwood et al., 2014; Bretherton, 2015; Vial et al., 2016), such a prospect would allow us to improve our knowledge of cloud feedbacks, and hence of climate sensitivity.

With this in mind, we assess the errors associated with z_{orig} estimates from δD_0 measurements, and discuss whether ~~there~~ they are small enough for z_{orig} estimates to be useful. In strato-cumulus clouds where the air is believed to ~~be entrained~~ originate from the first few tens of meters above cloud top (Faloona et al., 2005; Mellado, 2017), z_{orig} estimates are not useful if the errors are larger than a few tens of meters, e.g. 20 m. In cumulus clouds where mixing processes are more diverse and possibly deeper (Fig. 1), z_{orig} estimates may be useful if errors are of the order of 80 m.

Let's assume that we have a field campaign where we measure δD_0, surface meteorological variables, temperature and humidity profiles (e.g. radio-soundings), and a few δD profiles (e.g. by aircraft). This is what we can expect for example from the future EUREC4A (Elucidating the role of clouds-circulation coupling in climate) campaign to study trade-wind cumulus clouds (Bony et al., 2017). Below we quantify the effects of five sources of uncertainty on z_{orig} estimates.

6.1 Measurement errors

The first source of uncertainty ~~that we have highlighted in this article is the effect of rain evaporation. As long as the microphysical processes and associated isotopic fractionation processes are not well constrained~~are measurement errors. We re-calculate z_{orig} assuming an error of 0.4 ‰ on δD_0 (typical of what we can measure with in-situ laser instruments, Aemisegger et al. (2012); Benetti et al. (2014)) and 1 ‰ on δD_f (larger errors due to lower humidity and the increased complexity of measurements in altitude). The averaged errors on z_{orig} and their standard deviations are plotted as a function of EIS in Fig. 14a. Whereas errors on δD_f lead to errors on z_{orig} of the order of 20 m (Fig. 14a, green), errors on δD_0 lead to errors on z_{orig} of the order of 80 m (Fig. 14a, red). Yet in strato-cumulus, none expects the air to originate from a higher altitude than 80 m above the inversion. Therefore, δD_0 measurements would need to be more accurate than usual to be useful in strato-cumulus regions, i.e. 0.1 ‰ to yield a 20 m precision on z_{orig}. In trade-wind cumulus regions, the precision of 0.4 ‰ is enough for z_{orig} to be useful.

6.2 Neglecting rain evaporation

The second source of uncertainty is associated with neglecting rain evaporation. This effect can be quantified in a model, but it is very difficult to quantify in nature because it is complicated and uncertain to measure η (Rosenfeld and Mintz, 1988), and it is even more complicated to measure or predict α_{evap}. Rain evaporation can have a depleting or enriching effect depending on microphysical details that are too complex to be addressed here (Graf et al., 2019). Neglecting rain evaporation leads to an error of the order of 500 m in regions of low EIS and 250 m in regions of strong EIS (Fig. 14b, brown). In regions of strato-cumulus regions, rain evaporation is a significant source of error in spite of the relatively small amount of precipitation available to evaporate. This is because total evaporation of the rain efficiently enriches the SCL, and easily modifies δD_0 by more than the 0.1‰ targeted precision explained above. However, it is ~~safer to restrain z_{orig} estimates to non-precipitating clouds~~possible that LMDZ overestimates this source of error in trade-wind cumulus and strato-cumulus regions. LMDZ is one of the GCMs producing the strongest rain in srato-cumulus regions (Zhang et al., 2013), and GCMs are known to trigger convection to often in trade-wind cumulus regions (Nuijens et al., 2015a, b).

~~The second~~

6.3 Neglecting horizontal advection

The third source of uncertainty is ~~the~~ associated with horizontal advection. In nature, ϕ can be estimated from meteorological analyzes and β can be estimated from near-surface isotopic measurements at several locations (e.g. sounding arrays during typical field campaigns). In absence of these additional measurements, neglecting this effect leads to an error of the order of 800 m (Fig. 14b, purple). This limits the usefulness of z_{orig} estimates for all cloud regimes.

6.4 Daily variability in the steepness of δD profiles

The fourth source of uncertainty arises from the daily variability in α_{eff} ~~. Measuring daily~~ (appendix D2). Estimating α_{eff} requires to measure δD_f at 500 hPa. Satellite measurements are available but are affected by random errors that are too large for our application (Worden et al., 2011, 2012; Lacour et al., 2015). Precise in-situ measurements of water vapor δD ~~profiles is~~ in altitude are costly and difficult (Sodemann et al., 2017).

Let's assume that we have only one ~~profile~~ δD_f value that represents the seasonal-average at a given location. ~~The daily standard deviation of α_{eff} ($\sigma_{\alpha_{eff}}$) for a given season ranges from 5‰ in the Central Atlantic to 40‰ near the Maritime Continent (Fig. D1d).~~ To estimate the resulting error on z_{orig}, we re-estimate z_{orig} every day and at each location using $\bar{\alpha_{eff}} + \sigma_{\alpha_{eff}}$ and $\bar{\alpha_{eff}} - \sigma_{\alpha_{eff}}$. The error on z_{orig} is calculated as $\left(z_{orig}(\bar{\alpha_{eff}} - \sigma_{\alpha_{eff}}) - z_{orig}(\bar{\alpha_{eff}} + \sigma_{\alpha_{eff}})\right)/2$. The averaged error and its standard deviation is plotted as a function of EIS in Fig. 14c (black). It is of the order of 400m, and rarely below 200m. If we attempt to estimate α_{eff} as the fractionation coefficient as a function of local temperature, errors would be even more dissuasive (Fig. 14c, blue).

Therefore, estimating z_{orig} from daily δD_0 measurements cannot be useful unless we measure ~~daily δD profiles~~ δD_f on a daily basis as well. Practically, we could imagine measuring FT properties (δD_f) at the top of a mountain while we measure δD_0 at the sea level (e.g. on Islands such as Hawaii or La Réunion, ~~Galewsky et al. (2007); Bailey et al. (2013); Guilpart et al. (2017)). We could also imagine retrieving α_{eff} from daily~~ Galewsky et al. (2007); Bailey et al. (2013); Guilpart et al. (2017)).

6.5 Rayleigh assumption for the shape of δD profiles

Finally, a fifth source of uncertainty comes the assumption that the δD ~~profiles retrieved from space by IASI (Infrared Atmospheric Sounding Interferometer, Lacour et al. (2012, 2015)) , but this would be associated with additional errors whose estimate is beyond the scope of this paper~~profile follows a Rayleigh distillation line (section 2.2). However, both in LMDZ (appendix D1) and nature (Sodemann et al., 2017), δD profiles are usually intermediate between Rayleigh and mixing lines. The precision of our z_{orig} estimate is maximum in the Rayleigh distillation case.

~~The third source of uncertainty are measurements errors. We recalculate~~ When trying to find a numerical solution for z_{orig} ~~assuming an error of 0.4 ‰ on δD_0 (typical of what we can measure with in-situ laser instruments, Benetti et al. (2014))and 1 ‰ on δD_f (larger errors due to lower humidity and the increased complexity of measurements in altitude). Whereas errors on δD_f lead to errors on~~ directly from Eq. (6), a solution can be found only in 0.1 % of cases. This is because simulated δD profiles are often close to a mixing line in the lower troposphere (appendix D1). Whatever z_{orig} ~~of the order of 20 m (Fig. 14, green), errors on~~ in the lower troposphere, the δD_0 ~~lead to errors on~~ calculated from Eq. (6) is nearly constant because the δD profile is close to a mixing line (appendix A, Fig. 4b). Whatever z_{orig} ~~of the order of 80 m. This is higher than the upper bound for the expected entrainment altitude in strato-cumulus. Therefore,~~ in the middle troposphere, the δD_0 ~~measurements would need to be more accurate than usual to be useful in strato-cumulus regions, i.e. 0.1 ‰ to yield a 20 m precision on~~ calculated from Eq. (6) is also nearly constant because r_{orig} there is very small. So whatever z_{orig}~~. In~~, the δD calculated from Eq. (6) is nearly constant, and the numerical solution fails.

However, it is possible that δD profiles simulated by LMDZ are closer to mixing lines than real profiles, since GCMs are known to overestimate vertical mixing through the troposphere (Risi et al., 2012b) and to mix the lower free troposphere too frequently by deep convection in trade-wind ~~cumulus regions , the precision is enough for z_{orig} to be useful.~~ regions (Nuijens et al., 2015a, b). Therefore, the shape of δD profiles simulated by LMDZ is not a sufficient reason to reject the Rayleigh assumption. The uncertainty associated with this assumption is very difficult to quantify in LMDZ. More measurements of full δD profiles are very welcome to help quantify it.

To summarize, δD_0 measurements could potentially be useful to estimate z_{orig} with a useful precision~~in cumulus and strato-cumulus clouds, but only if we are able to measure daily~~, but if we measure daily δD_f in the mid-troposphere, if the shape of δD profiles ~~and if~~ can be better documented, if we measure δD_0 at different places to quantify the effect of horizontal advection, and if we can invent innovative techniques to better quantify the effect of rain evaporation. In addition in strato-cumulus clouds, we need to measure δD_0 with an accuracy of 0.1 ‰~~and 0.4 ‰ in trade-wind cumulus and strato-cumulus clouds respectively~~.

7 Conclusion

We propose an analytical model to predict the water vapor isotopic composition δD_0 of the sub-cloud layer (SCL) over tropical oceans. ~~Benetti et al. (2015) extended the Merlivat and Jouzel (1979)~~ This model relies on the hypothesis that the altitude from which the air originates, z_{orig}, is an important factor. We build on Benetti et al. (2015) who extended the Merlivat and Jouzel (1979) closure equation to make explicit the link between δD_0 and ~~FT entrainment~~mixing processes. We further extend ~~the Benetti et al. (2015) equationin two ways: first, we assume that we know the shape of~~ their equation: we assume a shape for the δD vertical profiles ~~, and second, we let the altitude from which the air originates, z_{orig}, vary~~as a function of q, and we account for horizontal advection and rain evaporation effects.

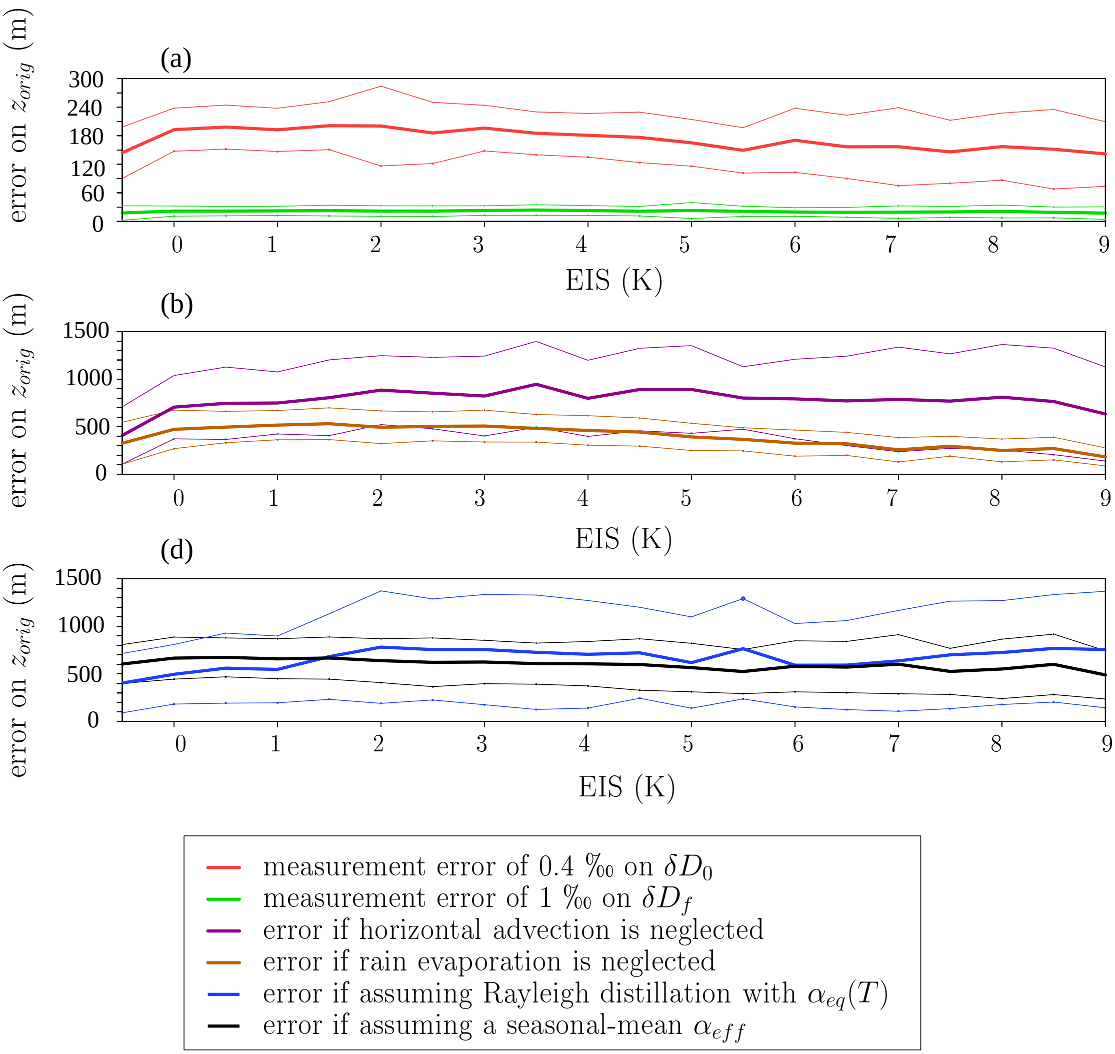

Figure 14. Errors when estimating z_{orig} from δD_0 observations, as a function of EIS, as predicted by LMDZ~~: error if one uses α_{eq} as~~. a~~function of local temperature to estimate α_{eff} , error if one uses the seasonal-mean profile instead of the daily profile to estimate α_{eff} (black~~) ~~, error~~ Error we would make if δD_0 is measured with a 1‰ error (red), and error we would make if δD_f is measured with a 1‰ error (green). b) error we would make if we neglect horizontal advection effects (purple) and rain evaporation effects (brown). c) Error if one uses α_{eq} as a function of local temperature to estimate α_{eff} (blue), error if one uses the seasonal-mean profile instead of the daily profile to estimate α_{eff} (black). The standard deviations among all daily errors estimated in each bin of EIS are also shown.

The resulting equation highlights the fact that δD_0 is not sensitive to the intensity of ~~entrainment~~mixing processes. Therefore, it is unlikely that water vapor isotopic measurements could help estimate the entrainment velocity that many studies have ~~strived~~ striven to estimate (Bretherton et al., 1995). In contrast, δD_0 is sensitive to the altitude from which the air originates. Based on a simulation with LMDZ and observations during the STRASSE cruise, we show that z_{orig} is an important factor explaining the seasonal-spatial and daily variations in δD_0, especially in subsidence regions. In turn, could δD_0 measurements, combined with vertical profiles of humidity, temperature and δD, help estimate z_{orig} and thus discriminate between different mixing processes? ~~This should rely on a good knowledge of the δD vertical profiles. We find that for~~ For such isotope-based estimates of z_{orig} to be useful, we would need ~~frequent vertical profiles of~~ a precision of a few hundreds meters in deep convective regions and smaller than 20 m in strato-cumulus regions. To reach this target, we would need daily measurements of δD in the mid-troposphere and very accurate measurements of δD_0, which are currently difficult to obtain. ~~In precipitating clouds and deep convection~~We would also need information on the horizontal distribution of δD to account for horizontal advection effects, and full δD profiles to quantify the uncertainty associated with the assumed shape for δD profiles. Finally, rain evaporation is ~~too large a source of uncertainty, whereas in~~ an issue in all regimes, even for strato-cumulus ~~regions, very precised estimates of z_{orig} (no larger than 20 m) would be needed to be useful. Therefore, it is in regions of shallow cumulus clouds that such isotope-based estimates of z_{orig} would be most useful.~~ clouds. Innovative techniques would need to be developed to quantify this effect from observations.

This study is preliminary in many respects. First, it would be safe to check using water tagging experiments in LMDZ that z_{orig} estimates really ~~represents~~ represent the altitude from which the air ~~is~~ originates, and is not ~~to biases~~ biased by our simplifying assumptions. Second, the coarse vertical resolution of LMDZ, and the simplicity of mixing parameterizations (e.g. cloud top entrainment is not represented) are a limitation of this study. Ideally, the relationship between δD_0, z_{orig} and the type of mixing processes should be investigated in isotope-enabled Large Eddy Simulations (LES) (Blossey et al., 2010; Moore et al., 2014). Artificial tracers and structure detection methods (Park et al., 2016; Brient et al., 2019), combined with conditional sampling methods (Couvreux et al., 2010), could help detect the different kinds of mixing structures, estimate their contributions to vertical transport, and describe their isotopic signature. This would allow us to confirm, or infirm, many of the hypotheses and conclusions in this paper. Finally, if the sensitivity of δD_0 to the type of mixing processes is confirmed, paired isotopic simulations of single-column model (SCM) versions of general circulation models (GCM) and LES, forced by the same forcing, could be very useful to help evaluate and improve the representation of mixing and entrainment processes in GCMs, as is routinely the case for non-isotopic variables (Randall et al., 2003; Hourdin et al., 2013; Zhang et al., 2013).

Code and data availability. LMDZ can be downloaded from http://lmdz.lmd.jussieu.fr/. Program codes used for the analysis are available on https://prodn.idris.fr/thredds/catalog/ipsl_public/rlmd698/article_mixing_processes/d_pgmf/catalog.html.

Isotopic measurements from STRASSE can be downloaded from http://cds-espri.ipsl.fr/isowvdataatlantic/. All other datasets and processed files are available on https://prodn.idris.fr/thredds/catalog/ipsl_public/rlmd698/article_mixing_processes/catalog.html.

Appendix A: Closure if the tropospheric profile follows a mixing line

For simplicity, we neglect here horizontal advection and rain evaporation effects, but results would be similar otherwise. If we assume that R_{orig} is uniquely related to q_{orig} through a mixing line between the SCL air and a dry end-member (q_f, R_f):

$$q_{orig} = a \cdot q_0 + (1-a) \cdot q_f \tag{A1}$$

and

$$R_{orig} = a \cdot q_0 \cdot R_0 + (1-a) \cdot q_f \cdot R_f \tag{A2}$$

Reorganizing Eq. (A1), we get $a = \frac{r-p}{1-p}$ with $p = q_f/q_0$. Since $q_f \leq q_{orig} \leq q_0$, $p \leq r_{orig}$. Injecting Eq. (A2) into 6, we get:

$$R_0 = \frac{R_{oce}/\alpha_{eq} + p/(1-p) \cdot R_f \cdot \alpha_K \cdot (1-h_0)}{h_0 + \alpha_K \cdot (1-h_0)/(1-p)} \tag{A3}$$

As a consistency check, in the limit case where the end-member is totally dry ($p = 0$), we find the MJ79 equation, i.e. Eq. (10).

It is intriguing to realize that r_{orig} has disappeared from Eq. (A3). This can be understood physically: if the vertical profile follows a mixing line, it does not matter ~~at~~ from which altitude the air comes~~from~~: ultimately, what matters is how much dry air has been mixed directly or indirectly into the SCL. This can be visualize in Fig. 4b. Therefore, if R_{orig} follows a mixing line, we lose the sensitivity to z_{orig}.

Appendix B: ~~Modification in case of~~ Diagnostics for rain evaporation in LMDZ

~~An important assumption that led to Eq. (9)is the neglect of SCL moistening by rain evaporation. Here we test the sensitivity to this assumption by adding a rain evaporation component. The new water vapor~~ Rain evaporation can be accounted for in equation 8 if we can quantify η, the ratio of water vapor originating from rain evaporation to that originating from surface evaporation, and α_{evap}, the ratio of isotopic ratio in the rain evaporation flux to R_0.

B1 Equations

In LMDZ, two parameterization schemes can produce rain evaporation: the convective scheme and the large-scale condensation scheme. Their respective precipitation evaporation tendencies, $(dq/dt)_{evap,conv}$ and ~~isotopic budgets of the SCL write~~$(dq/dt)_{evap,lsc}$, are given in $kg_{water} \cdot kg_{air}^{-1} \cdot s^{-1}$ and are used to calculate F_{evap} in $kg_{water} \cdot m^{-2} \cdot s^{-1}$:

$$\cancel{M \cdot q_{orig} + F + E = (N + D) \cdot q_0}$$

$$F_{evap} = \sum_{k=1}^{k_{LCL}} \left((dq/dt)_{evap,conv} + (dq/dt)_{evap,lsc} \right) \cdot \frac{\Delta P_k}{g}$$

$$M \cdot q_{orig} \cdot R_{orig} + F \cdot R_F + E \cdot R_E = (N + D) \cdot q_0 \cdot R_0$$

~~where F is the rain evaporation flux~~ where k_{LCL} is the last layer below the LCL, ΔP_k is the depth of layer k in pressure coordinate and g is gravity.

The isotopic equivalent of this flux, $F_{evap,iso}$, is used to calculate $R_{evap} = F_{evap,iso}/F_{evap}$. ~~We note $F = \eta \cdot E$. We write the isotopic composition of the rain evaporation, R_F, as~~

Only grid boxes and days where $F_{evap} > 0.05$ mm/d are considered to calculate α_{evap}. This represents 94.0% of all tropical oceanic grid boxes.

B2 Results

Consistent with the larger amount of precipitation available for evaporation, η is maximum in regions of deep convection, reaching 30% around the Maritime continent (Fig. C1a). It is minimal over the dry descending regions, reaching 5% off the coasts of Mauritania, Peru or Namibia. The rain evaporation is more depleted than the SCL in regions of strong deep convection, by as much as 70‰ around the Maritime continent (Fig. C1b). When the fraction of raindrops that evaporate is small, as is the case in such moist regions, isotopic fractionation favors evaporation of the lighter isotopologues. In these regions, rain evaporation has a depleting effect on the SCL, consistent with Worden et al. (2007). In contrast, in other regions, rain evaporation has a enriching effect on the SCL, up to 70‰ in dry regions. This is because in dry regions, rain evaporates almost totally, so that the evaporation flux has almost the same composition as the initial rain, which is more enriched than the water vapor.

Appendix C: Diagnostics for horizontal advection in LMDZ

We can account for horizontal advection in Eq. (8) if we can quantify parameters $\phi = \frac{F_{adv} \cdot q_{adv}}{E}$, the ratio of water vapor coming from horizontal advection to that coming from surface evaporation, and $\beta = R_{adv}/R_0$, the ratio of isotopic ratios of horizontal advection to that of the SCL.

C1 Equations

Let's assume that the box representing the SCL has a zonal extent Δy, a meridional extent Δx and is composed of k_{LCL} layers of vertical extent Δz_k. The quantity $F_{adv} \cdot q_{adv}$ represents the mass flux of water entering the grid box by horizontal advection per surface area, expressed in $kg_{water} \cdot s^{-1} \cdot m^{-2}$. Assuming an upstream advection scheme, it can be expressed as:

$$F_{adv} \cdot q_{adv} = \frac{\sum_{k=1}^{k_{LCL}} (\rho_k \cdot |u_k| \cdot q_{uk} \cdot \Delta y \cdot \Delta z_k + \rho_k \cdot |v_v| \cdot q_{vk} \cdot \Delta x \cdot \Delta z_k)}{\Delta x \cdot \Delta y} \tag{C1}$$

where u_k and v_k are the zonal and meridional wind components at layer k, ρ_k is the volumic mass of air at layer k, and q_{uk} and q_{vk} are the humidities of the incoming air from zonal and meridional advection at layer k. When $u_k > 0$, q_{uk} is the humidity in the grid box to the West. When $u_k < 0$, q_{uk} is the humidity in the grid box to the East. When $v_k > 0$, q_{vk} is the humidity in the grid box to the South. When $v_k < 0$, q_{vk} is the humidity in the grid box to the North.

Applying the hydrostatic equation at each layer ($\Delta P_k = \rho_k \cdot g \cdot \Delta z_k$, where g is gravity and ΔP_k is the vertical extent of the layer k in pressure coordinate), we get:

$$F_{adv} \cdot q_{adv} = \sum_{k=1}^{k_{LCL}} \frac{\Delta P_k}{g} \cdot \left(\frac{|u_k| \cdot q_{uk}}{\Delta x} + \frac{|v_k| \cdot q_{vk}}{\Delta y} \right)$$

The quantity F_{adv} represents the incoming air mass flux by horizontal advection, and q_{adv} represents the humidity of the incoming air. We can thus write them as:

$$F_{adv} = \sum_{k=1}^{k_{LCL}} \left(\frac{|u_k|}{\Delta x} + \frac{|v_k|}{\Delta y} \right) \cdot \frac{\Delta P_k}{g}$$

and

$$q_{adv} = \frac{\sum_{k=1}^{k_{LCL}} \left(\frac{|u_k|}{\Delta x} \cdot q_{uk} + \frac{|v_k|}{\Delta y} \cdot q_{vk} \right) \cdot \frac{\Delta P_k}{g}}{\sum_{k=1}^{k_{LCL}} \left(\frac{|u_k|}{\Delta x} + \frac{|v_k|}{\Delta y} \right) \cdot \frac{\Delta P_k}{g}}$$

The same budget as in Eq. C1 can be written for water isotopes:

$$F_{adv} \cdot q_{adv} \cdot R_{adv} = \frac{\sum_{k=1}^{k_{LCL}} (\rho_k \cdot |u_k| \cdot q_{uk} \cdot R_{uk} \cdot \Delta y \cdot \Delta z_k + \rho_k \cdot |v_v| \cdot q_{vk} \cdot R_{vk} \cdot \Delta x \cdot \Delta z_k)}{\Delta x \cdot \Delta y}$$

where R_{adv} represents the isotopic ratio of the incoming water vapor:

$$R_{adv} = \frac{\sum_{k=1}^{k_{LCL}} \left(\frac{|u_k|}{\Delta x} \cdot q_{uk} \cdot R_{uk} + \frac{|v_k|}{\Delta y} \cdot q_{vk} \cdot R_{vk} \right) \cdot \frac{\Delta P_k}{g}}{\sum_{k=1}^{k_{LCL}} \left(\frac{|u_k|}{\Delta x} \cdot q_{uk} + \frac{|v_k|}{\Delta y} \cdot q_{vk} \right) \cdot \frac{\Delta P_k}{g}}$$

Note that the upstream advection scheme assumed here overestimates the effect of advection compared to the Van Leer (1977) advection scheme used in LMDZ. We thus estimate here an upper bound for the advection effect.

In practice, rather than calculating $\beta = R_{adv}/R_0$, we calculate $\beta = R_{adv}/R_{SCL}$ where R_{SCL} is the isotopic ratio in average through the SCL:

$$R_{\cancel{F}SCL} = \cancel{\alpha_{re} \cdot R_0} \frac{\sum_{k=1}^{k_{LCL}} q_k \cdot R_k \frac{\Delta P_k}{g}}{\sum_{k=1}^{k_{LCL}} q_k \frac{\Delta P_k}{g}}$$

~~where α_{re} is an effective fractionation coefficient. For example, if droplets are formed near the cloud base, some of them precipitate and evaporate totally in the SCL (e. g. in non-precipitating shallow cumulus clouds), then $\alpha_{re} = \alpha(T_{cloudbase})$. In contrast, if droplets are formed in deep convective updrafts after total condensation of the SCL vapor, and then a very small fraction of the rain is evaporated in a very dry SCL, then $\alpha_{re} = 1/\alpha(T_{SCL})/\alpha_K$ (Stewart, 1975).~~ This prevents the advected water vapor to be systematically more depleted when the mixed-layer hypothesis is not exactly verified.

~~Combining all equations, in the case of a logarithmic δD profile, we get:~~

C2 Results

$$\cancel{R_0 = \frac{R_{oce}}{\alpha_{eq}} \cdot \frac{1}{h_0 + \alpha_K \cdot (1-h_0) \cdot \frac{1-r_{orig}^{\alpha_{eff}}}{1-r_{orig}} + \eta \cdot \alpha_K \cdot (1-h_0) \cdot (1-\alpha_{re})}}$$

Parameter ϕ is maximum where winds are maximum, such as near the extra-tropics or in the North Atlantic (Fig. C1a). Horizontal advection has an enriching effect in deep convective regions (probably because water vapor comes from nearby drier regions that have been less depleted by deep convection), and a depleting effect near the coasts (probably because of winds bringing vapor from the nearby land that is depleted by the continental effect) (Fig. C1b).

~~Rain evaporation can have a depleting or enriching effect depending on the sign of $1-\alpha_{re}$ (Fig~~ Note that in this formulation, parameters ϕ and β are resolution-dependent. For example, in a finer resolution, ϕ would be larger and β would be closer to 1, but $F_{adv} \cdot q_{adv} \cdot R_{adv}$ and thus the contribution of horizontal advection in Eq. (8) would remain the same.

Appendix D: LMDZ free tropospheric profiles

The goal of this appendix is to document the spatio-temporal variability in the shape (section D1) and steepness (section D2) of simulated free tropospheric δD profiles. Note that a detailed interpretation of these profiles is beyond the scope of this paper. This paper aims at understanding δD_0, which is the first step towards understanding full tropospheric profiles. In turn, understanding full tropospheric profiles in future studies will help refine our model for δD_0. ~~3 pink, blue). In the paper, we thus well neglect rain evaporation effects, to avoid dealing with such an unknown parameter as α_{re}.~~

D1 Shape of tropospheric profiles

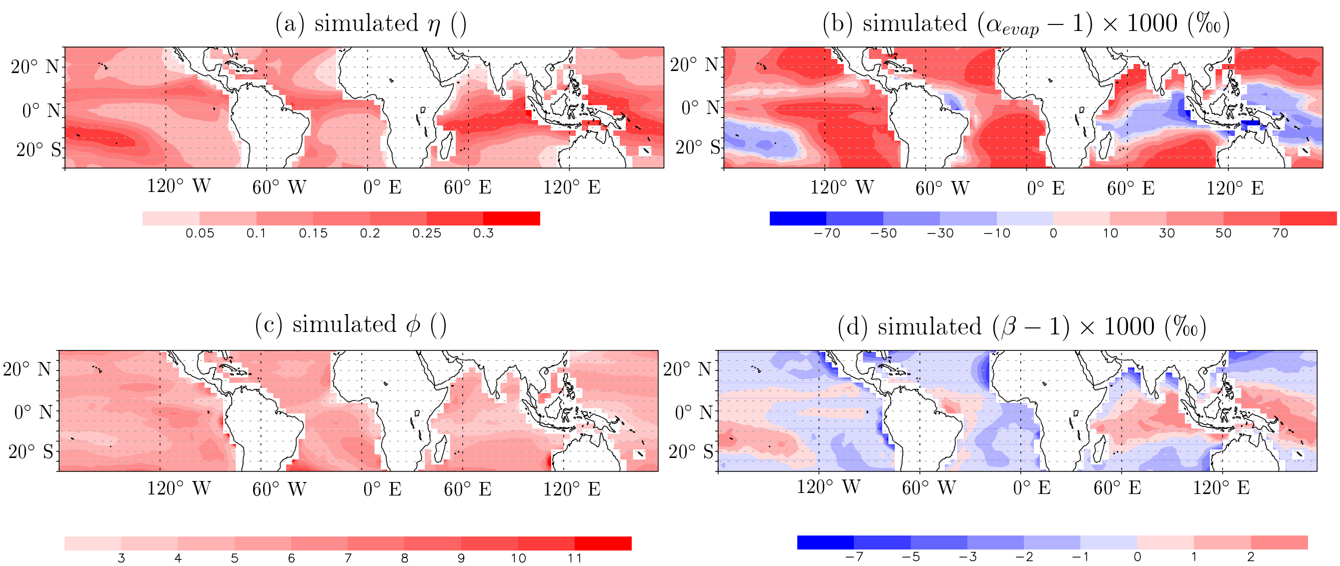

Figure C1. a) Ratio η of water in the SCL coming from rain evaporation to that coming from surface evaporation. b) Effective fractionation coefficient α_{evap} between the SCL water vapor and the rain evaporation. c) Ratio ϕ of water in the SCL coming from horizontal advection to that coming from surface evaporation. d) Effective fractionation coefficient β between the SCL water vapor and the water vapor coming from horizontal advection.

First, we test whether the δD vertical profiles simulated by LMDZ follow a Rayleigh or mixing line as a function of q. For the Rayleigh curve, α_{eff} is estimated as explained in section 3.3. For the mixing line (appendix A), the end member (q_f, R_f) is also taken at 500 hPa.

The tropical-mean vertical δD profiles simulated by LMDZ is bounded by Rayleigh and mixing lines (Fig. D1a). To better document the spatial variability in the shape of δD profiles, we plot parameter $f = \frac{\delta D_{LMDZ} - \delta D_{Rayleigh}}{\delta D_{mix} - \delta D_{Rayleigh}}$, describing how close is the simulated δD (δD_{LMDZ}) to the Rayleigh ($\delta D_{Rayleigh}$) and mixing (δD_{mix}) lines. We have $f = 0$ in case of a Raleigh line, $f = 1$ in case of a mixing line, and $f > 1$ if δD is more enriched than a mixing line. In the lower-troposphere, δD_{LMDZ} is close to a mixing line (and sometimes even more enriched) in deep convective regions (Indian Ocean, South Pacific Convergence Zone, Atlantic ITCZ), probably because deep convection efficiently mixes the lower troposphere. Elsewhere, δD_{LMDZ} is intermediate between the two lines (Fig D1e). In the middle troposphere, δD_{LMDZ} is relatively closer to Rayleigh everywhere (Fig D1b).

The daily variability of f is large everywhere and at all levels (Fig D1c,e), with standard deviation of 0.23 and 0.44 on tropical average at 1000 m and 4000 m respectively. A large daily variability in the shape of profiles is also observed in nature (Sodemann et al., 2017).

D2 Steepness of tropospheric profiles

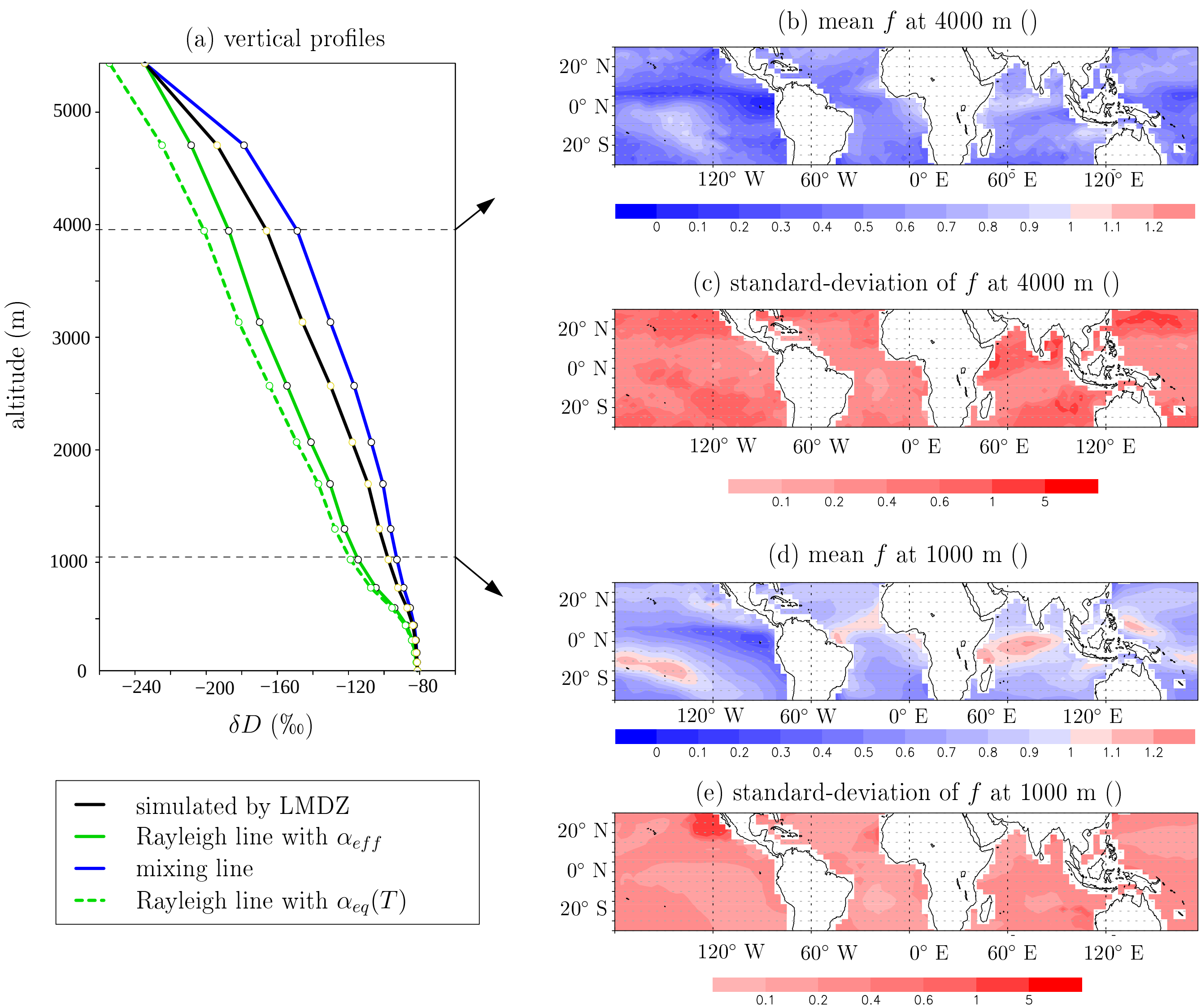

Figure D1. a) Vertical profiles of water vapor δD simulated by LMDZ (black), calculated if assuming a Rayleigh-type curve with α_{eff} estimated from $(q_f, \delta D_f)$ at 500 hPa (green), calculated if assuming a Rayleigh-type curve with $\alpha_{eq}(T)$ (dashed green) and calculated if assuming a mixing curve between the first layer and $(q_f, \delta D_f)$ at 500 hPa (blue), in average over all tropical oceanic locations and days. b) Winter-mean map of parameter $f = \frac{\delta D_{LMDZ} - \delta D_{Rayleigh}}{\delta D_{mix} - \delta D_{Rayleigh}}$ at 4000 m, i.e. slightly below 500 hPa where q_f and δD_f are taken. Parameter f describes how close is the simulated δD (δD_{LMDZ}) to the Rayleigh ($\delta D_{Rayleigh}$) and mixing lines (δD_{mix}): $f = 0$ in case of a Raleigh line, $f = 1$ in case of a mixing line, and $f > 1$ if δD is more enriched than a mixing line. c) Standard deviation of parameter f among all days in winter of all years, at 4000 m. d) Same as b but at 1000 m, i.e. slightly above the LCL. e) Same as c but at 1000 m. To avoid numerical problems, only days and locations where $|\delta D_{mix} - \delta D_{Rayleigh}| > 5$‰ are used in the calculations.

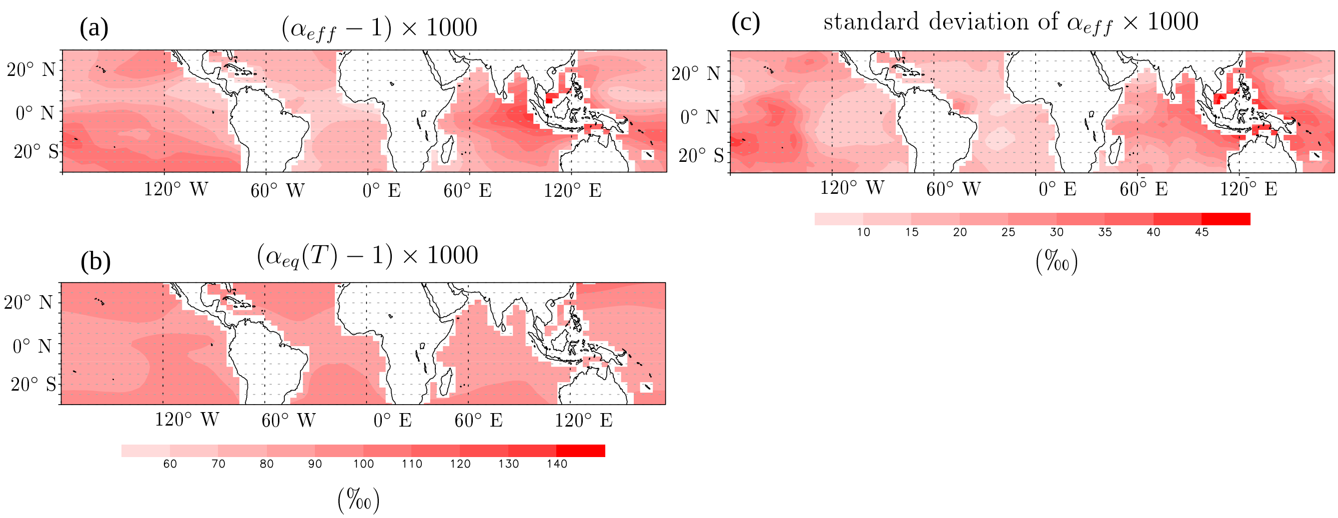

Figure D2. a) $\alpha_{eff} - 1$, where α_{eff} is the effective fractionation coefficient, expressed in ‰. b) $\alpha_{eq}(T) - 1$ expressed in ‰. All daily values are averaged over all days in winters of all years. c) Standard deviation of α_{eff} among all days in winter of all years, expressed in ‰.

The steepness of the δD gradient from the surface to the middle troposphere is described by the parameter α_{eff}. It is maximum in regions of deep convection, for example around the Maritime Continent (Fig. D2a). This is consistent with the maximum depletion simulated in deep convective regions in the mid-troposphere simulated by models (Bony et al., 2008), leading to steeper δD profiles. The pattern of α_{eff} may also reflect horizontal advection effects, where strong isotopic gradients align with winds (e.g. from the Eastern to the Western Pacific, Dee et al. (2018)).

Values of α_{eff} are of the same order of magnitude as real fractionation factors, but the spatial variations do not reflect those predicted if using a fractionation coefficient α_{eq} as a function of temperature T (Fig. D2b).

The daily standard deviation of α_{eff} ($\sigma_{\alpha_{eff}}$) for a given season ranges from 5‰ in the Central Atlantic to 40‰ near the Maritime Continent (Fig. D2c). On average over all seasons and locations, daily $\alpha_{eff} - 1$ at a given location varies within ±25 % of its seasonal-mean mean value.

Author contributions. CR thought about the equations, ran the LMDZ simulations, made the analysis and wrote the manuscript. JG initiated the discussion on the subject and discussed regularly about the results. GR provided the STRASSE radiosoundings. FB provided insight and references about cloud processes. JG, GR and FB all gave comments on the manuscript.

Competing interests. The authors declare that they have no conflict of interest.

Acknowledgements. This work was granted access to the HPC resources of IDRIS under the allocation 2092 made by GENCI. J. Galewsky was supported by the LABEX-IPSL visitor program, the Franco-American Fulbright Foundation, and NSF AGS Grant 1738075 to JG. We thank Marion Benetti and Sandrine Bony for her previous studies on this subject and useful discussions. We thank ~~Sandrine Bony for stimulating discussions~~two anonymous reviewers for their comments.

References

Aemisegger, F., Sturm, P., Graf, P., Sodemann, H., Pfahl, S., Knohl, A., and Wernli, H.: Measuring variations of [delta] 18O and [delta] 2H in atmospheric water vapour using two commercial laser-based spectrometers: an instrument characterisation study, Atmospheric Measurement Techniques, 5, 1491, 2012.

Aggarwal, P. K., Romatschke, U., Araguas-Araguas, L., Belachew, D., Longstaffe, F. J., Berg, P., Schumacher, C., and Funk, A.: Proportions of convective and stratiform precipitation revealed in water isotope ratios, Nature Geoscience, 9, 624, 2016.

Albrecht, B. A.: Effects of precipitation on the thermodynamic structure of the trade wind boundary layer, Journal of Geophysical Research: Atmospheres, 98, 7327–7337, 1993.

Bailey, A., Toohey, D., and Noone, D.: Characterizing moisture exchange between the Hawaiian convective boundary layer and free troposphere using stable isotopes in water, Journal of Geophysical Research: Atmospheres, 118, 8208–8221, 2013.

Benetti, M., Reverdin, G., Pierre, C., Merlivat, L., Risi, C., and Vimeux., F.: Deuterium excess in marine water vapor: Dependency on relative humidity and surface wind speed during evaporation, J. Geophys. Res, 119, 584–593, DOI: 10.1002/2013JD020 535, 2014.

Benetti, M., Aloisi, G., Reverdin, G., Risi, C., and Sèze, G.: Importance of boundary layer mixing for the isotopic composition of surface vapor over the subtropical North Atlantic Ocean, Journal of Geophysical Research: Atmospheres, 120, 2190–2209, 2015.

Benetti, M., Reverdin, G., Aloisi, G., and Sveinbjörnsdóttir, Á.: Stable isotopes in surface waters of the A tlantic O cean: Indicators of ocean-atmosphere water fluxes and oceanic mixing processes, Journal of Geophysical Research: Oceans, 122, 4723–4742, 2017a.

Benetti, M., Steen-Larsen, H. C., Reverdin, G., Sveinbjörnsdóttir, Á. E., Aloisi, G., Berkelhammer, M. B., Bourlès, B., Bourras, D., De Coetlogon, G., Cosgrove, A., et al.: Stable isotopes in the atmospheric marine boundary layer water vapour over the Atlantic Ocean, 2012–2015, Scientific data, 4, 160 128, 2017b.

Betts, A. K. and Ridgway, W.: Climatic equilibrium of the atmospheric convective boundary layer over a tropical ocean, Journal of the Atmospheric Sciences, 46, 2621–2641, 1989.

Blossey, P. N., Kuang, Z., and Romps, D. M.: Isotopic composition of water in the tropical tropopause layer in cloud-resolving simulations of an idealized tropical circulation, J. Geophys. Res., 115, D24 309, doi:10.1029/2010JD014 554, 2010.

Bolot, M., Legras, B., and Moyer, E. J.: Modelling and interpreting the isotopic composition of water vapour in convective updrafts, Atmospheric Chemistry and Physics, 13(16), 7903–7935, 2013.

Bony, S., Lau, K., and Sud, Y.: Sea surface temperature and large-scale circulation influences on tropical greenhouse effect and cloud radiative forcing, Journal of Climate, 10, 2055–2077, 1997.

Bony, S., Dufresne, J.-L., Le Treut, H., Morcrette, J.-J., and Senior, C.: On dynamic and thermodynamic components of cloud changes, Climate Dynamics, 22, 71–86, https://doi.org/10.1007/s00382-003-0369-6, 2004.

Bony, S., Risi, C., and Vimeux, F.: Influence of convective processes on the isotopic composition (deltaO18 and deltaD) of precipitation and water vapor in the Tropics. Part 1: Radiative-convective equilibrium and TOGA-COARE simulations, J. Geophys. Res., 113, D19 305, doi:10.1029/2008JD009 942, 2008.

Bony, S., Bellon, G., Klocke, D., Sherwood, S., Fermepin, S., and Denvil, S.: Robust direct effect of carbon dioxide on tropical circulation and regional precipitation, Nature Geoscience, 6(6), 447–451, 2013.

Bony, S., Stevens, B., Ament, F., Bigorre, S., Chazette, P., Crewell, S., Delanoë, J., Emanuel, K., Farrell, D., Flamant, C., et al.: EUREC4A: a field campaign to elucidate the couplings between clouds, convection and circulation, Surveys in Geophysics, pp. 1–40, 2017.

Bretherton, C. S.: Insights into low-latitude cloud feedbacks from high-resolution models, Phil. Trans. R. Soc. A, 373, 20140 415, 2015.

Bretherton, C. S., Austin, P., and Siems, S. T.: Cloudiness and marine boundary layer dynamics in the ASTEX Lagrangian experiments. Part II: Cloudiness, drizzle, surface fluxes, and entrainment, Journal of the atmospheric sciences, 52, 2724–2735, 1995.

Brient, F., Couvreux, F., Najda, V., Rio, C., and Honnert, R.: Object-oriented identification of coherent structures in large-eddy simulations: importance of downdrafts in stratocumulus, Geophy. Res. Lett., 2019.

Ciais, P., White, W., Jouzel, J., and Petit, J.: The origin of present-day Antarctic precipitation from surface snow deuterium excess data, J. Geophys. Res., 100, 18 917–18 927, 1995.

Couvreux, F., Hourdin, F., and Rio, C.: Resolved versus parametrized boundary-layer plumes. Part I: A parametrization-oriented conditional sampling in large-eddy simulations, Boundary-layer meteorology, 134, 441–458, 2010.

Craig, H. and Gordon, L. I.: Deuterium and oxygen-18 variations in the ocean and marine atmosphere, Stable Isotope in Oceanographic Studies and Paleotemperatures, Laboratorio di Geologia Nucleate, Pisa, Italy, 9–130, 1965.

Dansgaard: Stable isotopes in precipitation, Tellus, 16, 436–468, 1964.

Davini, P., D?Andrea, F., Park, S.-B., and Gentine, P.: Coherent Structures in Large-Eddy Simulations of a Nonprecipitating Stratocumulus-Topped Boundary Layer, Journal of the Atmospheric Sciences, 74, 4117–4137, 2017.

De Roode, S. R., Sandu, I., Van Der Dussen, J. J., Ackerman, A. S., Blossey, P., Jarecka, D., Lock, A., Siebesma, A. P., and Stevens, B.: Large-eddy simulations of EUCLIPSE–GASS Lagrangian stratocumulus-to-cumulus transitions: Mean state, turbulence, and decoupling, Journal of the Atmospheric Sciences, 73, 2485–2508, 2016.

De Rooy, W. C., Bechtold, P., Fröhlich, K., Hohenegger, C., Jonker, H., Mironov, D., Siebesma, A. P., Teixeira, J., and Yano, J.-I.: Entrainment and detrainment in cumulus convection: An overview, Quarterly Journal of the Royal Meteorological Society, 139, 1–19, 2013.

Dee, S. G., Nusbaumer, J., Bailey, A., Russell, J. M., Lee, J.-E., Konecky, B., Buenning, N. H., and Noone, D. C.: Tracking the Strength of the Walker Circulation With Stable Isotopes in Water Vapor, Journal of Geophysical Research: Atmospheres, 123, 7254–7270, 2018.

Delaygue, G., Masson, V., Jouzel, J., Koster, R. D., and Healy, R. J.: The origin of Antarctic precipitation: A modelling approach, Tellus, 52B, 19–36, 2000.

Dufresne, J.-L., Foujols, M.-A., Denvil, S., Caubel, A., Marti, O., Aumont, O., alkanski, Y., Bekki, S., Bellenger, H., Benshila, R., Bony, S., Bopp, L., Braconnot, P., Brockmann, P., Cadule, P., Cheruy, F., Codron, F., Cozic, A., Cugnet, D., de Noblet, N., Duvel, J.-P., Ethé, C., Fairhead, L., Fichefet, T., Flavoni, S., Friedlingstein, P., Grandpeix, J.-Y., Guez, L., Guilyardi, E., Hauglustaine, D., Hourdin, F., Idelkadi, A., Ghattas, J., Joussaume, S., Kageyama, M., Krinner, G., Labetoulle, S., Lahellec, A., Lefebvre, M.-P., Lefevre, F., Levy, C., Li, Z. X., Lloyd, J., Lott, F., Madec, G., Mancip, M., Marchand, M., Masson, S., Meurdesoif, Y., Mignot, J., Musat, I., Parouty, S., Polcher, J., Rio, C., Schulz, M., Swingedouw, D., Szopa, S., Talandier, C., Terray, P., and Viovy, N.: Climate change projections using the IPSL-CM5 Earth System Model: from CMIP3 to CMIP5, Clim. Dyn, 40 (9-10), 1–43, DOI 10.1007/s00 382–012–1636–1, 2012.

Duynkerke, P. G., de Roode, S. R., van Zanten, M. C., Calvo, J., Cuxart, J., Cheinet, S., Chlond, A., Grenier, H., Jonker, P. J., Köhler, M., et al.: Observations and numerical simulations of the diurnal cycle of the EUROCS stratocumulus case, Quarterly Journal of the Royal Meteorological Society: A journal of the atmospheric sciences, applied meteorology and physical oceanography, 130, 3269–3296, 2004.

Ehhalt, D. H.: Vertical profiles of HTO, HDO, and H2O in the troposphere, NCAR technical note, NCAR-TN-STR-100, 1974.

Ehhalt, D. H., Rohrer, F., and Fried, A.: Vertical profiles of HDO/H2O in the troposphere, J. Geophy. Res., 110, D13, 2005.

Emanuel, K., Neelin, D., and Bretherton, C.: On large-scale circulations in convecting atmospheres, Quaterly Journal of the Royal Meteorological Society, 120, 1111–1143, 1994.

Ent, R. J. and Savenije, H. H.: Oceanic sources of continental precipitation and the correlation with sea surface temperature, Water Resources Research, 49(7), 3993–4004, 2013.

Faloona, I., Lenschow, D. H., Campos, T., Stevens, B., Van Zanten, M., Blomquist, B., Thornton, D., Bandy, A., and Gerber, H.: Observations of entrainment in eastern Pacific marine stratocumulus using three conserved scalars, Journal of the atmospheric sciences, 62, 3268–3285, 2005.

Field, R. D., Jones, D. B. A., and Brown, D. P.: The effects of post-condensation exchange on the isotopic composition of water in the atmosphere, J. Geophy. Res., 115, D24305, doi:10.1029/2010JD014 334, 2010.

Galewsky, J.: Using Stable Isotopes in Water Vapor to Diagnose Relationships Between Lower-Tropospheric Stability, Mixing, and Low-Cloud Cover Near the Island of Hawaii, Geophysical Research Letters, 45, 297–305, 2018a.

Galewsky, J.: Relationships between inversion strength, lower-tropospheric moistening, and low-cloud fraction in the subtropical Southeast Pacific derived from stable isotopologues of water vapor, Geophysical Research Letters, 45, 7701–7710, 2018b.

Galewsky, J. and Rabanus, D.: A stochastic model for diagnosing subtropical humidity dynamics with stable isotopologues of water vapor, Journal of the Atmospheric Sciences, 73, 1741–1753, 2016.

Galewsky, J. and Samuels-Crow, K.: Water vapor isotopic composition of a stratospheric air intrusion: Measurements from the Chajnantor Plateau, Chile, Journal of Geophysical Research: Atmospheres, 119, 9679–9691, 2014.

Galewsky, J., Strong, M., , and Sharp, Z. D.: Measurements of water vapor D/H ratios from Mauna Kea, Hawaii, and implications for subtropical humidity dynamics, Geophy. Res. Lett., 34, L22 808, doi:10.1029/2007GL031 330, 2007.

Galewsky, J., Steen-Larsen, H. C., Field, R. D., Worden, J., Risi, C., and Schneider, M.: Stable isotopes in atmospheric water vapor and applications to the hydrologic cycle, Reviews of Geophysics, 54, 809–865, 2016.

Garratt, J. R.: The atmospheric boundary layer, Earth-Science Reviews, 37, 89–134, 1994.

Gates, W. L.: AMIP: The Atmospheric Model Intercomparison Project, Bull. Am. Meteor. Soc., 73, 1962–1970, 1992.

Gerber, H., Frick, G., Malinowski, S., Brenguier, J., and Burnet, F.: Holes and entrainment in stratocumulus, Journal of the atmospheric sciences, 62, 443–459, 2005.

Gerber, H., Frick, G., Malinowski, S. P., Jonsson, H., Khelif, D., and Krueger, S. K.: Entrainment rates and microphysics in POST stratocumulus, Journal of Geophysical Research: Atmospheres, 118, 12–094, 2013.

Gimeno, L., A., Drumond, R., Nieto, Trigo, R. M., and Stohl, A.: On the origin of continental precipitation, Geophys. Res. Lett., 37, L13 804, doi:10.1029/2010GL043 712., 2010.

Glenn, I. B. and Krueger, S. K.: Downdrafts in the near cloud environment of deep convective updrafts, Journal of Advances in Modeling Earth Systems, 6, 1–8, 2014.

Good, S. P., Noone, D., Kurita, N., Benetti, M., and Bowen, G. J.: D/H isotope ratios in the global hydrologic cycle, Geophysical Research Letters, 42, 5042–5050, 2015.

Graf, P., Wernli, H., Pfahl, S., and Sodemann, H.: A new interpretative framework for below-cloud effects on stable water isotopes in vapour and rain, Atmospheric Chemistry and Physics, 19, 747–765, 2019.

Guilpart, E., Vimeux, F., Evan, S., Brioude, J., Metzger, J.-M., Barthe, C., Risi, C., and Cattani, O.: The isotopic composition of near-surface water vapor at the Maïdo observatory (Reunion Island, southwestern Indian Ocean) documents the controls of the humidity of the subtropical troposphere, Journal of Geophysical Research: Atmospheres, 122, 9628–9650, 2017.

Heus, T. and Jonker, H. J.: Subsiding shells around shallow cumulus clouds, Journal of the Atmospheric Sciences, 65, 1003–1018, 2008.

Heus, T., Pols, C. F. J., Jonker, H. J., Van den Akker, H. E., and Lenschow, D. H.: Observational validation of the compensating mass flux through the shell around cumulus clouds, Quarterly Journal of the Royal Meteorological Society, 135, 101–112, 2009.

Hourdin, F., Musat, I., Bony, S., Braconnot, P., Codron, F., Dufresne, J.-L., Fairhead, L., Filiberti, M.-A., Friedlingstein, P., Grandpeix, J.-Y., Krinner, G., Levan, P., Li, Z.-X., and Lott, F.: The LMDZ4 general circulation model: climate performance and sensitivity to parametrized physics with emphasis on tropical convection, Clim. Dyn., 27, 787–813, https://doi.org/10.1007/s00382-006-0158-0, 2006.

Hourdin, F., Grandpeix, J.-Y., Rio, C., Bony, S., Jam, A., Cheruy, F., Rochetin, N., Fairhead, L., Idelkadi, A., Musat, I., et al.: LMDZ5B: the atmospheric component of the IPSL climate model with revisited parameterizations for clouds and convection, Climate Dynamics, 40, 2193–2222, 2013.

Jonas, P.: Observations of cumulus cloud entrainment, Atmospheric research, 25, 105–127, 1990.

Jouzel, J. and Koster, R. D.: A reconsideration of the initial conditions used for stable water isotope models, J. Geophys. Res., 101, 22 933–22 938, https://doi.org/10.1029/96JD02362, 1996.

Khalsa, S. J. S.: Direct sampling of entrainment events in a marine stratocumulus layer, Journal of the atmospheric sciences, 50, 1734–1750, 1993.

Kurita, N.: Water isotopic variability in response to mesoscale convective system over the tropical ocean., Journal of Geophysical Research, 118(18), 10–376, 2013.

Lacour, J.-L., Risi, C., Clarisse, L., Bony, S., Hurtmans, D., Clerbaux, C., and Coheur, P.-F.: Mid-tropospheric deltaD observations from IASI/MetOp at high spatial and temporal resolution, Atmos. Chem. Phys., 12, 10 817–10 832, doi:10.5194/acp–12–10 817–2012, 2012.

Lacour, J.-L., Clarisse, L., Worden, J., Schneider, M., Barthlott, S., Hase, F., Risi, C., Clerbaux, C., Hurtmans, D., and Coheur, P.-F.: Cross-validation of IASI/MetOp derived tropospheric ?D with TES and ground-based FTIR observations, Atmospheric Measurement Techniques, 8, 1447–1466, https://doi.org/10.5194/amt-8-1447-2015, http://www.atmos-meas-tech.net/8/1447/2015/, 2015.

Lacour, J.-L., Flamant, C., Risi, C., Clerbaux, C., and Coheur, P.-F.: Importance of the Saharan heat low in controlling the North Atlantic free tropospheric humidity budget deduced from IASI δD observations, Atmospheric Chemistry and Physics, 17, 9645–9663, 2017a.

Lacour, J.-L., Risi, C., Worden, J., Clerbaux, C., and Coheur, P.-F.: Isotopic signature of convection's depth in water vapor as seen from IASI and TES D observations, Earth Planet. Sci. Lett., 7, 9645–9663, doi.org/10.5194/acp–17–9645–2017, 2017b.

Lawrence, J. R., Gedzelman, S. D., Gamache, J., and Black, M.: Stable isotope ratios: Hurricane Olivia, J. Atmos. Chem, 41, 67–82, 2002.

Lawrence, J. R., Gedzelman, S. D., Dexheimer, D., Cho, H.-K., Carrie, G. D., Gasparini, R., Anderson, C. R., Bowman, K. P., and Biggerstaff, M. I.: Stable isotopic composition of water vapor in the tropics, J. Geophys. Res., 109, D06 115, doi:10.1029/2003JD004 046, https://doi.org/10.1029/2003JD004046, 2004.

Lee, J.-E., Pierrehumbert, R., Swann, A., and Lintner, B. R.: Sensitivity of stable water isotopic values to convective parameterization schemes, Geophy. Res. Lett., 36, doi:10.1029/2009GL040 880, 2009.

Lozar, A. and Mellado, J. P.: Evaporative cooling amplification of the entrainment velocity in radiatively driven stratocumulus, Geophysical Research Letters, 42, 7223–7229, 2015.

Majoube, M.: Fractionnement en Oxygène 18 et en Deutérium entre l'eau et sa vapeur, Journal de Chimie Physique, 10, 1423–1436, 1971.

Masunaga, H. and Sumi, Y.: A toy model of tropical convection with a moisture storage closure, Journal of Advances in Modeling Earth Systems, 9, 647–667, 2017.

McGrath, R., Semmler, T., Sweeney, C., and Wang, S.: Impact of balloon drift errors in radiosonde data on climate statistics, Journal of climate, 19, 3430–3442, 2006.

Mellado, J. P.: Cloud-top entrainment in stratocumulus clouds, Annual Review of Fluid Mechanics, 49, 145–169, 2017.

Merlivat, L. and Jouzel, J.: Global climatic interpretation of the Deuterium-Oxygen 18 relationship for precipitation, J. Geophys. Res., 84, 5029–5332, 1979.

Moore, M., Kuang, Z., and Blossey, P. N.: A moisture budget perspective of the amount effect, Geophys. Res. Lett., 41, 1329–1335, doi:10.1002/2013GL058 302., 2014.

Moyer, E. J., Irion, F. W., Yung, Y. L., and Gunson, M. R.: ATMOS stratospheric deuterated water and implications for troposphere-stratosphere transport, Geophys. Res. Lett., 23, 2385–2388, https://doi.org/10.1029/96GL01489, 1996.

Neggers, R., Stevens, B., and Neelin, J. D.: A simple equilibrium model for shallow-cumulus-topped mixed layers, Theoretical and Computational Fluid Dynamics, 20, 305–322, 2006.

Nicholls, S. and Turton, J.: An observational study of the structure of stratiform cloud sheets: Part II. Entrainment, Quarterly Journal of the Royal Meteorological Society, 112, 461–480, 1986.

Nuijens, L., Medeiros, B., Sandu, I., and Ahlgrimm, M.: Observed and modeled patterns of covariability between low-level cloudiness and the structure of the trade-wind layer, Journal of Advances in Modeling Earth Systems, 7, 1741–1764, 2015a.

Nuijens, L., Medeiros, B., Sandu, I., and Ahlgrimm, M.: The behavior of trade-wind cloudiness in observations and models: The major cloud components and their variability, Journal of Advances in Modeling Earth Systems, 7, 600–616, 2015b.

Oke, T. R.: Boundary layer climates, Halsted press, New York, 1988.

Oueslati, B., Bony, S., Risi, C., and Dufresne, J.-L.: Interpreting the inter-model spread in regional precipitation projections in the tropics: role of surface evaporation and cloud radiative effects, Climate Dynamics, pp. 1–15, 2016.

Park, S.-B., Gentine, P., Schneider, K., and Farge, M.: Coherent structures in the boundary and cloud layers: Role of updrafts, subsiding shells, and environmental subsidence, Journal of the Atmospheric Sciences, 73, 1789–1814, 2016.

Randall, D., Krueger, S., Bretherton, C., Curry, J., Duynkerke, P., Moncrieff, M., Ryan, B., Starr, D., Miller, M., Rossow, W., et al.: Confronting models with data: The GEWEX cloud systems study, Bulletin of the American Meteorological Society, 84, 455–469, 2003.

Risi, C., Bony, S., and Vimeux, F.: Influence of convective processes on the isotopic composition (O18 and D) of precipitation and water vapor in the Tropics: Part 2: Physical interpretation of the amount effect, J. Geophys. Res., 113, D19 306, doi:10.1029/2008JD009 943, 2008.

Risi, C., Bony, S., Vimeux, F., Chong, M., and Descroix, L.: Evolution of the water stable isotopic composition of the rain sampled along Sahelian squall lines, Quart. J. Roy. Meteor. Soc., 136 (S1), 227 – 242, 2010a.

Risi, C., Bony, S., Vimeux, F., Frankenberg, C., and Noone, D.: Understanding the Sahelian water budget through the isotopic composition of water vapor and precipitation, J. Geophys. Res, 115, D24110, doi:10.1029/2010JD014 690, 2010b.

Risi, C., Bony, S., Vimeux, F., and Jouzel, J.: Water stable isotopes in the LMDZ4 General Circulation Model: model evaluation for present day and past climates and applications to climatic interpretation of tropical isotopic records, J. Geophys. Res., 115, D12118, doi:10.1029/2009JD013 255, 2010c.

Risi, C., Landais, A., Bony, S., Masson-Delmotte, V., Jouzel, J., and Vimeux, F.: Understanding the 17O-excess glacial-interglacial variations in Vostok precipitation, J. Geophys. Res, 115, D10112, doi:10.1029/2008JD011 535, 2010d.

Risi, C., Noone, D., Worden, J., Frankenberg, C., Stiller, G., Kiefer, M., Funke, B., Walker, K., Bernath, P., Schneider, M., Wunch, D., Sherlock, V., Deutscher, N., Griffith, D., Wernberg, P., Bony, S., Jeonghoon Lee, D. B., Uemura, R., and Sturm, C.: Process-evaluation of tropical and subtropical tropospheric humidity simulated by general circulation models using water vapor isotopic observations. Part 1: model-data intercomparison, J. Geophy. Res., 117, D05 303, 2012a.

Risi, C., Noone, D., Worden, J., Frankenberg, C., Stiller, G., Kiefer, M., Funke, B., Walker, K., Bernath, P., Schneider, M., Wunch, D., Sherlock, V., Deutscher, N., Griffith, D., Wernberg, P., Bony, S., Lee, J., Brown, D., Uemura, R., and Sturm, C.: Process-evaluation of tropical and subtropical tropospheric humidity simulated by general circulation models using water vapor isotopic observations. Part 2: an isotopic diagnostic of the mid and upper tropospheric moist bias, J. Geophy. Res., 117, D05 304, 2012b.

Risi, C., Noone, D., Frankenberg, C., and Worden, J.: Role of continental recycling in intraseasonal variations of continental moisture as deduced from model simulations and water vapor isotopic measurements, Water Resour. Res., 49, 4136–4156, doi: 10.1002/wrcr.20 312, 2013.

Rodts, S. M., Duynkerke, P. G., and Jonker, H. J.: Size distributions and dynamical properties of shallow cumulus clouds from aircraft observations and satellite data, Journal of the atmospheric sciences, 60, 1895–1912, 2003.

Rosenfeld, D. and Mintz, Y.: Evaporation of rain falling from convective clouds as derived from radar measurements, Journal of Applied Meteorology, 27, 209–215, 1988.

Salati, E., Dall'Olio, A., Matsui, E., and Gat, J.: Recycling of water in the Amazon basin: An isotopic study, Water Resources Research, 15, 1250–1258, 1979.

Seidel, D. J., Ao, C. O., and Li, K.: Estimating climatological planetary boundary layer hheight from radiosonde observations: comparison of methods and uncertainty analysis, J. Geophy. Res., 115, D16113, 2010.

Seidel, D. J., Sun, B., Pettey, M., and Reale, A.: Global radiosonde balloon drift statistics, Journal of Geophysical Research: Atmospheres, 116, 2011.

Sherwood, S., Bony, S., and Dufresne, J.-L.: Spread in model climate sensitivity traced to atmospheric convective mixing, Nature, 505, 37–42, doi:10.1038/nature12 829, 2014.

Sherwood, S. C.: Maintenance of the free tropospheric tropical water vapor distribution. part II: simulation of large-scale advection, J. Clim., 11, 2919–2934, 1996.

Siebert, P., Beyrich, F., Gryning, S. E., Joffre, S., and Rasmussen, A.: Review and intercomparison of operational methods for the determination of the mixing height, Atmos. Environ., 34, 1001–1027, 2000.

Sodemann, H., Aemisegger, F., Pfahl, S., Bitter, M., Corsmeier, U., Feuerle, T., Graf, P., Hankers, R., Hsiao, G., Schulz, H., et al.: The stable isotopic composition of water vapour above Corsica during the HyMeX SOP1 campaign: insight into vertical mixing processes from lower-tropospheric survey flights, Atmospheric Chemistry and Physics, 17, 6125–6151, 2017.

Sorbjan, Z.: Structure of the atmospheric boundary layer, Prentice Hall, Englewood Cliffs, N. J., 1989.

Stevens, B.: Bulk boundary-layer concepts for simplified models of tropical dynamics, Theoretical and Computational Fluid Dynamics, 20, 279–304, 2006.

Stewart, M. K.: Stable isotope fractionation due to evaporation and isotopic exchange of falling waterdrops: Applications to atmospheric processes and evaporation of lakes, J. Geophys. Res., 80, 1133–1146, 1975.

Stull, R. B.: An intruduction to boundary layer meteorology, Dordrect Kluwer, 1988.

Taylor, K. E., Stouffer, R. J., and Meehl, G. A.: An overview of CMIP5 and the experiment design, Bulletin of the American Meteorological Society, 93(4), 485–498, 2012.

Thayer-Calder, K. and Randall, D.: A numerical investigation of boundary layer quasi-equilibrium, Geophysical Research Letters, 42, 550–556, 2015.

Tremoy, G., Vimeux, F., Soumana, S., Souley, I., Risi, C., Cattani, O., Favreau, G., and Oi, M.: Clustering mesoscale convective systems with laser-based water vapor delta18O monitoring in Niamey (Niger), J. Geophys. Res., 119(9), 5079–5103, DOI: 10.1002/2013JD020 968, 2014.

Uppala, S., Kallberg, P., Simmons, A., Andrae, U., da Costa Bechtold, V., Fiorino, M., Gibson, J., Haseler, J., Hernandez, A., Kelly, G., Li, X., Onogi, K., Saarinen, S., Sokka, N., Allan, R., Andersson, E., Arpe, K., Balmaseda, M., Beljaars, A., van de Berg, L., Bidlot, J., Bormann, N., Caires, S., Chevallier, F., Dethof, A., Dragosavac, M., Fisher, M., Fuentes, M., Hagemann, S., Holm, E., Hoskins, B., Isaksen, L., Janssen, P., Jenne, R., McNally, A., Mahfouf, J.-F., Morcrette, J.-J., Rayner, N., Saunders, R., Simon, P., Sterl, A., Trenberth, K., Untch, A., Vasiljevic, D., Viterbo, P., and Woollen, J.: The ERA-40 re-analysis, Quart. J. Roy. Meteor. Soc., 131, 2961–3012, 2005.

Van Leer, B.: Towards the ultimate conservative difference scheme : IV. a new approach to numerical convection, J. Computational Phys., 23, 276–299, 1977.

Vial, J., Bony, S., Dufresne, J.-L., and Roehrig, R.: Coupling between lower-tropospheric convective mixing and low-level clouds: Physical mechanisms and dependence on convection scheme, Journal of Advances in Modeling Earth Systems, 8, 1892–1911, 2016.

Wang, Q. and Albrecht, B. A.: Observations of cloud-top entrainment in marine stratocumulus clouds, Journal of the atmospheric sciences, 51, 1530–1547, 1994.

Webster, C. R. and Heymsfield, A. J.: Water Isotope Ratios D/H, 18O/16O, 17O/16O in and out of Clouds Map Dehydration Pathways, Science, 302, 1742–1746, https://doi.org/10.1126/science.1089496, 2003.

Williams, K., Ringer, M., and Senior, C.: Evaluating the cloud response to climate change and current climate variability, Climate Dynamics, 20, 705–721, 2003.

Wood, R.: Stratocumulus clouds, Monthly Weather Review, 140, 2373–2423, 2012.

Wood, R. and Bretherton, C. S.: Boundary layer depth, entrainment, and decoupling in the cloud-capped subtropical and tropical marine boundary layer, Journal of climate, 17, 3576–3588, 2004.

Wood, R. and Bretherton, C. S.: On the relationship between stratiform low cloud cover and lower-tropospheric stability, Journal of climate, 19, 6425–6432, 2006.

Worden, J., Noone, D., and Bowman, K.: Importance of rain evaporation and continental convection in the tropical water cycle, Nature, 445, 528–532, 2007.

Worden, J., Noone, D., Galewsky, J., Bailey, A., Bowman, K., Brown, D., Hurley, J., Kulawik, S., Lee, J., and Strong, M.: Estimate of bias in Aura TES HDO/H2O profiles from comparison of TES and in situ HDO/H2O measurements at the Mauna Loa Observatory, Atmos. Chem. Phys., 11, 4491–4503, doi: 10.5194/acp–11–4491–2011, 2011.

Worden, J., Kulawik, S., Frankenberg, C., Bowman, K., Payne, V., Cady-Peirara, K., Wecht, K., Lee, J.-E., and Noone, D.: Profiles of CH4, HDO, H2O, and N2O with improved lower tropospheric vertical resolution from Aura TES radiances, Atmos. Meas. Tech. Discuss, 5, 397–411, doi:10.5194/amt–5–397–2012, 2012.

Wyant, M. C., Bretherton, C. S., Bacmeister, J. T., Kiehl, J. T., Held, I. M., Zhao, M., Klein, S. A., and Soden, B. J.: A comparison of low-latitude cloud properties and their response to climate change in three AGCMs sorted into regimes using mid-tropospheric vertical velocity, Climate Dynamics, 27, 261–279, 2006.

Yanai, M., Esbensen, S., and Chu, J.-H.: Determination of bulk properties of tropical cloud clusters from large-scale heat and moisture budgets, Journal of the Atmospheric Sciences, 30, 611–627, 1973.

Zhang, M., Bretherton, C. S., Blossey, P. N., Austin, P. H., Bacmeister, J. T., Bony, S., Brient, F., Cheedela, S. K., Cheng, A., Del Genio, A. D., et al.: CGILS: Results from the first phase of an international project to understand the physical mechanisms of low cloud feedbacks in single column models, Journal of Advances in Modeling Earth Systems, 5, 826–842, 2013.

Zipser, E.: Mesoscale and convective scale downdrafts as distinct components of squall-line structure, Mon. Wea. Rev., 105, 1568–1589, 1977.